LA-11527-MS

UC-721
Issued: March 1989

LA--11527-MS

DE89 009687

Studies of Ancient Concrete as Analogs of Cementitious Sealing Materials for a Repository in Tuff

*Della M. Roy**
*C. A. Langton**

DISCLAIMER

*Consultants at Los Alamos, Materials Research Laboratory, Pennsylvania State University, University Park, PA 16802.

Los Alamos National Laboratory
Los Alamos, New Mexico 87545

DISCLAIMER

CONTENTS

STUDIES OF ANCIENT CONCRETE AS ANALOGS OF CEMENTITIOUS SEALING MATERIALS FOR A REPOSITORY IN TUFF

by

D. M. Roy and C. A. Langton

ABSTRACT

The durability of ancient cementitious materials has been investigated to provide data applicable to determining the resistance to weathering of concrete materials for sealing a repository for storage of high-level radioactive waste. Because tuff and volcanic ash are used in the concretes in the vicinity of Rome, the results are especially applicable to a waste repository in tuff. Ancient mortars, plasters, and concretes collected from Rome, Ostia, and Cosa dating to the third century BC show remarkable durability. The aggregates used in the mortars, plasters, and concretes included basic volcanic and pyroclastic rocks (including tuff), terra-cotta, carbonates, sands, and volcanic ash. The matrices of ancient cementitious materials have been characterized and classified into four categories: (1) hydraulic hydrated lime and hydrated lime cements, (2) hydraulic aluminous and ferruginous hydrated lime cements (± siliceous components), (3) pozzolana/hydrated lime cements, and (4) gypsum cements. Most of the materials investigated are in category (3). The materials were characterized to elucidate aspects of the technology that produced them and their response to the environmental exposure throughout their centuries of existence. Their remarkable properties are the result of a combination of chemical, mineralogical, and microstructural factors. Their durability was found to be affected by the matrix mineralogy, particle size, and porosity; aggregate type, grading and proportioning; and the methodology of placement. In these respects the properties of ancient cementitious materials are subject to controlling factors similar to those of modern portland cement-containing materials. The evidence from the detailed investigations of these analog materials suggests that sealing materials compositionally and microstructurally similar to the ancient pozzolanic cementitious materials will be likely to adjust slowly to such an environment.

1. INTRODUCTION

1.1 Origin and Importance of Study

The need to isolate high-level wastes and transuranic wastes from the biosphere for relatively long periods of time has given rise to a plan for isolation of radioactive waste in mined repositories. It is necessary to predict the performance of repository systems for a period of thousands of years.

Most current repository conceptual designs use portland cement-based materials as components in multiple-barrier waste-disposal systems. The need for extraordinarily long-term durability and phase stability of borehole-plugging and shaft-sealing systems places unique requirements on materials such as cement, mortar, grouts, and concrete. It is difficult to determine the ultimate design suitability based solely on operating experience, experimentation, or prototype testing. One approach is to predict stability from thermodynamic properties (Sarkar et al., 1982). In addition, researchers are currently placing increased emphasis on the extrapolation of performance data for engineered materials based on knowledge from natural analogs. The concrete materials investigated in this study provide information on comparable man-made analogs.

An attempt is made in the present study to develop a chemical and physical explanation for the observed durability of selected ancient cement-containing materials. This should serve as a means of obtaining supporting data to aid in the assessment of durability, long-term performance, and thermodynamic stability of portland cement-containing materials that may be used for borehole and shaft sealing. Ultimately, these data are intended to aid in the performance and risk assessment of multiple-barrier systems for radionuclide containment.

1.2 Statement of the Problem

The overall requirements for long-term performance of sealing materials were not as stringent in most previous sealing experiences associated with segments of industrial applications, such as mining and chemical waste disposal, as those for nuclear waste isolation. It is assumed that portland cement-based materials will be important for repository sealing efforts. Historically, cement chemistry/engineering has been primarily concerned with bulk properties of the cements themselves and has provided little information on the long-term behavior of cement-containing materials in adverse subsurface environments. Some of the factors of concern for long-term durability and stability of these materials have been reviewed elsewhere (Roy et al., 1979).

This study of ancient cementitious building materials and their longevity provides an independent source of data for predicting longevity of modern cementitious materials used in repository sealing. Certain cement-containing ancient structures (up to about 2200 years old) are still functioning today and thereby provide historical documentation of the extended durability of these materials. They have survived environmental conditions which in many respects are more severe than those anticipated for borehole-plugging materials. These specific materials are particularly appropriate analogs for the NNWSI sealing program. They include concretes which contain tuff and volcanic ash aggregate, providing strong mineralogical and chemical composition similarities. The results are especially applicable to the assessment of long-term durability of near-surface sealing elements. concrete shaft covers, linings, and associated elements.

The objectives of this study are as follows:

Primary objectives

1. Provide information regarding the potential for long-term durability of cementitious sealing materials.
2. Provide information on the phase stabilities of the hydrated calcium silicate components of portland cement.
3. Provide information on performance of ancient cementitious analog materials under conditions similar to those in NNWSI sealing studies.

Secondary objectives

4. Obtain representative samples of a variety of ancient calcium silicate-containing building materials.
5. Establish procedures for characterization of these samples.
6. Characterize samples.
7. Determine and evaluate the interaction between these ancient materials and the environments in which they exist.

1.3 Background Information

A brief review of the literature on the history of building materials and construction techniques has been presented by Roy and Langton (1982). In addition to this review, the history of cementing materials from antiquity to the middle of the 19th century is discussed by Znatchko-Javorsky (1958). In his study Znatchko-Javorsky describes the historical development of gypsiferous and calcareous cementing materials in Eastern and Western Europe as well as in the USSR. The late T. A. Wertime, Smithsonian Associate, first interested the author (D. M. Roy) in the studies and provided valuable information. Roy and Langton (1982) and Langton and Roy (1984) have also summarized the results of a comprehensive literature survey of the following topics: chemical studies of ancient mortars and concretes, matrix-aggregate reactions in ancient mortars and concretes, and engineering studies of ancient concretes.

1.4 Sample and Site Location Information

A description of the sites in Rome, Ostia, and Cosa is given in Appendix A. The oldest samples were from Cosa, mid-third century BC, which is soon after Roman influence came through Latin colonization of the earlier Etruscan port colony at Cosa, in about 273 BC (Brown, 1951). Some specimens from the Roman Forum were attributed to late second century BC [the late Republican period (Blake, 1947)], while others from familiar structures are Early Empire (50 BC-50 AD) and later. Although the port colony of Ostia originated in the fourth century BC, most of the more permanent building took place later, during the Augustan period (43 BC-14 AD) and later into the second and third century AD.

Thus, the materials collected provide representatives of building materials over a span of several centuries.

1.5 Field Description of Samples and Site Locations; Terminology

Terminology used to describe the materials is given in Appendix B. Field descriptions of the hand specimens and site descriptions are presented in Appendix C. Where possible, site locations were noted on the site plans. Site and sample locations at Rome and Ostia were photographically documented and this information was stored in the archives at the Materials Research Laboratory, The Pennsylvania State University. Those specimens from Cosa were collected and documented by F. E. Brown.

1.6 Technical Approach

Samples analyzed in this study were collected specifically for this research effort. The author (D. M. Roy) collected 27 hand specimens from a variety of archaeological structures and excavations in Rome and Ostia, Italy. Several specimens were collected for her from Cosa by F. E. Brown, American Academy in Rome, at the time the other specimens were collected. Hand-specimens and sample locations were photographically documented, and samples were catalogued in accordance with a numerical system which also took into account the site location.

Intensive study of these specimens combined analytical and interpretive methods in a multi-method analysis. Analytical techniques and tests used on these samples are described in Appendix D and listed below:

Macroscopic and Microscopic Analyses

1. Hand-specimen examinations
2. Binocular microscope examinations
3. Thin section preparation and petrographic microscopic examinations
4. Scanning electron microscope (SEM) studies (including energy-dispersive x-ray (EDX) analysis)

Chemical Analyses of Selected Fractions

1. Wet chemical analyses

2. Emission spectroscopic analyses
3. Specialized chemical analyses

Structural (Phase Identification) Studies

1. X-ray diffraction analyses of matrix fractions
2. Silicate structure analysis-trimethylsilylation (TMS) and gas chromatography/gel permeation chromatography (GPC) (in the latter, Eric Lachowski provided some analyses) (Tamas et al., 1976; Sarkar and Roy, 1979)

Thermal Analyses

1. Thermogravimetric analyses
2. Differential thermal analyses

2. Results

2.1 Macroscopic Results

Macroscopic descriptions of ancient cementitious materials, concretes, mortars, and plasters from Rome, Ostia, and Cosa, are presented in Appendix E.

2.2 Microscopic Results

Petrographic data for the samples are summarized in Table 2-1 and selected thin sections are discussed in the following narrative.

A summary of microscopic descriptions of specimens from Ostia, Rome, and Cosa is given in Table 2-1. Photomicrographs of selected ancient building materials from Ostia and Rome, CR-1, OS-27, CF-4B, and CO-19A, are shown in Fig. 2-1 (a-d), respectively, and illustrate microtextures typical of ancient plasters, mortars, and concretes from Italy. Coarser volcanic aggregates are incorporated in a cementitious matrix. The aggregates generally account for 50 to 80% of the sample volume. These aggregates have glassy, opaque to slightly anisotropic groundmasses which range in color from black to orange, to red or yellow. They range from vesicular [Fig. 2-1(a,b)] to dense [Fig. 2-1(c,d)] and from irregular to subangular to rounded in shape. Some aggregates also display flow banding.

Leucite, olivine, augite, apatite, biotite, alkali feldspar, and amphibole are the most common phenocrysts, and augite and alkali feldspar are the most common microlites. Figure 2-1(d) illustrates an aggregate containing large leucite phenocrysts in a glassy groundmass. In some ancient building materials examined, the coarse aggregate fractions were predominantly made up of a single rock type, whereas in others, aggregates with various textures, colors, and phenocrysts were observed. Most of the aggregates can be classified as silica undersaturated pyroclastic rocks with a trachyte mineralogy; hence the name trachytic tuff applies to most of the coarse aggregate fractions in these specimens.

In general, the matrix phases were too fine grained for identification by optical techniques. At low magnification, the cementitious material appears mottled and patchy [Fig. 2-1(a-d)]. These color and textural inhomogeneities are due to variations in both mineralogy and grain size of the constituent phases. Very fine grained regions with diffuse to well-defined selvages range from clear or light yellow, displaying high birefringence (probably made up of calcite) to darker, dusky yellow to gray, displaying lower birefringence. Other small patches, up to 0.5 mm, are red, orange, or brown, subangular to irregular in shape, and have diffuse selvages. In addition, irregular patches of slightly coarser grained calcite are abundant and ubiquitous throughout the matrices of these samples and are illustrated in Fig. 2-1(a-c) (bright areas). At low magnification, the interfacial regions between the cementitious matrix and the coarse volcanic aggregates appear coherent and sharp. Often the matrix material was observed filling vesicles within these aggregates and occasionally replacing the phenocrysts and groundmass as illustrated in Fig. 2-1(d), where leucite crystals, apparently replaced by matrix phases, are shown.

Petrographic analyses of these volcanic aggregate-containing materials conducted at high magnification (400 to 1000X) revealed that the associated matrix fractions contained a sizeable amount (10-30% of the matrix) of fine aggregate. Most of this fine aggregate fraction (up to 0.5 mm) was made up of volcanic glass or palagonite (altered volcanic glass); a minor proportion of small phenocrysts was also present. These fine red to yellowish-orange, glassy ash particles were characterized by the development of extensive matrix-aggregate reaction zones. (Reaction rims were not commonly observed between coarse volcanic aggregates and matrix phases.) The nature and extent of these reaction products

TABLE 2-1. Microscopic Descriptions of Ancient Concretes, Mortars, and Plasters from Italy.*

Sample No.	Matrix	Aggregates+	Miscellaneous
		COSA	
CS-1	v. fn. gr.; dusty gray-yel. with diffuse patches and webbing of dk. gray-yel; <1% fn. red opaque volcanic glass or palagonite (calcite matrix)	1. siltstone, rounded, contains aligned quartz and feldspar crystals 2. med. gr. limestone (marble) displaying irregular selveges. One frag. ≈25% slide.	matrix/agg. reaction rims were not observed; matrix is characterized by tension cracks which have subsequently been filled with sl. coarser gr. calcite than that constituting the bulk matrix
CS-2A	v. fn. gr.; lt. orange-yel. to red-yel.; fn. gr. red volcanic glass or palagonite ≲5% (calcite matrix)	1. schist frag. containing quartz, feldspar, mica, and opaque crystals, sub-angular 2. quartzite frag. sub-angular 3. carbonate frag.	matrix/fn. agg. reaction zones were not observed; tension cracks were not characteristic; patches of med. to coarse gr. calcite were common; about 30% of sample consists of v. fn. gr. chunks of poorly crushed lime which have recarbonated to form calcite
CS-2B (Layer 1)	v. fn. gr.; orange-yel. to lt.-yel.; abundant, ≳20% red opaque volcanic glass or palagonite (calcite + pozzolona reaction product matrix)	1. black, opaque crystal-rich tuff containing olivine and augite, sub-angular 2. red opaque tuff 3. red opaque lithic tuff showing flow banding 4. strained quartz gr. in an opaque ground mass, sub-angular to rounded	reaction rims developed around fn. agg.; in places there is a fracture between the exterior layer (2) and the bulk plaster
(Layer 2)	v. fn. gr.; dk. orange-gray with dk. gray stringers parallel to exterior surface		unidentified greenish colored crystals make up a layer up to ≈0.4 mm thick
CS-3	v. fn. gr.; orange-yel. mottled to lt. and dk. orange; patches of gray-yel. are sl. coarser crystals of calcite (calcite matrix)	1. terra-cotta frag. containing strained quartz gr. and clay. Some frag. show an alignment of the fabric; frag. up to 1 cm	matrix/agg. reaction zones were not observed. Tension cracks were common; few chunks of recarbonated poorly crushed lime were observed
CS-4	no matrix	crystal-rich pyroclastic rock (trachytic tuff)	at least 95% of this sample is composed of olivine, augite, alkali feldspar, nepheline, and analcime crystals
		OSTIA	
OS-1A	v. fn. gr.; dk. gray-yel. mottled to med. gray-yel. to lt. orange; patches of sl. coarser gr. calcite with discrete to diffuse boundaries. ≈30% of matrix = dk. red opaque, subrounded volcanic glass or palagonite; matrix ∿ 30% sample (calcite + pozzolana reaction product matrix)	1. dk. red opaque vesicular tuff 2. black, opaque volcanic tuff; augite and olivine phenocrysts 3. red-orange, non-porous tuff, alkali feldspar and augite phenocrysts 4. red-orange, vesicular tuff, leucite, biotite, and augite phenocrysts plus microlites 5. dk. gray tuff, alkali feldspar phenocrysts 6. feldspar, biotite, augite, olivine crystals	well developed reaction zones between matrix and fn. volcanic agg.; reaction products have low bf. and commonly exhibit lath-like or plate-like crystal habits. (Phenocrysts do not display reaction rims)

TABLE 2-1. (CONTINUED).

Sample No.	Matrix	Aggregates[†]	Miscellaneous
OS-1B	v. fn. gr.; clear to br. or gray-yel. depending on slide thickness; abundant red and black, opaque subangular to rounded volcanic glass or palagonite; also v. small olivine, augite, biotite, alkali feld. crystals (calcite + pozzolana product matrix)	1. black opaque, vesicular tuff, subangular 2. dk. red vesicular tuff, biotite and olivine phenocrysts 3. lt. yel. br. vesicular tuff, few microlites 4. m. red br. v. vesicular tuff	same as above
OS-2 (Layer 1)	v. fn. gr., m. gray.-yel. mottled to orange-yel., stringers of orange-yel; abundant red, opaque volcanic glass or palagonite ≈30% of matrix (calcite + pozzolana reaction product matrix)	1. orange-red, opaque, vesicular tuff 2. black, opaque vesicular tuff, needle-shaped microlites	same as above. Contact between layers 1 and 2 is regular but layer 1 was not polished prior to application of layer 2
(Layer 2)	v. fn. gr. gray. br. mottled to br. yel; patches of sl. coarser gr. crystals (calcite matrix)	1. limestone with corroded selveges (possibly partially calcined and subsequently hydrated and carbonated), up to 2 mm 2. limestone, rounded v. fn. gr. texture similar to matrix (possibly uncrushed chunks of lime, subsequently hydrated and carbonated)	layer 2 (exterior plaster) is a lime plaster. The outer surface is smooth (polished) and is overlain by a v. thin layer up to 0.15 mm thick of unidentified material
OS-18	v. fn. gr.; dk. red-br. to red-orange with dk. br. webbing and mottling; abundant red opaque volcanic glass or palagonite (calcite + pozzolana reaction product matrix)	1. one agg. ≈98% of sample, black, opaque, vesicular tuff 2. smaller, up to 0.5 cm rounded volcanic frag. with reaction (weathered) rims	well developed reaction zones between matrix and fn. volcanic agg.; matrix contains veins and vug fillings of secondary minerals (biaxial neg., low bf. inclined extinction, lath habit)
OS-27	v. fn. gr.; lt. br.-yel., abundant dk. gray volcanic glass or palagonite; angular patches of material with same texture as bulk matrix but rimmed by a dk., discrete selvage (calcite + pozzolana reaction product matrix)	1. dk. red tuff, subrounded, feldspar microlites 2. black, vesicular tuff, rounded, few microlites	well developed reaction zones between matrix and fn. volcanic agg.; v. fn. gr. calcite fills pores and fractures throughout the matrix and between agg. and matrix.
OS-33	v. fn. gr.; med. gray-yel., mottled to various shades of gr.-yel.-red; abundant dk. red opaque volcanic glass or palagonite, angular (calcite + pozzolana reaction product matrix)	1. dk. red-br., glassy tuff, few olivine crystals, small vesicles lined with calcite 2. red opaque, vesicular tuff with dk. colored salvages 3. yel.-orange, vesicular tuff, few microlites, subrounded 4. dk. gray, vesicular tuff, phenocrysts of olivine and pyroxene 5. biotite, olivine, augite, leucite, apatite crystals	same as above

TABLE 2-1. (CONTINUED).

Sample No.	Matrix	Aggregates[†]	Miscellaneous
OS-7-MHN	v. fn. gr.; gray-yel. mottled to lt. and dk. areas; also dk. webbing especially around agg.; abundant fn. red volcanic glass or palagonite; matrix ≈20% of sample (calcite + pozzolana reaction product matrix)	1. black, opaque, vesicular tuff 2. crystals of leucite, biotite, augite, feldspar 3. silty carbonate frag. containing microfossils 4. red, opaque leucite-rich tuff	well developed matrix/fn. agg. reaction zones; irregular patches of sl. coarser gr. calcite throughout matrix and in agg. vesicules
		ROME	
CA-1	v. fn. gr.; clear to lt. yel. mottled to med. gray-yel; abundant (≈30% matrix) red, opaque volcanic glass or palagonite surrounded by low bf. phase with texture similar to the fn. gr. calcite in the matrix (calcite + pozzolan reaction product matrix)	1. black, vesicular tuff, few microlites 2. med. red.-br. vesicular tuff, ≤10 3. lt. orange glassy tuff, ≤5% 4. one frag. med. gr. limestone, angular 5. crystals of biotite, olivine, augite, alkali feldspar	well developed reaction zones between matrix and fn. agg.; patches and veins of fn. gr. calcite are common; vesicles in the agg. are commonly lined or filled with calcite
CA-2 (Layer 1)	v. fn. gr.; lt. yel. mottled to med. gray-yel.; abundant (≤20% of matrix) red, opaque volcanic glass or palagonite (calcite + pozzolana reaction product matrix)	1. red, opaque, vesicular tuff 2. black, opaque, vesicular tuff 3. tuff breccia 4. biotite crystals	well developed reaction zones between matrix and fn. agg.; small patches of coarser gr. calcite throughout matrix; a thin layer (≈0.07 mm thick) of needle-shaped crystals exhibiting low bf. is present between layers 1 and 2
(Layer 2)	fn. gr.; clear to lt. yel.; carbonate bf. and extinction; uniform texture (calcite matrix)		exterior layer is a lime plaster
CF-2	v. fn. gr.; lt. yel. to lt. gray; v. fn. red and black opaque volcanic glass or palagonite (calcite + pozzolana reaction product matrix)	1. black, opaque vesicular tuff, small feldspar microlites 2. dk. red, opaque tuff, angular	well developed reaction zones between matrix and fn. agg.; reaction products include low bf. crystals in the interfacial region in addition to v. fn. gr. low bf. material with a texture similar to the matrix calcite
CF-4A	v. fn. gr.; clear to lt. yel.; predominantly calcite, ≤20% sample vol = matrix (primarily calcite matrix + minor amount of pozzolana reaction products)	1. red opaque vesicular tuff, rounded to subangular, apatite, biotite, opaque phenocrysts 2. dk. br.-red. tuff, same as above 3. one large red to yel. vesicular tuff frag. 4. black, vesicular tuff, <5%	matrix-agg. reaction less obvious than generally observed in ancient Roman pozzolana-containing materials
CF-4B	fn. gr.; laths up to 0.03 mm, clear, biaxial neg., undulatory extinction; few patches of fn. gr. calcite	1. dk. red vesicular crystal-rich tuff, contains abundant opaque crystals, olivine, zoned augite, biotite, alkali feldspar phenocrysts 2. black, vesicular tuff	crystals making up the matrix are probably zeolites. They are also present as vug fillings. All agg. look corroded and replaced by secondary minerals similar to those in the matrix; this is probably a weathered tuff frag., not a man-made material

TABLE 2-1. (CONTINUED).

Sample No.	Matrix	Aggregates†	Miscellaneous
CF-4C (Layer 1)	v. fn. gr.; lt. gray webbed and mottled orange-gray; abundant ≳50% dk. gray to black opaque volcanic glass or palagonite, angular to subrounded (calcite + pozzolana reaction product matrix)	1. med. red tuff showing flow bonding, biotite and alkali feldspar phenocrysts 2. dk. red-br. opaque vesicular tuff, few microlites 3. v. dk. br. vesicular tuff, augite, olivine and biotite phenocrysts 4. biotite, olivine, augite, and feldspar crystals	well developed reaction zones between matrix and fn. agg.; in places there is a distinct fracture filled with calcite between layers 1 and 2; patches of calcite with discrete to diffuse boundaries are disseminated throughout the matrix
CF-4C (Layer 2)	v. fn. gr.; lt. yel. with lt. and dk. patches; abundant ≳40% of matrix is dk. to med. red volcanic glass or palagonite (calcite + pozzolana reaction products matrix)	1. red vesicular tuff ± phenocrysts 2. black vesicular tuff 3. crystals of alkali feldspar, augite, olivine, biotite	well developed reaction zones between matrix and fn. agg. which typically have opaque centers and diffuse boundaries
CF-4D	v. fn. gr.; lt. yel., predominantly calcite; abundant ≳30% of matrix is v. fn. volcanic glass or palagonite, ≳10% matrix is a v. low bf. phase with texture similar to calcite (calcite + pozzolan reaction product matrix)	1. crystals of alkali feldspar, olivine, augite, nosean, garnet 2. black, vesicular tuff, rounded to subangular 3. red. br., vesicular to non-vesicular tuff	same as above; abundant "pluck outs" in this thin section
CO-19A	v. fn. gr., gray-yel. to orange-yel., abundant, ≳30% of matrix fn. red opaque volcanic glass or palagonite (calcite + pozzolana reaction product matrix)	1. black, vesicular tuff, crystals, apatite, olivine and garnet phenocrysts 2. red, opaque leucite-rich tuff 3. crystals of biotite, olivine, garnet, leucite, apatite, alkali feldspar, and augite	same as above; matrix contains patches of sl. coarser gr. calcite and in places displays tension cracks; many of the agg. have calcite vesicle linings and fillings
CO-19B	v. fn. gr.; lt. yel. to clear with diffuse red-yel. patches; abundant ≳10-30% fn. red opaque volcanic glass or palagonite (calcite + pozzolana reaction product matrix)	1. black, opaque, vesicular tuff containing microlites 2. orange lithic tuff displaying flow banding 3. lt. yel. tuff containing alkali feldspar microlites 4. red vesicular tuff 5. crystals of leucite feldspar, olivine, and augite	well developed matrix/agg. reaction zones; abundant flow banded tuff; some areas of matrix display tension cracks
CR-1	v. fn. gr.; gray-yel. to clear (clear patches are composed of coarser crystals); abundant fn. red volcanic glass or palagonite (calcite + pozzolana reaction product matrix)	1. black, opaque, vesicular tuff 2. black, opaque, vesicular tuff containing leucite phenocrysts 3. yel. to orange vesicular tuff 4. crystals of biotite, alkali feldspar, and augite	well developed matrix/agg. reaction zones; calcite commonly lines pores of agg.; agg. fract. ≳70% of sample
CR-2	no matrix	1. dk. red brown vesicular tuff containing large olivine, and alkali feldspar, phenocrysts	this is a tuff frag.; there are concentric features in this thin section which suggest this rock is a tuffaceous breccia

TABLE 2-1. (CONTINUED).

Sample No.	Matrix	Aggregates[†]	Miscellaneous
CR-9A	v. fn. gr.; clear to lt. gray, yel. to lt. yel.-gray; patches of sl. coarser gr. calcite; abundant ≳30% fn. red volcanic glass or palagonite (calcite + pozzolana reaction product matrix)	1. black, opaque, vesicular tuff 2. dk. red-br. opaque, vesicular tuff, abundant leucite phenocrysts 3. lt. orange-red, opaque tuff containing feldspar microlites 4. crystals of alkali feldspar and leucite	well developed matrix/agg. reaction zones. Matrix is a mixture of calcite plus pozzolana reaction products with characteristically low bf., v. fn. gr. size and same texture as calcite
CR-9B	v. fn. gr.; med. dusty gray mottled to dk. gray-yel.; abundant, ≳30% of matrix; fn. red volcanic glass or palagonite (calcite + pozzolana reaction product matrix)	1. black, opaque, vesicular tuff 2. dk. red-br., sl. vesicular tuff containing feld. microlites 3. chunks of fn. gr. carbonate 4. few crystals of olivine	same as above. Calcite was observed filling fractures between certain large agg. and the surrounding matrix; the matrix makes up ≲20% of the total sample
FP-7	v. fn. gr.; med. grayish yel. to orange mottled to lt. gray-yel.; abundant ≳30% fn. red volcanic glass or palagonite; sample contains ≳30% matrix (calcite + pozzolana reaction product matrix)	1. crystals of biotite, augite, nepheline, olivine, and alkali feldspar 2. dk. red-brown, opaque, vesicular tuff, some frag. contain biotite, olivine, and augite phenocrysts 3. lt. red.-yel., leucite-rich tuff 4. black, opaque, vesicular tuff 5. chunks of uncrushed lime which have subsequently carbonated	extensive matrix/fn. agg. reaction zones; coarser gr. size in matrix fraction corresponds to lighter color and better developed carbonate bf.; calcite crystals were observed filling occasional fracture
FP-11B	fn. gr.; clear to lt. gray-yel.; fn. red volcanic glass or palagonite; at least 40% matrix = calcite (calcite + pozzolana reaction product matrix)	1. dk. red-brown, opaque, vesicular tuff 2. crystals of olivine, augite, biotite, and alkali feldspar 3. abundant chunks of uncrushed lime which have subsequently carbonated (sl. coarser gr. than matrix)	matrix contains equant, hexagonal crystals but they are too small for optical measurements; they are clear and display low bf.
FP-12	v. fn. gr.; clear to lt. yel. to gray-yel.; clear areas are sl. coarser gr.; abundant ≳30% of matrix is fn. red volcanic glass or palagonite; ≲20% of sample is matrix (calcite + pozzolana reaction product matrix)	1. black, opaque, vesicular tuff 2. black, opaque, feldspar-rich tuff 3. chunks of uncrushed lime which have subsequently carbonated	well developed matrix/fn. agg. reaction zones typically displaying low bf. and a texture similar to the surrounding calcite matrix
FP-18	fn. gr., clear to lt.-yel.; predominantly calcite, abundant ≲20% fn. black opaque volcanic agg. (primarily calcite matrix, minor amount of pozzolana reaction products)	1. dk. red, opaque, vesicular tuff, some of which appears to have corroded (weathered?) selvages 2. dk. red, opaque tuff containing olivine, feldspar, and augite phenocrysts	very limited reaction between matrix and fn. black agg.; med. to coarse gr. calcite was observed in large agg. pores and in fractures in the matrix; one surface of this sample is covered by a mat-like layer of fibrous crystals, up to 0.21 mm, which are aligned parallel to the surface; no area was located where this thin mat was in direct contact with the bulk sample

TABLE 2-1. (CONTINUED).

Sample No.	Matrix	Aggregates†	Miscellaneous
T-1	v. fn. gr.; lt. br.-yel., abundant, ≈30% of matrix, fn. red volcanic glass or palagonite; matrix ≈40% of sample (calcite + pozzolana reaction product matrix)	1. black, opaque, vesicular tuff 2. black, opaque, vesicular tuff containing leucite phenocrysts 3. dk. red.-br. opaque tuff containing leucite phenocrysts 4. crystals of biotite, apatite, leucite, olivine, augite, and feldspar	same as above

*Abbreviations are standard for petrographic descriptions.

†Aggregates are listed in order of decreasing relative abundance.

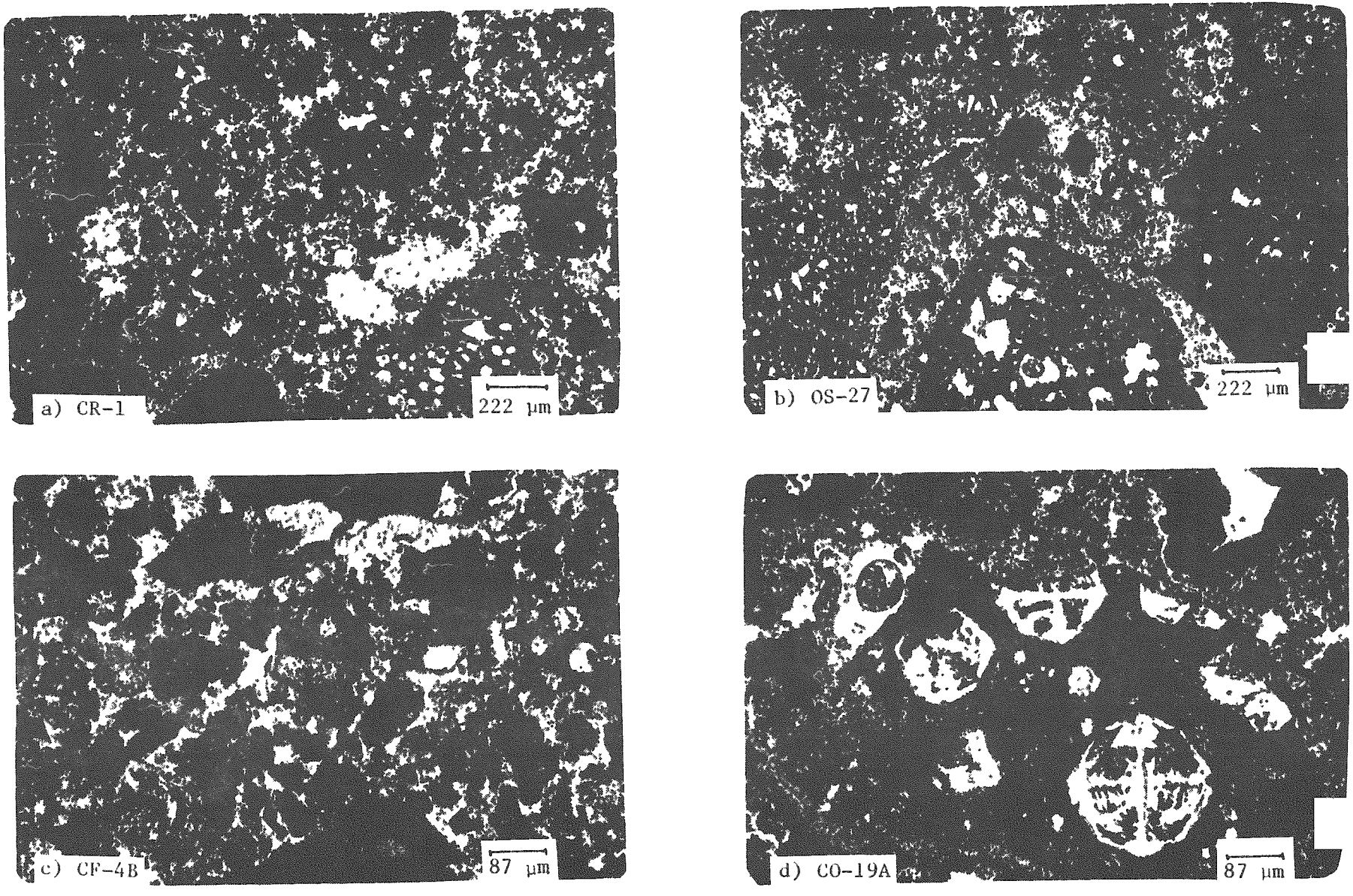

Fig. 2-1. Photomicrographs of Ancient Pozzolana-containing cementitious materials from Ostia, OS-27, and Rome, CR-1, CF-4B, CO-19A. a) Nicols = 70°; b) 20°; c) 0°; and d) 0°.

are best illustrated by comparisons of ordinary and polarized light images because the degree of anisotropy of these phases is a function of the compositional variations. For example, in ordinary light, the calcite (originally slaked lime, portlandite)-rich portions of the matrix are clear to light yellow in color, whereas the unreacted volcanic glass is red to yellowish-orange. In ordinary light the reaction products making up the interfacial zones range from red to light yellow. In polarized light, the calcite-rich areas display high (bright) birefringence, whereas the volcanic glass is isotropic or very slightly anisotropic. The pozzolana reaction products display a birefringence ranging between these two extremes, but it is most commonly low and appears medium gray in color. The reaction rims appear as halos around cores of unreacted volcanic glass and can be observed in ordinary or polarized light or both, depending on the particular area being investigated.

Figures 2-2(a-d), 2-3(a-d), and 2-4(a,b) are a series of paired (ordinary and polarized light) photomicrographs illustrating the nature and extent of the pozzolana reaction product. The microtexture of the reaction products varies from massive, similar to the glass particles (Figs. 2-2 and 2-3), to an intermediate texture [Fig. 2-4(c)], to well-developed partly isotropic crystallites growing outward from the aggregate surfaces [Fig. 2-4(a,b)]. The entire matrix fraction in these samples is composed of an intimate mixture of calcite-rich areas, pozzolana reaction products, and unreacted fine aggregate cores. In some places, calcite is slightly more abundant; in others, the reaction products are more abundant. The fine aggregate fractions appear to be relatively well dispersed throughout the matrix. Figure 2-4(c) shows a photomicrograph illustrating a fine aggregate agglomerate which clearly displays intergranular reaction rims. Figure 2-4(d) illustrates a replacement-type texture characterized by replacement of the fine aggregate selvages with matrix phases (lime-rich phases).

Specimens of the ancient cementitious building materials display varying degrees of secondary fracturing. Most samples examined were not noticeably fractured but some displayed extensive network-type cracking, as illustrated by photomicrographs of samples OS-1A and CO-19A, Fig. 2-5(a,b), respectively. The fractures in OS-1A are completely filled with secondary calcite, whereas those in CO-19A are open. It is impossible to determine if the cracks in the latter sample were induced during collection or thin section

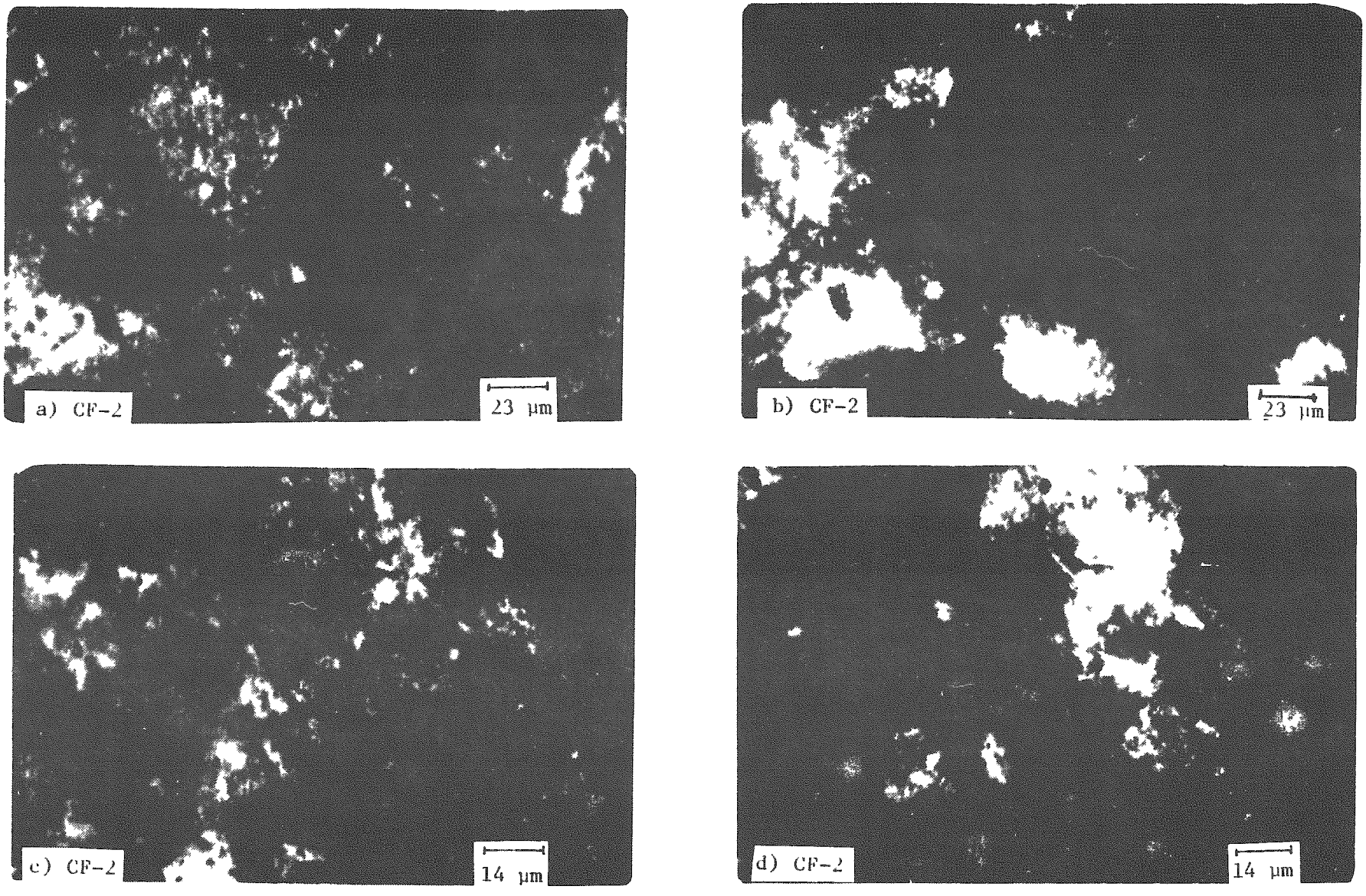

Fig. 2-2. Photomicrographs of interfacial zones formed by chemical reactions between fine pozzolanic volcanic ash particles and the lime-rich phases in the matrix fraction of CF-2, Rome. a,c) Nicols = 0°; b,d) Nichols = 90°.

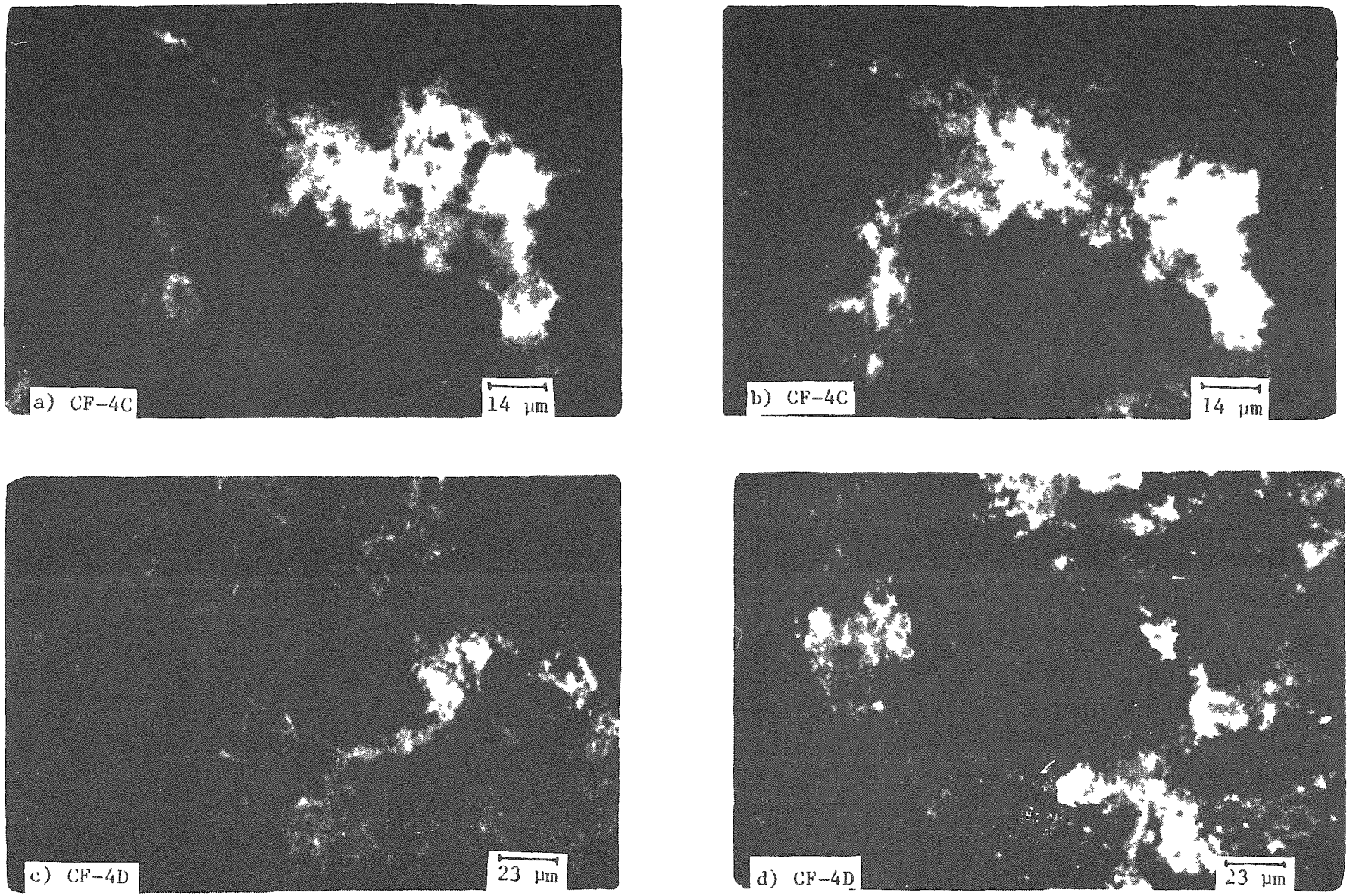

Fig. 2-3. Photomicrographs of interfacial zones formed by chemical reactions between the fine pozzolanic volcanic ash particles and the lime-rich phases in the matrices of CF-4C and CF-4D, Rome. a,c) Nicols = 0°: b,d) Nicols = 90°.

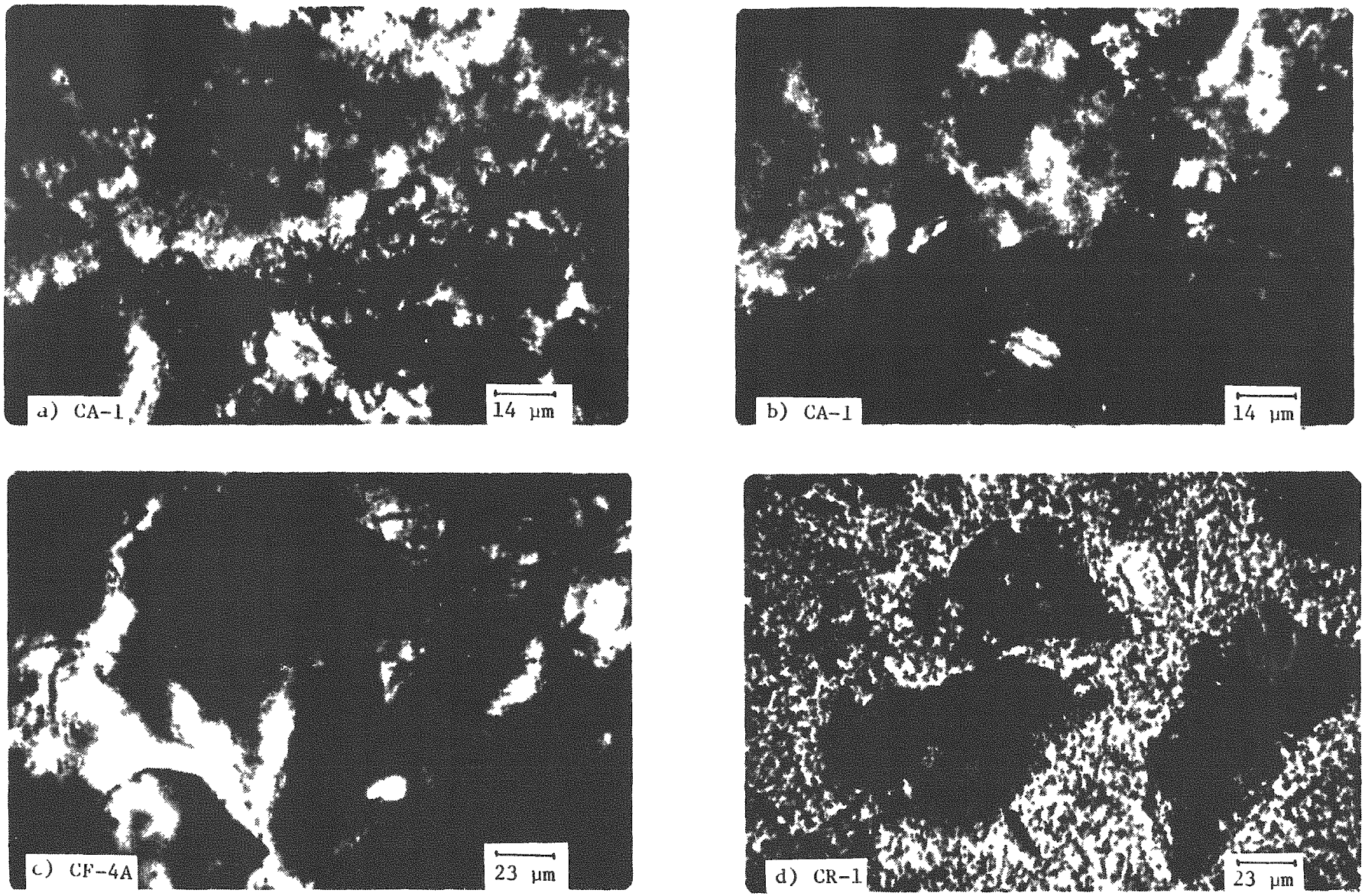

Fig. 2-4. Photomicrographs of interfacial zones formed by chemical reactions between the fine pozzolanic volcanic ash particles and the lime-rich phases in the matrices of CA-1, CF-4A, and CR-1, Rome. a,c) Nicols =0°; b,d) Nicols = 90°.

preparation, but it is certain that those which are filled with secondary minerals are not artifacts of recent handling. The lack of pattern fractures in most of the ancient samples studied implies that ancient builders established construction techniques and proportioning ratios which minimized drying shrinkage and volume changes caused by post-set chemical reactions.

Another type of building material is represented by sample CS-3. Photomicrographs of this particular specimen collected from Cosa [Fig. 2-5(c,d)] illustrate broken terra-cotta aggregates in various sizes and shapes (bottom) incorporated in a relatively homogeneous, fine-grained calcite matrix (top). These samples are characterized by an abundance of tension gashes throughout the matrix, which probably formed as the result of carbonation of the original slaked lime, portlandite. [An 11% volume reduction is involved in the reaction $Ca(OH)_2 + CO_2 \rightarrow CaCO_3 + H_2O$ (Lea, 1970).] Another feature of this specimen is that it contained up to 1% charcoal fragments which had been incorporated into the matrix, along with the crushed, calcined limestone. The black area in the center of Fig. 2-5(c) is a piece of porous charcoal impregnated with calcite. The matrix/terra-cotta interfacial zones observed in this thin section did not show evidence that pozzolana reactions had taken place. The terra-cotta aggregates were typically dark red or brown and very fine grained and contained feldspar, olivine, and quartz grains [Fig. 2-5(c,d)].

2.3 Scanning Electron Microscope Analysis Results

2.3.1 Description of Selected Samples from Cosa

Scanning electron photomicrographs of four ancient cementitious building materials from Cosa are shown in Fig. 2-6(a-f). The matrix fractions of samples CS-1, -3, and -4 consist of interlocking calcite crystals which formed as the result of carbonation of the slaked lime (portlandite), which initially constituted the binding phase in these materials. Secondary electron images of CS-1 are shown in Fig. 2-6(a,b), and the microstructure of this sample is coherent, relatively porous, and characterized by intergrown massive calcite and randomly oriented calcite crystals 0.01 to 1.0 μm in cross section. This specimen has an irregular, lumpy texture which was probably inherited from the original poorly crushed, slaked lime.

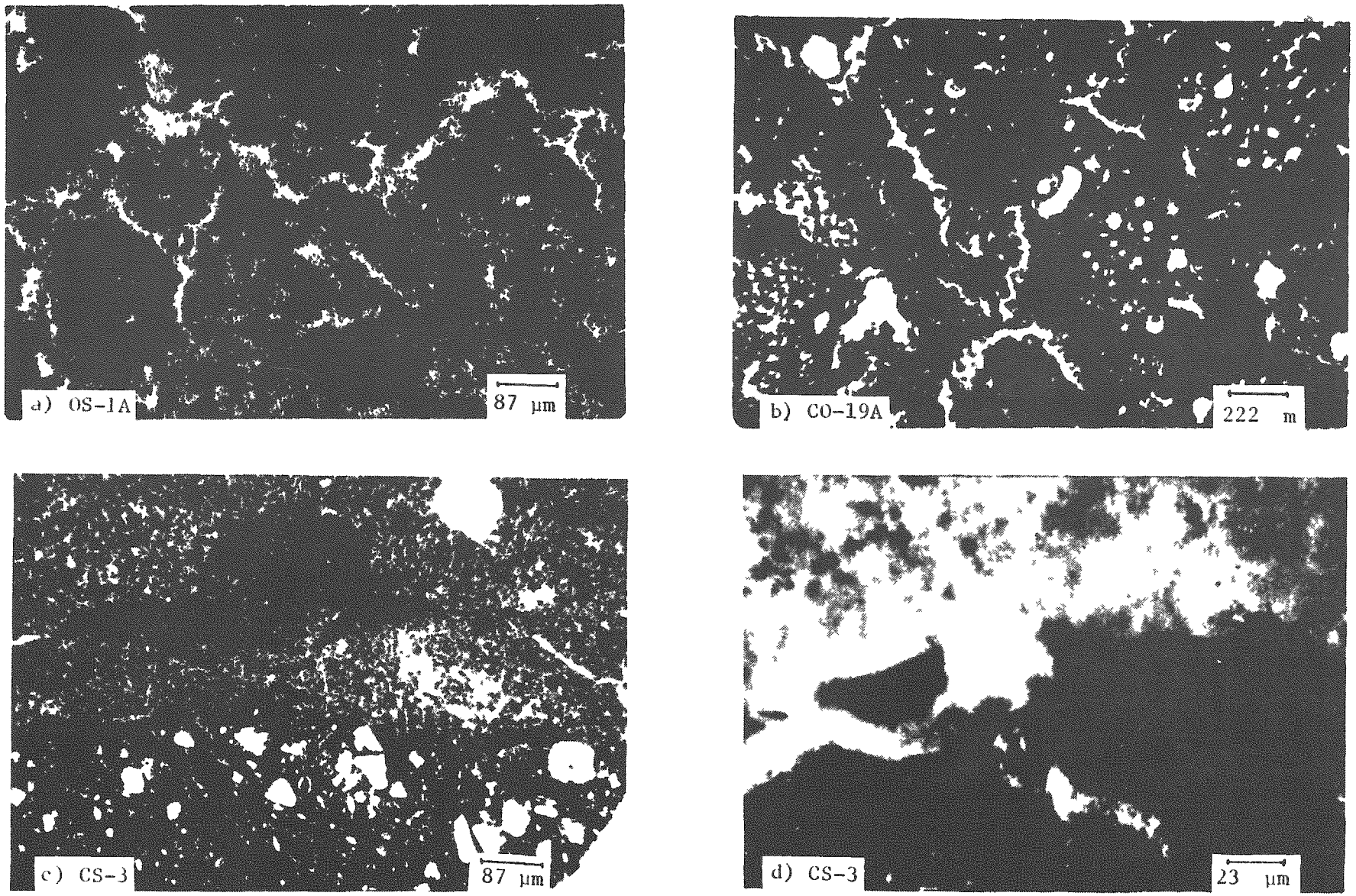

Fig. 2-5. Photomicrographs of ancient volcanic aggregate-containing cementitious materials from Ostia, OS-1A, and Rome, CO-19A (a and b), respectively; and of an ancient mortar/plaster from Cosa, CS-3, containing Terra-Cotta aggregate (c and d). a,b,c) Nicols =0°; d) Nicols = 20°.

For the most part, the microtexture and particle morphologies of the matrix fraction of CS-2B (layer 1) resemble those described for CS-1. However, there are regions within the matrix of CS-2B (layer 1) which have a more complex microstructure such as that illustrated in Fig. 2-6(c). In this secondary electron image, the matrix appears to be composed of very fine particles with an irregular, crumpled sheet-like morphology intergrown with small, well-developed calcite crystals to form a coherent material. The fine sheet- or foil-like particles typically appear to be fused or intergrown to such an extent that a massive microstructure is formed. Qualitative chemical analysis of this phase by energy dispersive x-rays (EDX) resulted in the detection of a minor amount of silicon and aluminum in addition to calcium. The EDX spectrum for the area labeled A in the upper right of Fig. 2-6(c) is shown in Fig. 2-7, and the phase which exhibits the crumpled foil-type morphology is thought to be the reaction product of pozzolanic ash and portlandite.

Sample CS-3 was a lime-containing material (opus signinum) in which broken terra-cotta fragments were used as coarse aggregate. The matrix of this specimen is shown in the bottom half of Fig. 2-6(d) and is composed entirely of well-developed calcite crystals up to 1.0 μm in size. Portions of the matrix have a lumpy texture which was probably inherited from the crushed lime; other portions are uniformly fine grained. The interfacial region formed between the matrix and a terra-cotta fragment is also shown in Fig. 2-6(d) (the upper half of this image is the terra cotta). Neither compositional gradations nor complex structural features were observed at the lime (calcite) matrix terra-cotta interfaces. However, the interfaces were not sharp planar contacts because the terra-cotta surfaces on which the portlandite and calcite crystallized were irregular.

Sample CS-4, a mortar from Cosa, is unique in that the matrix fraction constitutes less than 5% by volume of the total material. The bulk microtexture is illustrated in the low magnification SEM image in Fig. 2-6(e) and is characterized by rounded sand-like aggregates held together by a minor amount of calcite (carbonated portlandite). As shown in Fig. 2-6(f) (lower half), the calcite matrix consists of small, less than 10-μm, intergrown crystals.

The interfacial region formed between a volcanic sand grain (top half) and the matrix fraction (lower half) is also shown in Fig. 2-6(f). Compositional zoning and complex

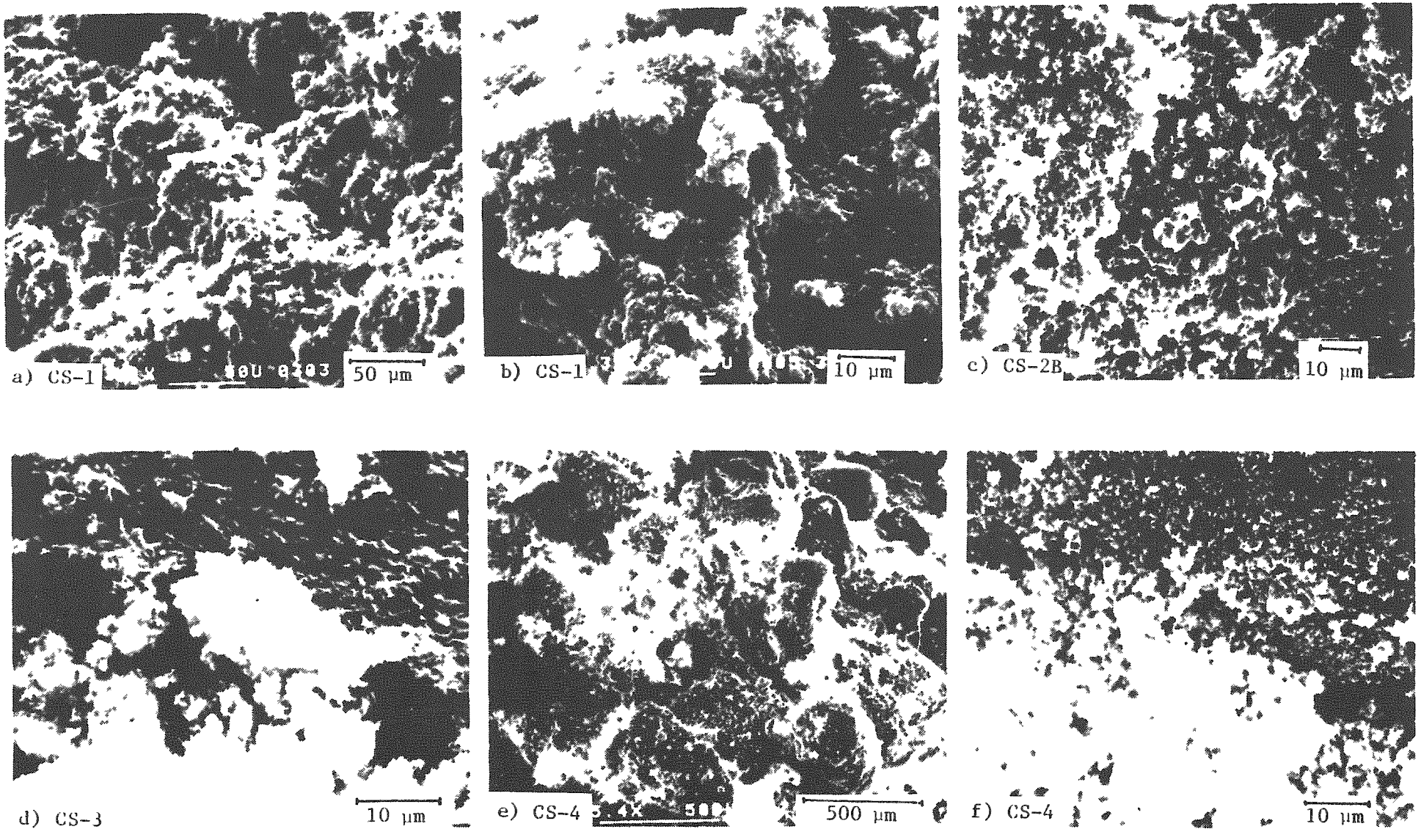

Fig. 2-6. Scanning electron photomicrographs (SEM secondary electron images) of four specimens from Cosa. CS-1, CS-2B (layer 1), CS-3, and CS-4.

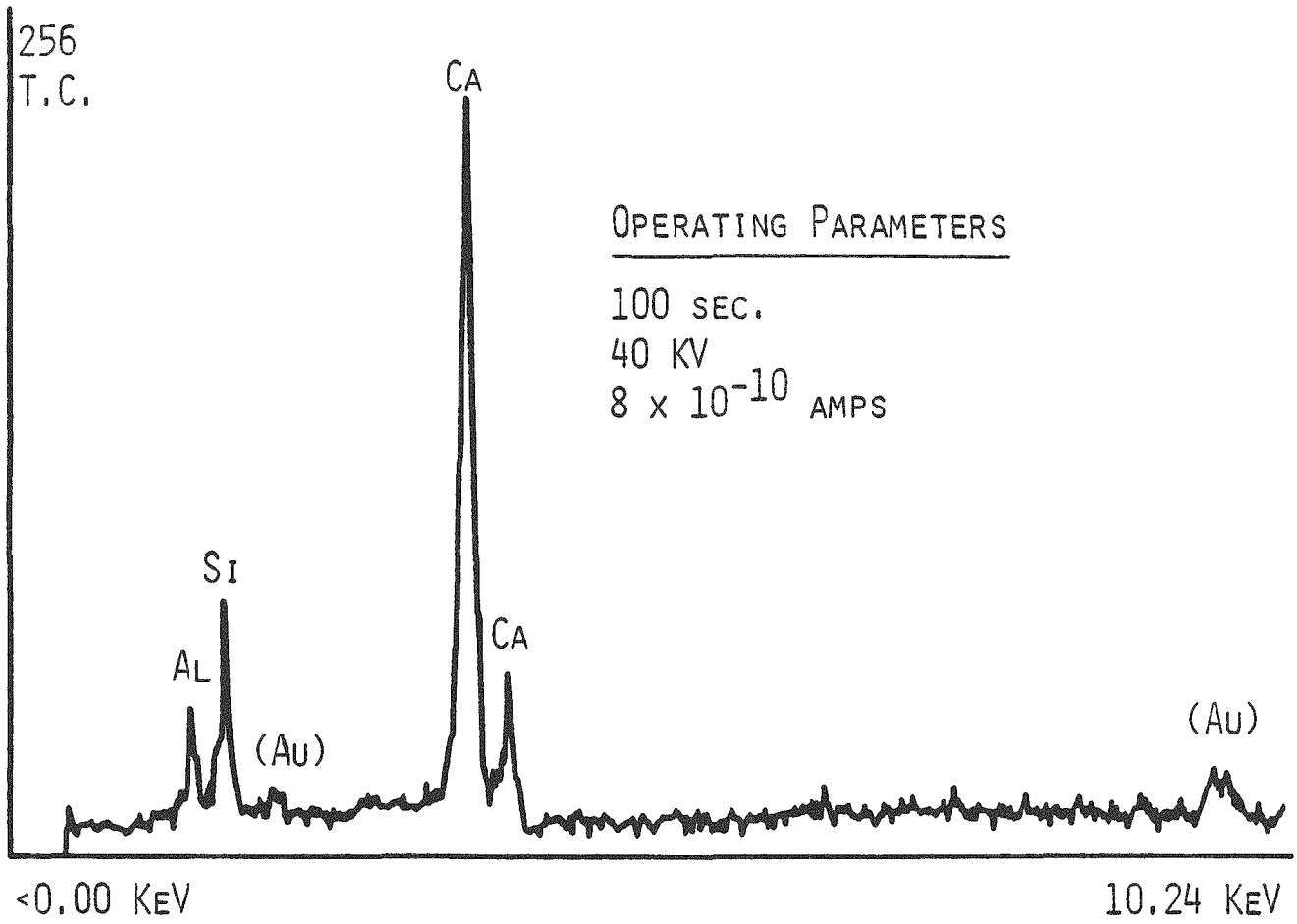

Fig. 2-7. Examples of an energy dispersive x-ray spectrum for the crumpled foil-like phase in CS-2B (layer 1). This analysis was taken from the area labeled A in Figure 2-6(c).

structural layering were not observed, and calcite crystals were found growing normal to the aggregate surface. These crystals were identical to those in the bulk matrix. Fracture of this sample commonly resulted in exposure of the aggregate surfaces, although often small calcite crystals remained attached to the volcanic sand.

2.3.2 Samples from Ostia

Scanning electron photomicrographs of selected samples, OS-13, -27, and -33, collected from ancient structures at Ostia, Italy, are shown in Figs. 2-8 and 2-9. These secondary electron images illustrate microstructures characterized by very fine grained, intergrown matrix phases surrounding fine volcanic ash particles 0.05-1 mm, which were used as pozzolana. The morphologies of the various matrix phases range from small, discrete euhedral crystals, needles, and platelets [Figs. 2-8(b,c) and 2-9(c-f)] to irregular particles often fused into sponge-like or undifferentiated masses [Figs. 2-8(d-f) and 2-9(c-f)]. The crystals and fine-structure particles appear to be intimately intergrown to form a coherent bulk material.

Photomicrographs of OS-13, -27, and -33 illustrate surface features developed on the fine aggregates, volcanic ash, or palagonite embedded in the matrix of these samples [Figs. 2-8(a-f), and 2-9(a,e), respectively]. These secondary electron images clearly show map cracking on the surfaces of the aggregates, which probably resulted from volume changes caused by dehydration shrinkage of an altered, outermost, water-rich layer. In many cases, several stages of fracturing are represented; the older cracks are filled with secondary phases, as illustrated in Fig. 2-9(e). Repeated stages of shrinkage were also inferred from cross-cutting relationships with the more recent fractures intersecting older, healed cracks.

Fractured surfaces were photographed in Figs. 2-8 and 2-9, and it is obvious that the phases formed and structures developed in the interfacial regions between the fine aggregate and matrix fractions account for a small but significant proportion of the volume in these samples. The overall microstructure of the interfacial regions shown in these photomicrographs is complex and characteristically is made up of two parts: a thin film layer which shows shrinkage cracks and is developed directly on the aggregate and a layer of very fine, irregularly shaped particles which appear to be growing from the film layer

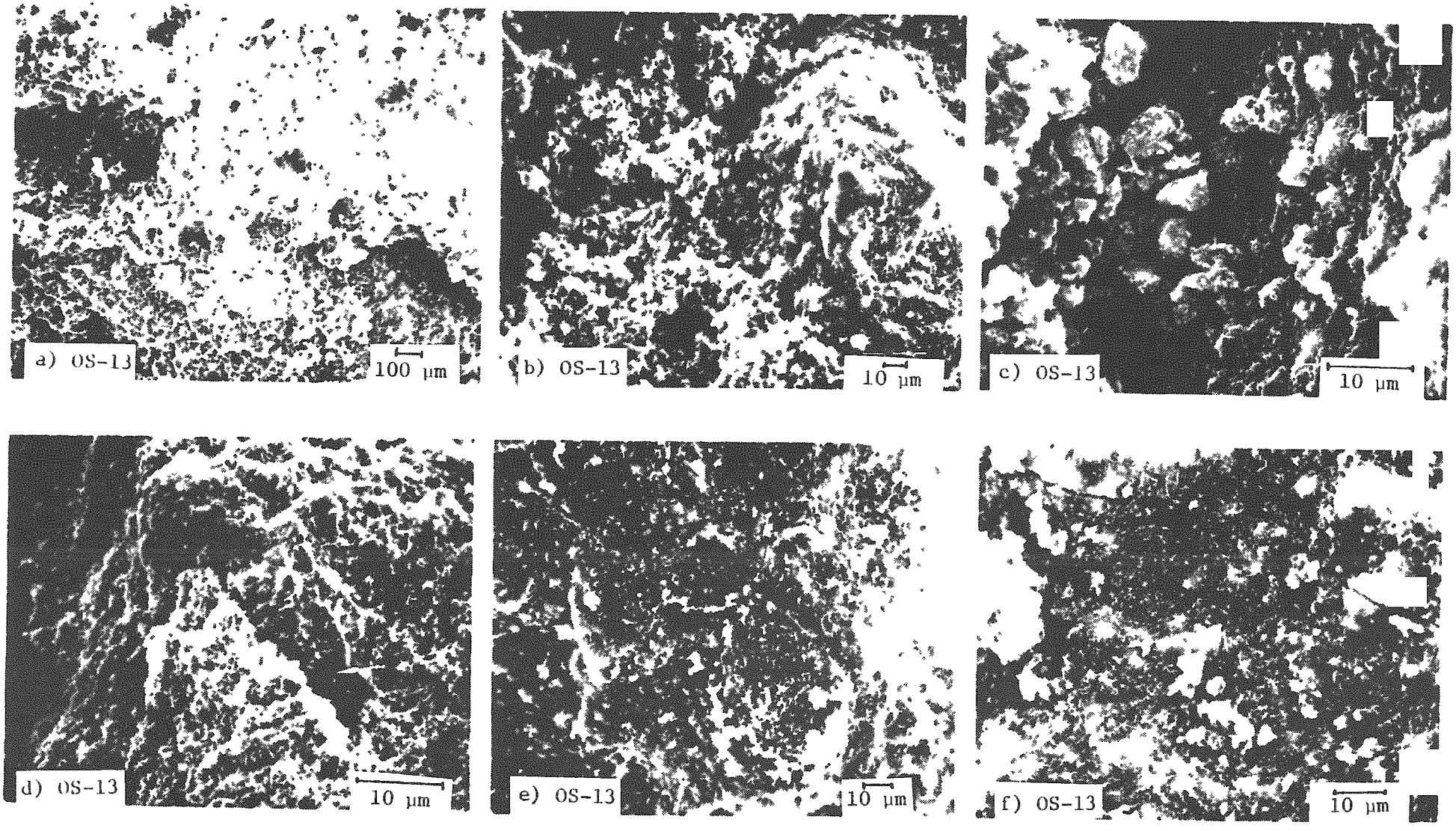

Fig. 2-8. Scanning electron photomicrographs (SEM secondary electron images) of sample OS-13 from Ostia.

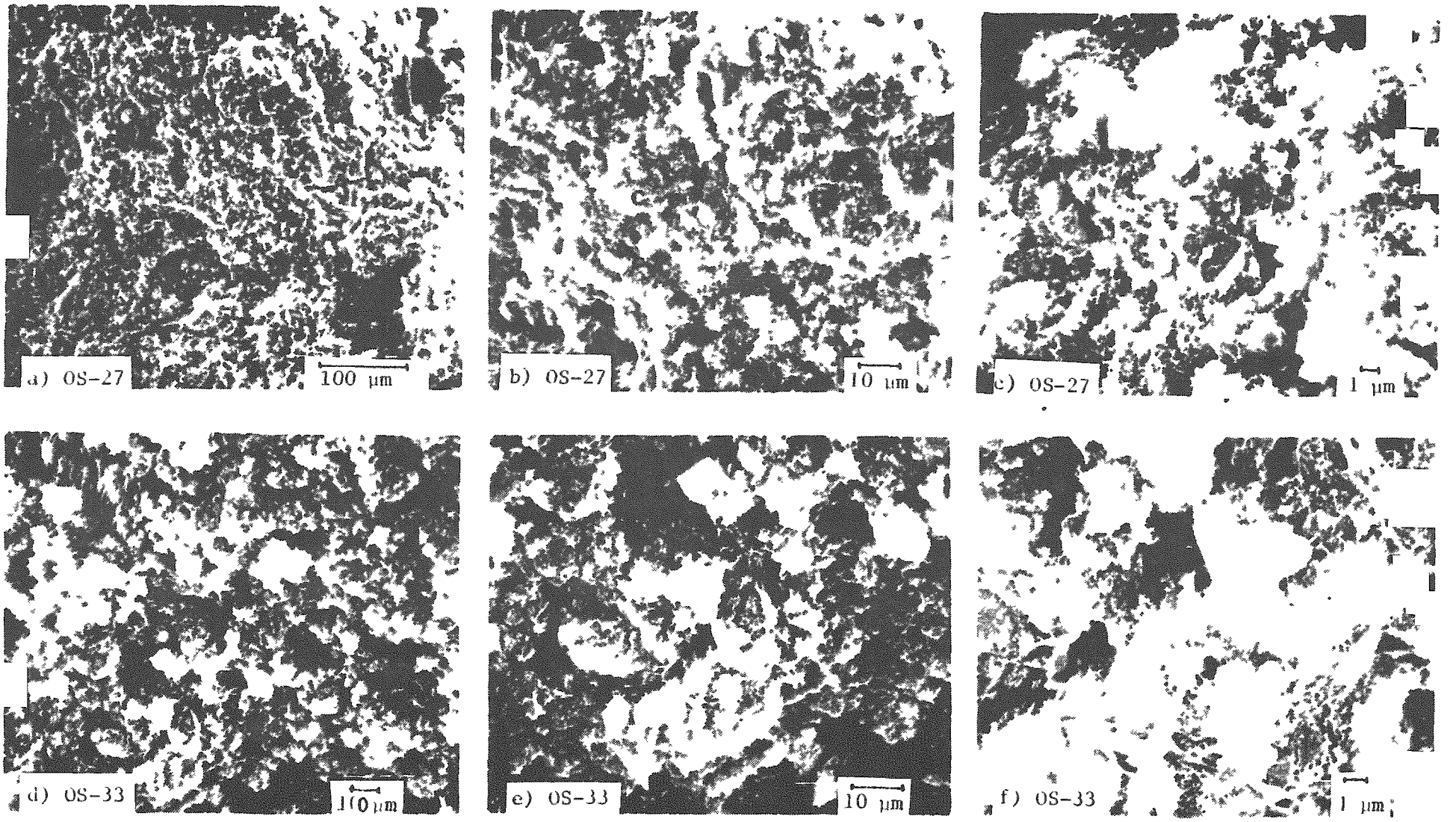

Fig. 2-9. Scanning electron photomicrographs (SEM secondary electron images) of sample OS-27 (a to c) and OS-33 (d to f) from Ostia a), b), and c) are successively higher magnifications, as are d), e), and f).

into the bulk matrix [Figs. 2-8(c,e) and 2-9(f)]. In places, calcite crystals up to 1 μm were observed growing directly from the film layer into the bulk paste. Fracture of the Ostia samples typically took place along these layers of interfacial zone and resulted in exposure of the film layer developed on the aggregate while leaving the very fine particle layer attached to the bulk matrix. This suggests that the interfacial regions in these samples are zones of relative weakness. This property of the Ostia specimens may be related to a characteristic of the type of volcanic ash which was used as pozzolana since this particular fracture pattern appears to be related to the extensive development of the film layer in the interfacial region of these samples.

Energy dispersive compositional data obtained from a variety of crystals, many of which displayed prismatic or rhombohedral crystal faces up to 1 μm in size, indicate that calcium was by far the most abundant cation detected. Therefore, it was concluded that calcite makes up a large proportion of matrix. EDX compositional data for the masses of very fine irregular particles and phases in the interfacial regions indicated the presence of silicon, potassium, and a minor amount of aluminum, in addition to calcium. Examples of EDX spectra for these phases are shown in Fig. 2-10. The spectra A, B, and C correspond to the areas marked in Figs. 2-8(b,f) and 2-9(b), respectively. Although these analyses are qualitative, they suggest that pozzolanic reactions between the slaked lime originally mixed with the volcanic aggregate have taken place and that the very fine particles and film layers contain silicon, potassium, and aluminum released from the volcanic ash in addition to calcium from the portlandite.

2.3.3 Descriptions of Samples from Rome

Scanning electron photomicrographs of selected samples from ancient buildings in Rome, CA-1, CA-2, CR-1 (Fig. 2-11), CF-2, and CO-19 (Fig. 2-12), illustrate a variety of crystal and particle morphologies in the matrix fractions of these materials. The crystals are typically prismatic, pinachoidal or rhombohedral, and can be massive [Figs. 2-11(d,e) and 2-12(f)] or granular [Figs. 2-11(f) and 2-12(b-e)]. EDX compositional data and the morphologies of these crystals support the conclusion that they are calcite (carbonated slaked lime). Masses of very small, irregularly formed particles also constitute a large

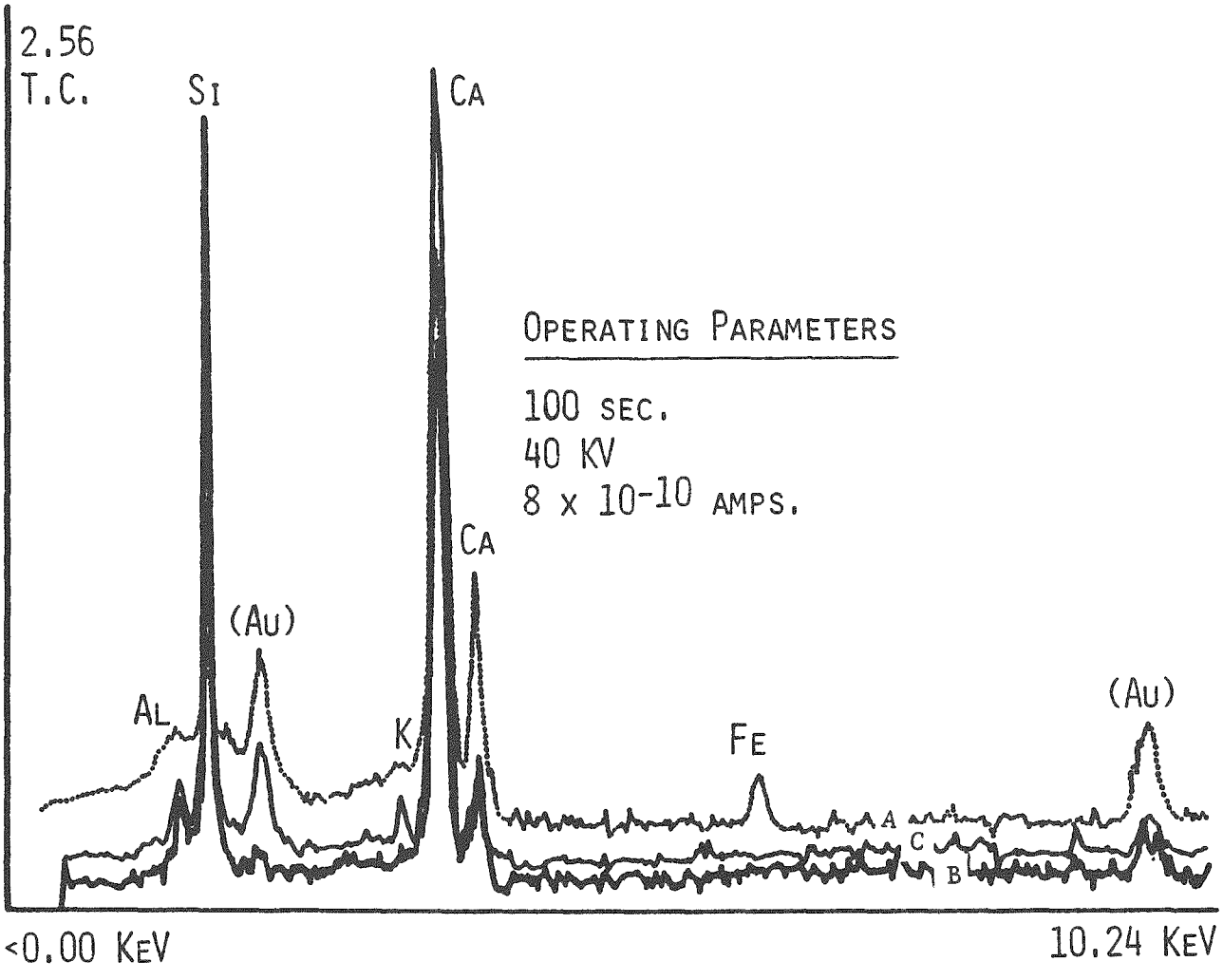

Fig. 2-10. Examples of energy dispersive x-ray spectra for hydrated matrix and interfacial phases in OS-13 and OS-27. Spectrum A was collected from massive fine-grained particles overlying a volcanic ash particle (Figure 2-8b). Spectrum B was collected from the hydrated surface of a volcanic ash particle (Figure 2-8f). Spectrum C was collected from a sponge-like mass of very fine matrix particles (Figure 2-9b).

proportion of the matrix fraction in the various samples collected from Rome [Figs. 2-11(b,c,e) and 2-12(b,c,f)]. These particles occur as dense masses and also in more open, very fine sponge-like masses which are intergrown with calcite crystals. In some areas the fine particles are the most abundant phase; other areas of the same sample are calcite-rich. The overall microstructures of the matrix fractions in these samples range from dense and coherent, for example CA-1 [Fig. 2-11(a-c)] and CA-2 [Fig. 2-11(d,e)], to somewhat less dense, such as that for CR-1 [Fig. 2-11(f)] and CO-19 [Fig. 2-12(d-f)].

These cementitious building materials from Rome contain a large proportion of volcanic ash approximately 0.05 to 1 mm in size. In most samples examined by scanning electron microscope imagery, only vague outlines of the fine aggregate particles were observed [Figs. 2-11(a-c) and 2-12(a,b)]. This is because fracture traces typically transect the bulk matrix instead of intersecting and following the fine aggregate/matrix interfacial regions, as in the case of the Ostia samples. The result is that the aggregates are covered with crystals and fine particles from the bulk matrix. Where the aggregate surface was observed [lower right of Fig. 2-11(b)], the interfacial region appeared to consist of a film layer on the aggregate surface which was attached to the bulk matrix by fine, irregular particles. The film layer when exposed typically shows shrinkage cracks, which are probably the result of dehydration. The complex microstructures of the exposed interfacial regions resemble those previously described for the samples from Ostia.

Energy dispersive x-ray analyses of areas within the matrix fractions of samples CA-1, CA-2, and CF-2, which contain a relatively large amount of the very fine particle phase, are presented in Fig. 2-13. Spectra A, B, and C were obtained from correspondingly labeled areas in Figs. 2-11(c,e) and 2-12(c), respectively. These data indicate that calcium is by far the most abundant cation detected. Analyses A (CA-1) and C (CF-2) indicate the presence of small amounts of silicon, minor potassium, and trace amounts of aluminum and iron (also possibly trace amounts of phosphorous and titanium) in the phases examined. Analysis B, obtained from an area in sample CA-2 which contains somewhat more massive matrix phases [Fig. 2-11(e)], also indicated the presence of silicon, phoshorous, and potassium, but in relatively lesser amounts compared to the fine sponge-like areas in CA-1 and CF-2.

The differences in these analyses of fine-structure particles with different morphologies in samples collected from different sites in Rome are surprisingly small.

2.4 Results of X-Ray Diffraction Analysis

Results of the x-ray diffraction analyses for the matrix fraction (separated from the bulk sample by method A) of the cementitious materials are summarized in Table 2-2. X-ray diffraction data for the aggregate fractions of the Roman samples were particularly important for accurate interpretation of the matrix data. In most cases, these samples contain considerable amounts of fine volcanic ash incorporated in the matrix-fraction which may or may not have been derived from the same rock source as the coarse aggregate. Therefore, Table 2-2 contains selected x-ray diffraction data for many aggregates as well as matrix fractions. Examples of powder diffraction x-ray data obtained as a result of the two separation techniques are also illustrated in Appendix F for OS-33, CF-2, and CS-3.

Mineralogical and phase determinations by x-ray diffraction do not permit detection of phases present in amounts less than 2 to 10 weight percent of the sample. (The exact value depends on x-ray absorption and diffraction characteristic of the particular material.) The mineralogy found agrees generally with that determined petrographically.

2.5 Results of Thermal Analysis

Examples of the results for the matrix fraction of selected specimens are given in Appendix G, Figs. G-1 and F-3, and Table G-1. Tabulated quantitative data obtained from thermogravimetric analysis (TGA) are included in Section 2.6 on chemical analysis. Confirmatory phase determinations are made from these studies, by measuring the temperature at which certain thermal effects take place, such as the decomposition of calcite. The peak areas [from differential thermal analysis (DTA) and TGA weight losses] determine the relative proportions of different phases. There is a significant difference between CS-2, which shows mostly calcite decomposition, and OS-33, FP-18, and FP-12 which also contain major amounts of other material exhibiting dehydration.

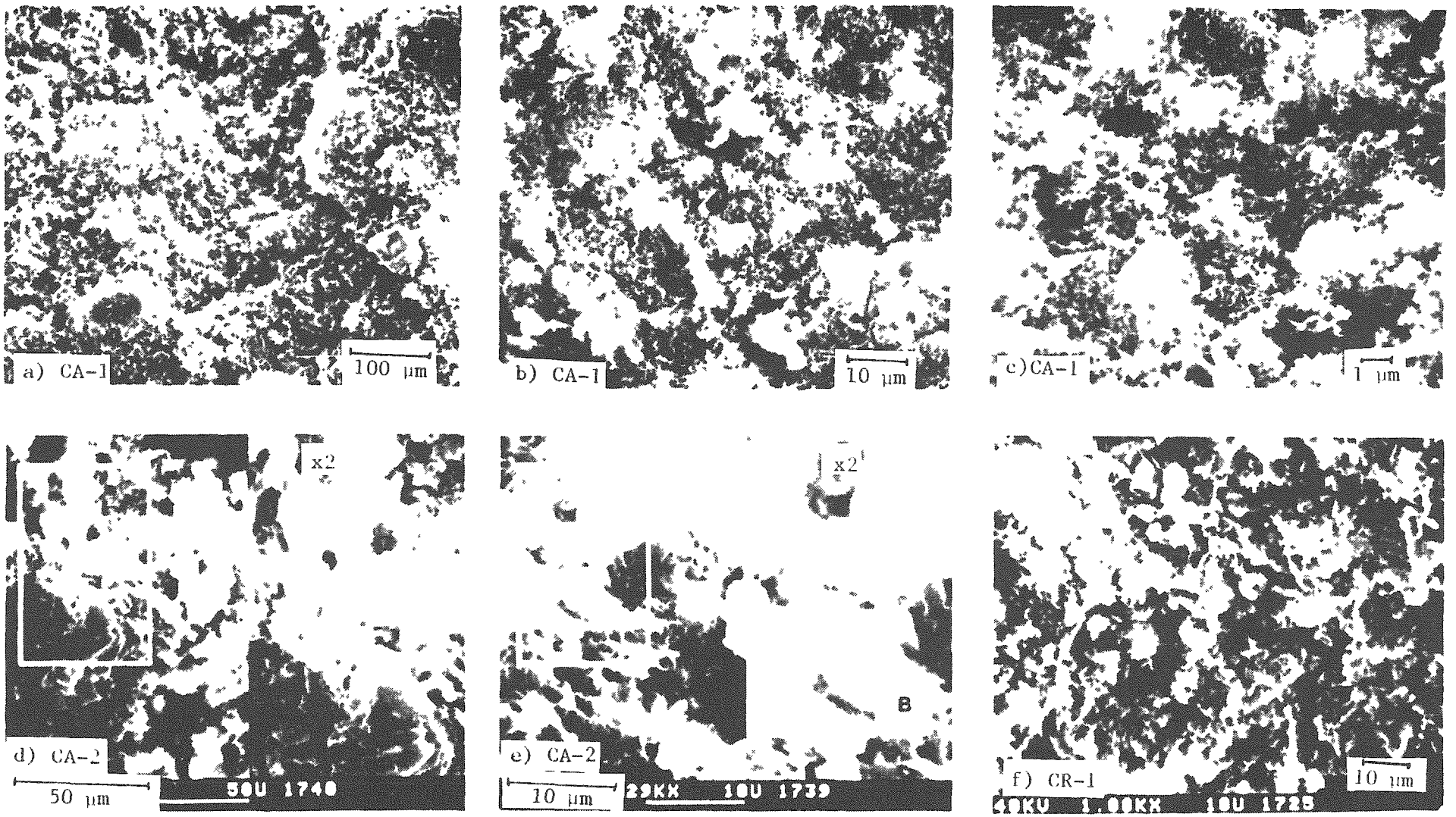

Fig. 2-11. Scanning electron micrographs (SEM secondary electron images) of samples CA-1, CA-2, and CR-1 from Rome. a), b) and c) are successively higher magnifications.

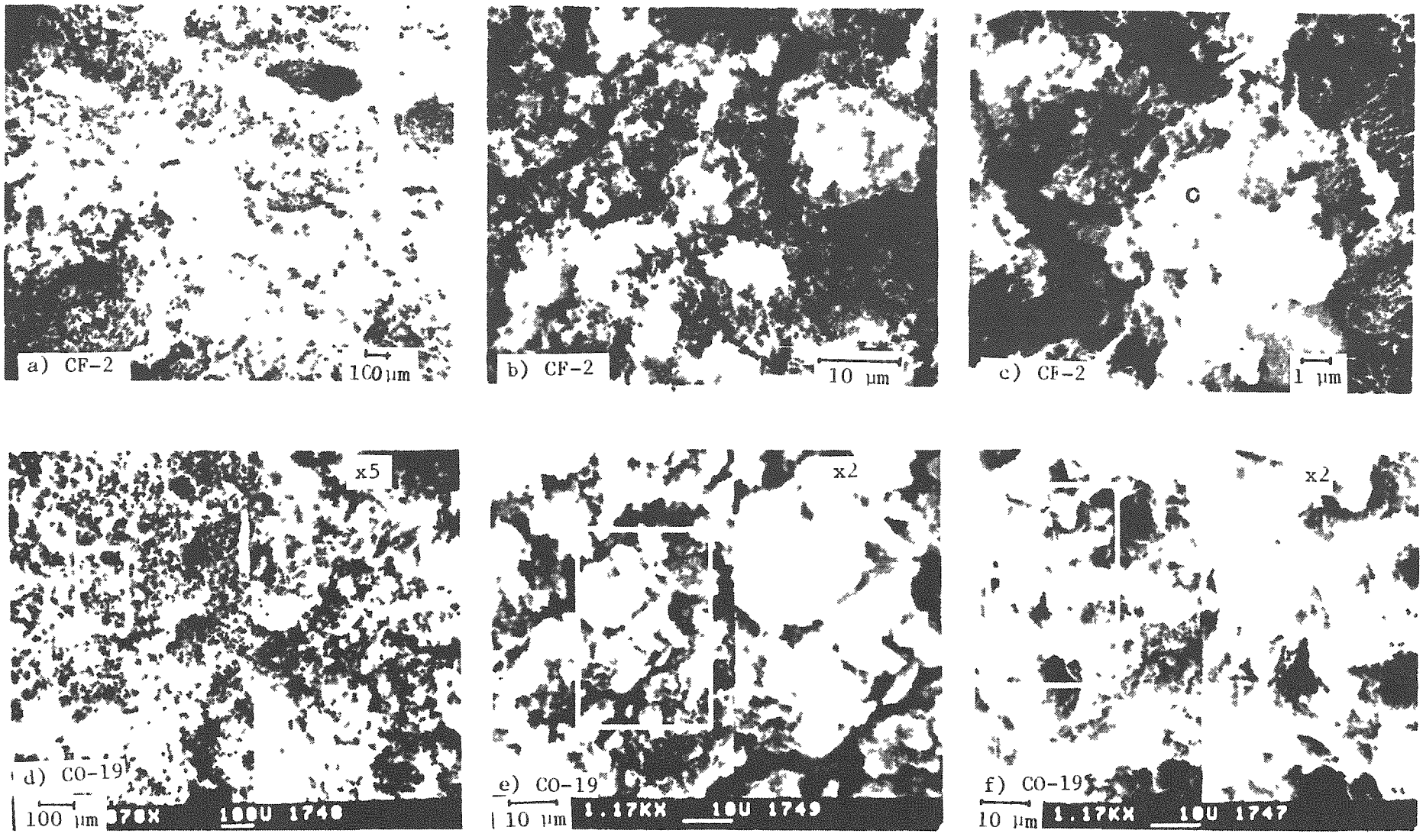

Fig. 2-12. Scanning electron photomicrograph (SEM secondary electron image) of samples CF-2 and CO-19 from Rome.

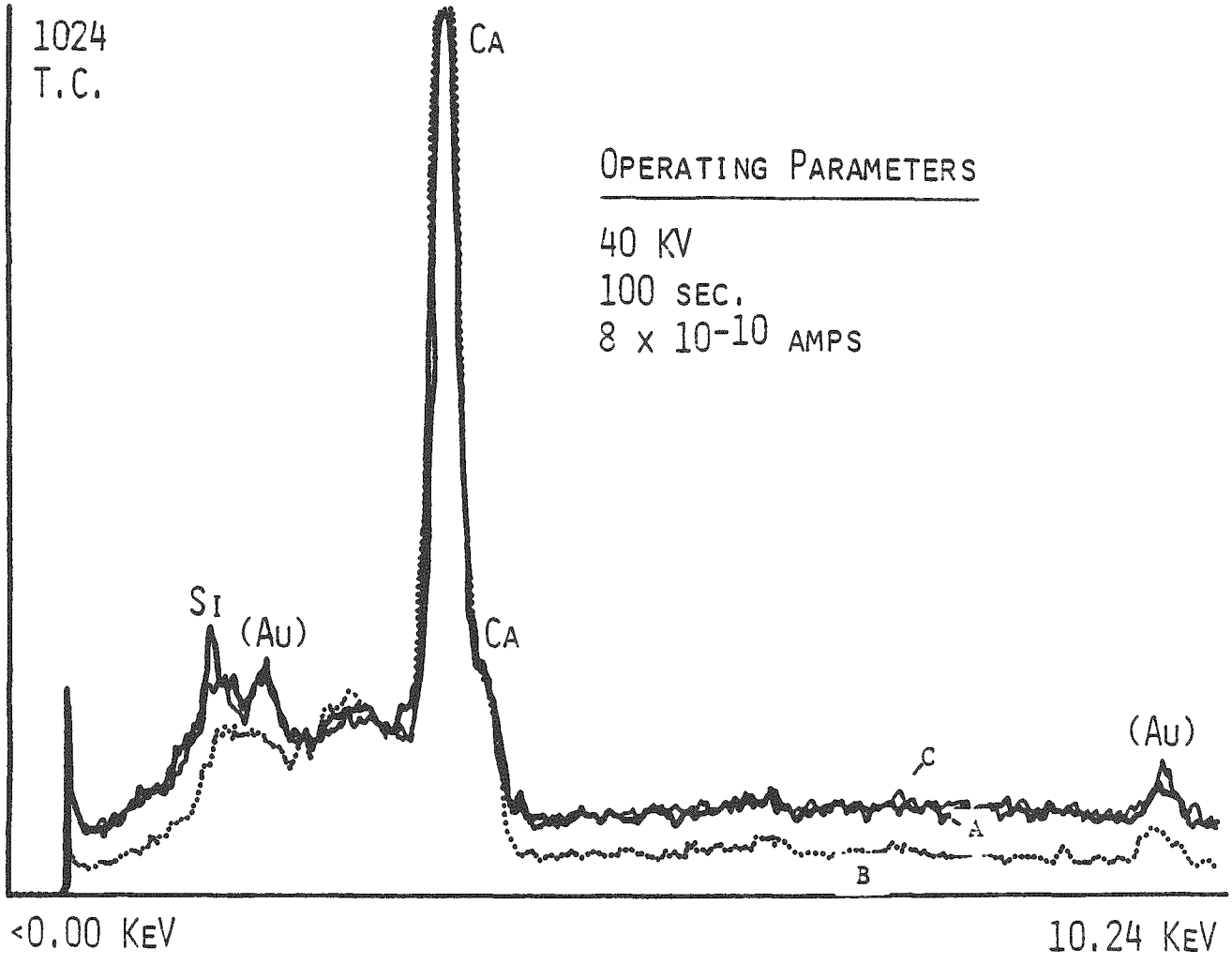

Fig. 2-13. Examples of energy-dispersive x-ray spectra for hydrated matrix phases in sample CA-1, CA-2, and CF-2. Spectrum A corresponds to the labeled area in Figure 2-11(c) (CA-1); spectrum B to labeled area in Figure 2-11(e) (CA-2); and spectrum C to the labeled area in Figure 2-12(c) (CF-2).

TABLE 2-2. X-ray Diffraction Data for the Matrix Fractions and Selected Aggregates from Ancient Plasters, Mortars, and Concretes from Italy.

X-ray Code	Sample No.	Results*†
		COSA
LCCS1MXR	CS1	CA, QU, AM
LCCS1AXR	CS1A (agg. 1)	CA, QU
LCCS2MXR	CS2	CA, QU, m.A
LCCS3MXR	CS3	CA, m.QU
LCCS3AX1	CS3A (agg. 1)	QU, CA
LCCS4MXR	CS4	CA, QU, AU, AM
LCCS4AX1	CS4 (agg. 1)	CA
LCCS4AX2	CS4 (agg. 2)	AM. m.CA
LCCS4AX3	CS4 (agg. 3)	AU, CA, QU
		OSTIA
LCOS1AMXR	OS1A	CA, A, AU, LE, HG, AM
LCOS1AAXR	OS1A(A) (agg. 1)	CA, A, AU, LE, BI, HG, NO, 2AM
LCOS1BMXR	OS1B	CA, A, AU, HG, AM
LCOS1BAXR	OS1B(A) (agg. 1)	CA, A, QU
LCOS2MXR	OS2	CA, vm.A
LCOS2AXR	OS2A (agg. 1)	CA, vm.A
LCOS13MXR	OS13	CA, m.AU, m.A. vm.LE, vm.HG
LCOS13AXR	OS13A (agg. 1)	CA, A, AU, LE, HG, AM
LCOS18MXR	OS18	CA, AU, LE, HG, PH
LCOS18AXR	OS18A (agg. 1)	QU, CA, AU, PH, LE, AM
LCOS27MXR	OS27	CA, AU, AP, HG, LE, QU, AM
LCOS27AX1	OS27A (agg. 1)	CA, AU, LE, HG

TABLE 2-2. (continued)

X-ray Code	Sample No.	Results*
LCOS33MXR	OS33	CA, A, AU, QU, AM
LCOS33AXR	OS33A (agg. 1)	CA, A, AU, QU, AM
		ROME
LCCA1MXR	CA1	CA, LE, AU, AP
LCCA1AX1	CA1A (agg. 1)	AU, LE, A, AP, QU, CA, HG
LCCA1AX2	CA1B (agg. 2)	AU, CA, LE, A, AP, NO
LCCA2MXR	CA2	CA, AU, GY, A, LE, AP, HG, AM
LCCF2MXR	CF2	CA, AU, A, AM
LCCF2AXR	CF2A (agg. 1)	CA, AU, A, LE, BI, AM
LCCF4MXR	CF4	CA, A, AF, QU, AP, AU, LE, GY, 2AM
LCCO19MXR	CO19	CA, A, LE, AU, QU, AM
LCCO19AXR	CO19A (agg. 1)	CA, A, LE, AU
LCCR9MXR	CR9	CA, AU, A, LE, QU, AM
LCCR9AXR	CR9A (agg. 1)	CA, AU, A, QU, LE
LCFP11AMX	FP11A	CA, A, AU, HG, GY, AM
LCFP12MXR	FP12	CA, AU, A, GY, m.HG, AM
LCFP12MXR	FP12	CA, AU, A, GY, m.HG, AM
LCFP12AXR	FP12A (agg. 1)	CA, AU, AF, BI, A, GY, AM
LCFP18MXR	FP18	CA, A, HG, AU, AM
LCT1MXR	T1	CA, A, AU, GY, 2AM
LCT1AXR	T1A (agg. 1)	BI, A, AU, CA, m.GY?

TABLE 2-2. (continued)

*Abbreviations used have the following meanings: AF = alkali feldspar; A = analcime; AM = amorphous material; AP = apatite; AU = augite; BI = biotite; CA = calcite; GY = gypsum; HG = hydrogarnet; LE = leucite; NO = nosean; PH = phillipsite; QU = quartz; m. = minor amount; vm. = very minor amount.

+Phases are listed in order of decreasing amount. Many matrix materials designated with "AM" contain glassy-type broad amorphous peak at ~29°2θ characteristic of amorphous calcium silicate hydrate (C-S-H).

2.6 Results of Chemical Analysis

2.6.1 Quantitative Analysis

Chemical analyses for the matrix fractions of the lime- and calcium silicate-based cementitious materials are presented in Table 2-3. The materials range from relatively high calcium (and CO_2) (51% CaO) to relatively high silica (34% SiO_2) content.

2.6.2 SEM Qualitative Analysis

Examples of qualitative chemical analyses (EDX) of the -1-μm matrix fractions which were ultrasonically separated from selected ancient composites are presented in Figs. 2-14 and 2-15. The -1-μm material is essentially x-ray amorphous as discussed in Section 2.4 and was obtained from those specimens containing hydraulic hydrated lime or pozzolana/hydrated lime matrices. The qualitative analyses presented in Figs. 2-14 and 2-15 (bottom) are from those areas shown in Figs. 2-14 and 2-15 (top), respectively. Although the morphologies of the -1-μm particles in each sample appear uniform, the compositions of the particles may be variable. Therefore the EDX spectrum for each sample is the average analysis of the area shown. The spectrum in Fig. 2-15 is typical of a silica-rich C-S-H gel.

2.6.3 Electron Microprobe Analysis

Three samples (CF-4C, T-1, and OS-1A), illustrating pozzolana/matrix reaction rims, were selected for study using microprobe techniques. Compositions for the fine volcanic aggregates, the matrix fractions, and the associated interfacial regions were obtained from selected regions of polished thin sections. Typical analyses of scans across opposite sides of the same fine aggregate in sample CF-4C are presented in Table 2-4. These data illustrate a compositional gradation between a pozzolana fine aggregate and the bulk matrix. That is, the aggregate is relatively richer in silica and poorer in calcium than the matrix, and the interfacial region typically displays values intermediate between the aggregate and surrounding matrix phases. Data in Table 2-4 also illustrate the variability observed in microprobe analyses of these samples. Averaging techniques were not utilized because of the problems associated with obtaining reasonable oxide totals (Roy and Langton, 1982).

TABLE 2-3. Quantitative Chemical Analyses for Selected Ancient Building Materials from Italy.

	COSA				OSTIA			ROME						
	CS-1	CS-2A	CS-3	CS-4	OS-18	OS-33	FP-MHN	CA-1	CA-2	CF-2	CR-9	FP-11A	FP-12	FP-18
SiO_2,%	15.3	20.8	3.60	12.5	37.8	30.5	31.4	33.4	25.1	34.6	25.4	35.1	31.4	34.0
Al_2O_3	1.50	3.82	0.98	2.70	15.8	11.8	10.15	11.5	9.16	11.25	9.02	15.8	10.45	12.3
TiO_2	0.083	0.196	0.042	0.51	0.533	0.407	0.496	0.605	0.450	0.555	0.428	0.541	0.499	0.525
Fe_2O_3	0.80	1.74	0.42	5.68	5.45	3.98	5.25	6.45	4.63	5.80	4.67	5.6	6.30	4.90
CaO	41.5	37.2	51.3	41.5	11.4	22.5	22.8	27.8	24.5	17.3	25.7	17.0	19.3	14.3
MgO	2.87	1.69	1.82	1.93	2.77	1.75	2.63	3.35	2.27	2.52	2.01	2.05	3.25	2.43
MnO	0.029	0.031	0.011	0.098	0.137	0.103	0.132	0.124	0.0905	0.141	0.102	0.127	0.113	0.081
Na_2O	0.22	0.21	0.06	0.222	1.81	1.96	1.59	1.24	0.775	2.09	1.38	2.93	0.73	1.965
K_2O	0.31	0.71	0.10	0.51	4.40	1.12	1.725	2.11	2.00	1.94	1.21	1.14	2.28	2.14
Ba,ppm	260	190	80	170	2530	990	1270	2230	1310	1460	2430	3010	1620	930
Cr	<5	5	<5	65	<5	<5	<5	<5	<5	<5	<5	5	<5	<5
Cu	45	10	<5	315	85	5	145	65	85	120	100	10	65	95
Ni	<5	<5	<5	<5	<5	<5	65	5	<5	<5	<5	<5	<5	<5
Sr	175	255	290			865	993	1095	1310	867	1135	1250	922	875
V	<5	10	<5	125	175	120	145	145	105	150	110	10	145	110
Zr	10	55	<5	195	325	210	235	285	240	240	125	55	50	270
SO_3	0.30	0.21	0.15	0.59	0.17	0.64	0.28	0.17	6.02	0.48	2.04	0.21	3.35	0.29
CO_2	30.73	26.0	39.7	30.0	7.49	12.24	11.0	7.49	9.34	8.64	11.38	6.38	7.97	8.96
$H_2O_{110°C}$	∿0	∿0	∿0	∿0	∿0	6.68	5.78	---	4.56	8.76	6.25	5.39	8.30	6.98
H_2O_{total}	5.48	8.60	3.03	5.99	13.85	12.24	13.81	6.59	14.80	14.48	14.45	12.1	16.31	17.40

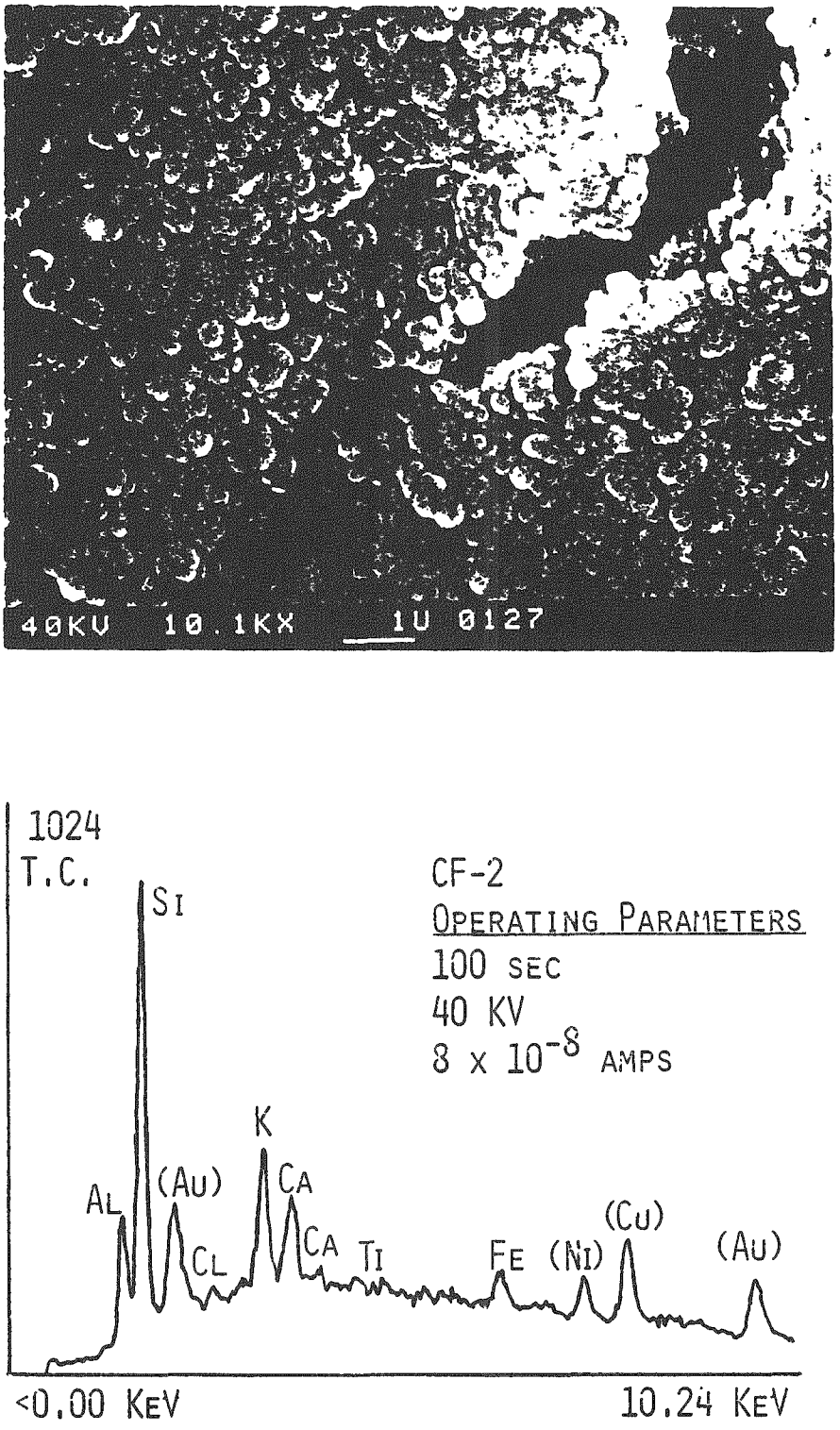

Fig. 2-14. EDX analyses of the -1-μm matrix fraction ultrasonically separated from sample CF-2, Rome.

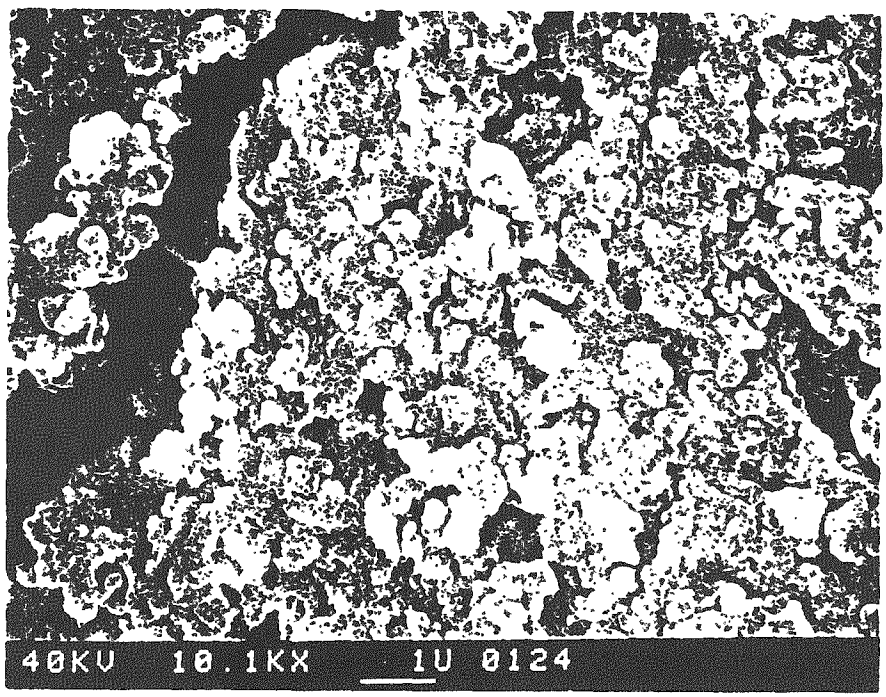

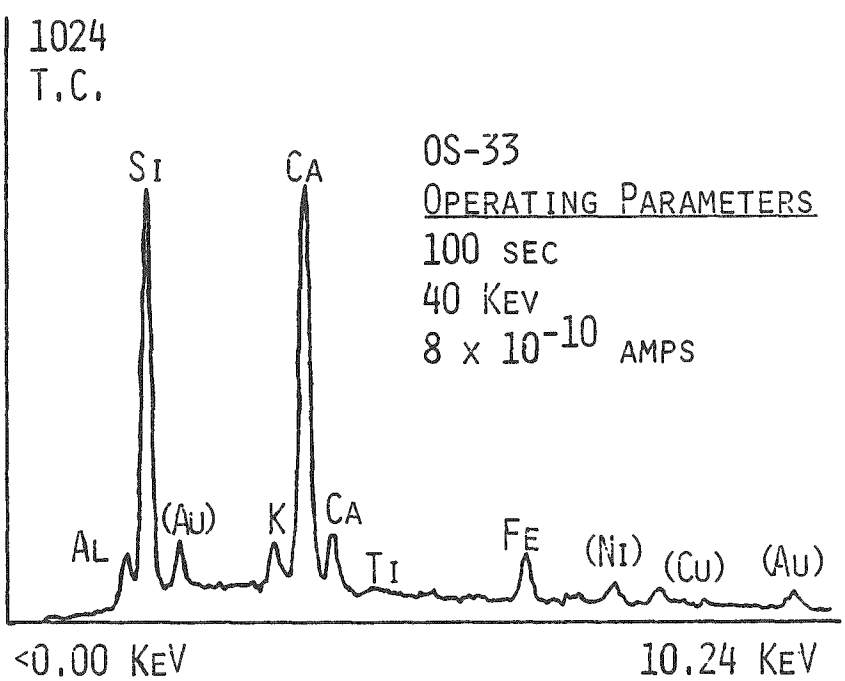

Fig. 2-15. EDX analyses of the -1-μm matrix fraction ultrasonically separated from specimen OS-33, Ostia.

TABLE 2-4
CHEMICAL DATA OBTAINED BY MICROPROBE ANALYSES
OF SAMPLE CF-4c FROM ROME

	(Weight percent)			(Weight percent)		
oxide	pozzolana aggregate 1	interfacial region 1	matrix 1	pozzolana aggregate 2	interfacial region 2	matrix 2
SiO_2	53.22	26.93	21.91	70.95	28.63	27.31
Al_2O_3	1.57	6.23	3.68	12.12	6.32	4.31
Fe_2O_3	18.63	1.51	x	3.02	1.53	1.22
CaO	6.56	9.75	29.03	5.39	9.26	23.81
MgO	13.58	0.44	0.49	0.33	0.39	0.42
Na_20	—	0.40	0.49	1.20	0.84	0.30
K_2O	0.71	2.15	0.82	2.58	2.21	0.94

2.6.4 TMS Results

Four peaks were distinguished in the gas-liquid chromatograms of trimethylsilyl derivatives of the matrix fractions of the ancient cementitious materials. Two of these were identified as monomer, SiO_4^{4-}, and dimer, $Si_2O_7^{6-}$, derivatives. The other two were attributed to the trimethylsilyl-esters of $Si_3O_{10}^{8-}$ and $Si_4O_{12}^{8-}$. The derivatives of larger silicate ions were not identified due to ineffective separation by the gas-liquid chromatographic technique. Additional peaks which were observed may be due to side reactions or branching effects of the various derivatives, although mass spectrometry analyses were not performed. Data for selected samples are plotted in Appendix H, Fig. H-1, as a function of relative amount of derivative versus elution time. In addition to the ancient building material samples, two reference materials were also analyzed. These materials were an alkali-silica gel from Denmark and a fragment of volcanic ash (pozzolana ash) from Rome. These data are shown in Fig. H-2. Note the large amount of monomeric silicate species present in the alkali-silica gel in contrast to the others.

The silylation products of two samples, OS-19 and CO-33, were investigated by gel permeation chromatography (GPC) (Sarkar and Roy, 1979), which determines the distribution of higher polymeric species beyond those detected by gas chromatography

(GC). Figure H-3 gives the spectra obtained and Table 2-5 summarizes the results in terms of weight percent monomer, dimer, and polysilicate, plus the average number of silicon ions in the polymeric silicate. These are compared with a specimen ADL-1 from another study of lime-rich cements (having no polysilicate species) for reference. The results from OS-33 show a larger percentage of polysilicate in comparison with CO-19. Both these cements show similarities to modern C-S-H binding species in hydrated portland cement (Sarkar and Roy, 1979; Glasser et al., 1981), although the percentage of silicate dimer is low and the total TMS-derivative soluble material is low, indicating that much of the binding phase is probably insoluble high silica content polymer.

TABLE 2-5
SUMMARY OF GPC RESULTS OF TMS DERIVATIONS OF ANCIENT ROMAN CEMENTS

No.	Weight of Sample (Mg)	Weight of Monomer (Mg) (SiO_2)	Weight of Dimer (Mg) (SiO_2)	Weight of Polysilicate total (Mg)	Weight of Polysilicate as SiO_2 (Mg)	
ADL-1*	381.8	2.60	0.12	0	0	
OS-33	517.5	6.70	0.22	31.5	11.2	
CO-19	110.2	4.30	0	11.0	0	
	%C	%H	$\bar{N}_n$	$\bar{N}_w$	$\bar{N}_n^+$	$\bar{N}_w^+$
OS-33	28.7	7.1	1480	3027	8.7	17.8
CO-19	—	—	2324	7488	—	—

* Lime-rich cement specimen from a Roman aqueduct in Greece.
$\bar{N}_n$ = no. ave. molecular wt.
$\bar{N}_w$ = wt. ave. molecular wt.
$\bar{N}_n^+$ = no. ave. silicons in silicate skeleton.
$\bar{N}_w^+$ = wt. ave. silicons in silicate skeleton.

3. Discussion

3.1 Types of Ancient Cementitious Building Materials

3.1.1 Hydrated Lime-Based Mortars and Plasters

Lime plasters and mortars were manufactured by calcining relatively pure calcite in the form of limestone, chalk, marble, or caliche at temperatures above approximately 800°C to produce lime. Combination of crushed lime and water results in crystallization of portlandite, $Ca(OH)_2$, which initially forms the binding phase in these materials. As discussed by Roy and Langton (1982), portlandite readily carbonates on exposure to air and most fresh groundwaters and hence, after some time, calcite becomes the binding phase.

The poor workability and nonhydraulic character of pure hydrated lime cements limited widespread use of these materials in ancient structures. However, one such type of material, opus signinum, which is a mixture of lime and fine terra-cotta fragments, was used extensively enough throughout the Roman empire for Vitruvius to describe its manufacture (Vitruvius, translated by Morgan, 1960).

Sample CS-3 from Cosa may be considered an example of opus signinum, although the terra-cotta in this specimen is not finely ground. (Coarse, angular terra-cotta fragments, greater than 1 cm, make up approximately 50 percent of sample CS-3.) Sample FP-7, thought to be opus signinum from hand specimen examination, contained instead a reddish volcanic ash. In general, hydrated lime-based materials had limited applications as plasters. The following ancient specimens examined in this study were classified as hydrated lime-based: CS-1, CS-2A, and CS-3 from Cosa, and OS-2 layer 2 (0.15 cm thick) from Ostia.

3.1.2 Hydraulic* Hydrated Lime-Based and Hydraulic Hydrated Lime-based/Soil Plasters and Mortars

* Hydraulic cements are cements that set and harden by chemical interaction with water and that are capable of doing so under water.

Primarily due to the limited number of outcrops of pure (99%) calcium carbonate formations, the use of pure hydrated lime-based plasters and mortars in ancient structures was relatively rare. Also, the construction applications of pure hydrated lime-based materials were somewhat limited. However, siliceous and/or argillaceous carbonate rocks, containing two to ten percent amorphous or crystalline silica and/or clay, respectively, are common throughout the Mediterranean region (Roy and Langton, 1982). When calcined at temperatures above about 850°C, silica in these rocks can react with lime to form dicalcium silicate, whereas the alumina in clays of various compositions can react with lime to form calcium aluminate and/or calcium aluminoferrite phases. Therefore, it is reasonable to expect that many of these cementitious materials initially may have contained reactive hydraulic calcium silicate, calcium aluminate, and aluminoferrite compounds, even in minor quantity. Hydration of the above calcined reaction products results in crystallization of portlandite plus formation of hydrated calcium silicate phases (poorly crystallized or amorphous, for example C-S-H) and hydrated calcium aluminate and ferrite phases. These latter phases crystallize in the presence of excess water, are relatively insoluble in water, and may even harden under water, hence the term hydraulic cements. Upon exposure to air or bicarbonate-containing groundwater, portlandite and the hydroxylated calcium aluminate and ferrite phases carbonate to form calcite and carbonated calcium aluminate and ferrites, respectively. With time, the calcium silicate hydrates may also carbonate to varying degrees, depending on the P_{CO_2}.

Samples CS-2 and possibly CS-4 were classified in this category. However, because pozzolanas were so abundant in the Rome and Ostia regions, only a few of the cementitious matrix materials collected from Rome and Ostia fit in this class. Most were in the third category described in the next section.

3.1.3 Pozzolana/Hydrated Lime-Based Plasters, Mortars, and Concretes

Although the use of pozzolana-hydrated lime cements has been reported in the Mediterranean Region Greek island areas, in structures of the fourth to fifth century BC (Efstathiadis, 1978), good pozzolanic raw materials were geographically limited. The matrix fractions in the samples collected from Italy (except those specified elsewhere as hydrated lime-based materials or rocks) contained relatively large proportions of very fine,

volcanic ash particles, pozzolana, in addition to hydrated lime. The lime component was prepared from carbonate rocks as described in Sections 3.1.1 and 3.1.2. Pure or impure carbonate rocks may have been used. Outcrops of volcanic ash are abundant near Rome and Ostia and are typical silica undersaturated pyroclastic ashes. These two ingredients were combined in the presence of water [in some instances the lime was initially slaked (Vitruvius, translated by Morgan, 1960)] to form a hydraulic cement. Chemical reactions between the lime, excess water, and volcanic ash particles produced very fine grained reaction products which were capable of setting under water (that is, they are relatively insoluble in water) in addition to portlandite. Subsequent carbonation of the portlandite and other hydrated phases resulted in a binding material composed of calcite plus very fine grained hydrated phases (partly C-S-H). Coarse and fine (sand size) aggregate fractions totaling 85 or more volume percent of the bulk sample were also added as extenders to make mortars or concrete.

3.1.4 Other Materials

A few rocks were mistaken for concretes and plasters. These include the samples CS-4, initially thought to be a concrete bound by carbonated lime.

3.1.5 Gypsum Plasters and Mortars

Although used widely in the Mediterranean regions, no representations of this class of materials were among the specimens collected; most of the Roman plasters as well as stuccos were lime and lime-pozzolana/sand materials (Blake, 1947).

3.2 Textures of the Bulk Samples, Microstructures and Particle Morphologies of the Matrix Fractions, and Matrix/Aggregate Interfacial Regions

3.2.1 Application of Techniques

Hand specimen, hand lens/binocular microscope, petrographic microscope, and scanning electron microscope and microprobe techniques were used to describe the textures, microstructures, and phase morphologies of the ancient cementitious materials analyzed in this study. Hand specimen analyses of fractured and sawed surfaces proved most useful in evaluating the relative proportions, grading, and sorting of the coarse and fine aggregate fractions in addition to the relative homogeneity of the bulk specimen. These macroscopic

techniques were useful to assess the gross sample similarities, which resulted in the ability to identify samples from the same geographic regions and in some cases even from the same excavation site or structure.

The maximum magnification of the petrographic microscope used in this study, approximately 1000X, proved too low for detailed analyses of the morphologies of the matrix phase. However, microtextures and in some instances matrix/fine aggregate reaction features were easily observed in thin sections. Characterization of the fine and coarse aggregate fractions was also best accomplished by petrographic techniques.

Characterization of the very fine grained matrix fractions in these ancient materials required utilization of various scanning electron microscopy techniques. Magnifications up to and greater than 20,000X permitted description of the morphologies of the matrix phases and of the microstructures in the bulk matrices and in the matrix/aggregate interfacial regions. Both fractured- and polished-surface samples were examined by electron microscope analyses which utilized secondary electron and backscattered imagery.

3.2.2 Hydrated Lime Plasters and Mortars

In hand specimen analyses, these ancient materials were usually white, reflecting the purity of the lime used, and were characterized by tension fractures caused by shrinkage resulting from an approximately 11 percent solid-volume decrease associated with the reaction of $Ca(OH)_2 + CO_2 \rightarrow CaCO_3 + H_2O$ (Lea, 1970). As a result of this reaction, the binding phase was, with time, converted from portlandite to calcite. Most of the hydrated lime-based samples examined in this study were plasters and contained less than 10 percent aggregate by volume. An exception to this is sample CS-3, which contains coarse terra-cotta fragments.

The microstructures of the calcite matrices examined were crystalline, uniform, and very fine grained. They were characterized by randomly oriented rhombohedra and elongated crystals ranging from about 0.5 to 2 μm in size. Variations in the microtexture were usually attributed to features inherited from coarsely crushed or poorly calcined raw materials. Where matrix/aggregate interfacial regions were observed, calcite crystals appeared to be growing directly from the aggregate substrates. Neither compositional nor structural zoning or layering was observed in these interfacial regions.

3.2.3 Pozzolana/Hydrated Lime (Hydraulic Lime)-Based Plasters, Mortars, and Concretes

Hand specimens of these materials are typically multimodal and contain up to and greater than 75 percent by volume coarse aggregates. The fine aggregate fractions in these materials often account for up to 75 percent of the remaining volume (bulk volume minus coarse aggregate fraction). In the hand specimens, coarse and fine aggregate fractions were composed of alkali-rich silica, undersaturated volcanic rock, and ash fragments (trachytic tuffs). In addition, these materials contained pozzolana, that is, very fine, reactive volcanic ash, less than 0.5 μm in size. The color of the pozzolana and fine aggregate fractions ranged from pink to red, to brown or gray and imparted a pale to moderate color to the matrix fractions in these samples. Tension fractures were not obvious features in these pozzolana-containing building materials, probably because of the lower amount of calcite formation. A qualitative degree of coherency appears also to be a function of the coarse and fine aggregate proportioning and grading. Chunks of coarsely crushed, or poorly calcined hydrated (and subsequently carbonated), lime are ubiquitous features throughout the matrices of these composite materials.

The microstructures of these pozzolana/hydrated lime matrices are very complex and are characterized by small, up to 2-μm, well-developed calcite crystals intergrown with abundant fine-structure particles up to 0.1 μm. The calcite crystals are generally randomly oriented and have morphologies similar to those previously described in Sections 3.2.1 and 3.2.2. The fine-structure particles display irregular morphologies resembling platelets, needles, and foils and typically are intergrown to form porous sponge-like masses or massive features. In thin sections, the matrices in these materials are very mottled in both color and texture.

Fracture of certain pozzolana/hydrated lime-containing materials resulted in exposure of matrix/very fine aggregate interfacial regions. This was especially true for the samples examined from Ostia. These matrix/very fine aggregate interfacial regions were complex and characterized by a film layer overlying the aggregate surfaces from which a layer of very fine particles appeared to be growing into the coarser grained bulk matrix. This type of interfacial zoning was also observed in the samples collected from Rome.

However, fracture of the latter materials less often resulted in exposure of the interfacial regions. Dehydration cracks in the interfacial film layers were very common features in the samples collected from Ostia, which suggests that this film may consist of a swelling gel. Complex interfacial layering and zoning were less commonly observed at matrix/coarse aggregate contacts.

3.3 Chemistry of the Matrix Fraction

As discussed in the previous sections, the mechanically separated matrix fractions are dominated by calcite in a number of cases. The extent to which this is true is shown from the calculations summarized in Table 3-1. Assuming that all CO_2 in the analyses is reacted to form calcite, the residual CaO (ΔCaO) is shown, which may be contained in other phases. No correction is made for magnesium carbonate or dolomite component, which would increase the ΔCaO.

The presence of significant amounts of cementing phases other than calcite is reflected by the presence of other major constituents, silica and alumina in particular, especially in those materials in which this is also accompanied by substantial (~10-20 percent) remaining CaO after accounting for calcite formation. The CaO remainder indicates potential for the presence of a calcium silicate (or aluminate/aluminosilicate) cementitious phase.

Another method of data treatment reveals the significant groupings in a different manner. Compositions of the mechanically separated matrix fractions are shown in Fig. 3-1 as a plot of sums of the weight percentages of CaO + MgO vs Al_2O_3 + Fe_2O_3, which were determined for the matrix fraction of selected cementitious materials collected for this study. These parameters were chosen for comparison purposes in order to minimize the effects of aggregate contamination and alteration or weathering. The composition of the matrix fraction obtained by light crushing and sieving was plotted because particle morphology studies have shown that most of the matrix phases are in the <45-μm to ~1-μm size range. Other major and minor constituents such as SiO_2, Na_2O, and K_2O are particularly sensitive to aggregate (quartz sand, igneous rock fragments, and unreacted pozzolana) contamination. Only a fraction of the total oxide components is represented in this type of graph, and there are a number of limitations with respect to interpreting

TABLE 3-1. Calculation of Residual CaO (ΔCaO) After Consumption by CO_2 to Form $CaCO_3$.*

Cosa	CO_2	ΔCaO
CS-1	30.73	2.34
CS-2A	26.0	4.07
CS-3	39.7	0.71
CS-4	30.0	3.27

Ostia	CO_2	ΔCaO
OS-18	7.49	1.86
OS-33	12.24	6.90
OS-7-MHN	11.0	8.78

Rome	CO_2	ΔCaO
CA-1	7.49	18.26
CA-2	9.34	12.60
CF-2	8.64	6.29
CR-9	11.38	11.20
FP-11A	6.38	8.87
FP-12	7.97	9.14
FP-18	8.96	2.88

*Using data from Table 2-3; assumption that all CO_2 is reacted with CaO to form calcite. ΔCaO gives remainder to form other cementitious phase: (C-S-H) or silicates in fine mineral powder.

these plots. For example, it is not possible to distinguish a pure lime (portlandite) cement from a hydraulic lime (portlandite plus hydrated calcium silicates) cement which may have been prepared from siliceous limestones low in clay, on the basis of $(CaO + MgO)/(Al_2O_3 + Fe_2O_3)$ ratios since SiO_2 is not represented. Likewise, it is not possible to distinguish cements prepared from argillaceous limestones (natural cement stones in which case a single material was calcined) from portland cements (prepared from a two-component raw material mix) with the same composition.

Compositional data presented in Fig. 3-1 have been grouped into four categories which are consistent with cement terminology: hydrated lime and hydraulic (siliceous) hydrated lime cements; hydraulic (aluminous and/or ferruginous) hydrated lime cements with and without siliceous components; volcanic ash (pozzolana)/hydrated lime cements; and for completeness, gypsum cements not found in the present materials. The boundaries of the four categories are only approximate and probably overlap to varying degrees. As information is obtained on a larger number of samples from future studies, the boundaries of these categories are expected to become better defined.

Figure 3-1 shows that the matrix fractions in hydrated lime cements and hydraulic hydrated lime cements in which hydration of calcium silicate phases is responsible for the hydraulic properties may contain up to 4 weight percent $(Al_2O_3 + Fe_2O_3)$ (in addition to hydraulic siliceous components). They were represented primarily by the materials from Cosa. Five specimen compositions plotted in the figure were materials collected and previously studied from ancient structures in Greece and Cyprus (Roy and Langton, 1983). The matrices of these materials are generally rich in CaO, Al_2O_3, and Fe_2O_3, containing up to 12 weight percent $Al_2O_3 + Fe_2O_3$. The pozzolana-containing cementitious materials from Rome and Ostia contained greater than 12 weight percent $(Al_2O_3 + Fe_2O_3)$ and relatively low amounts of $(CaO + MgO)$. Their compositions appear much more compatible with the general chemistry of tuff.

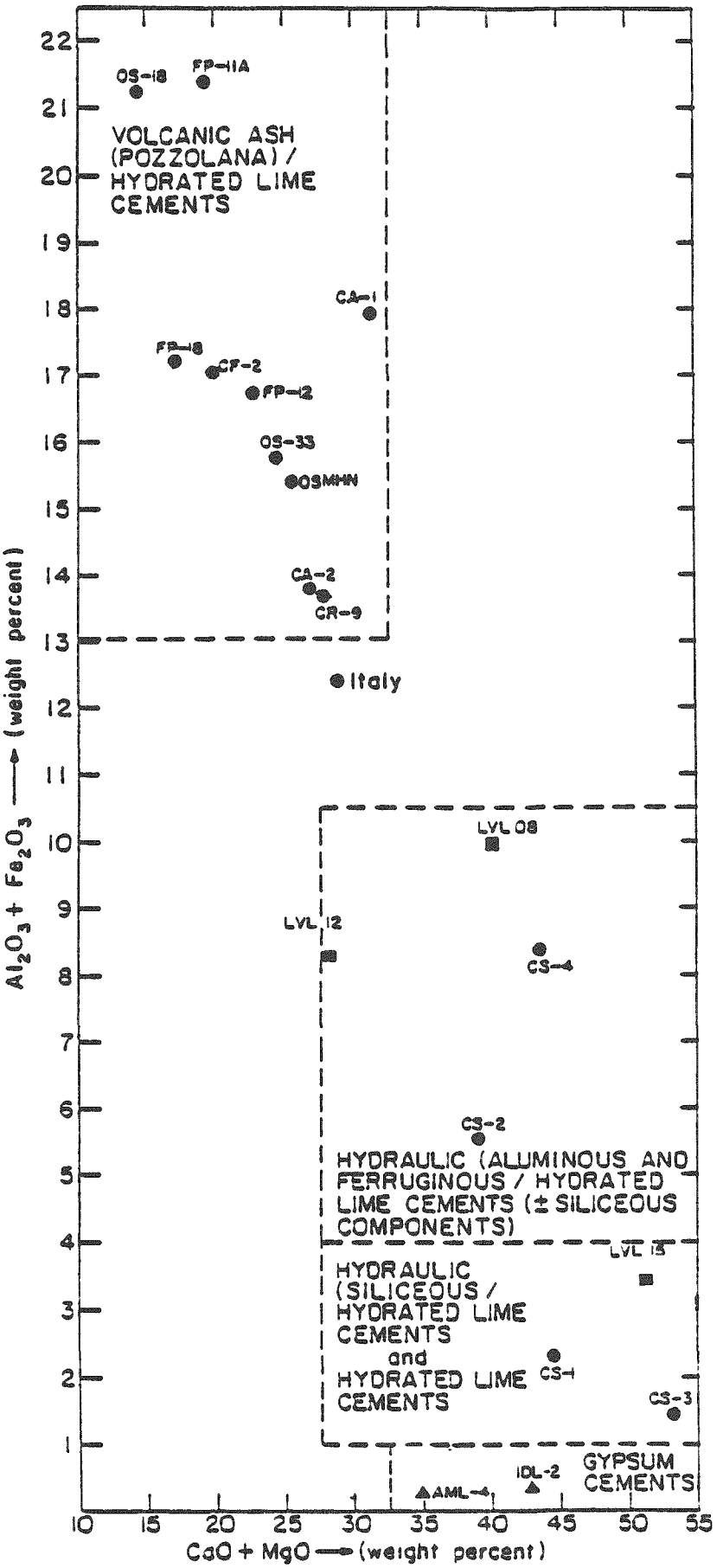

Fig. 3-1. Classification of cement types. Circles represent current materials from Italy; squares and triangles from Greece and Cyprus, respectively (Roy and Langton, 1983).

3.4 Phase Identification and Phase Relations of the Matrix Fractions

The pozzolana-hydrated lime cements which form the binding phases in most of the materials described here are composed of calcite (carbonated portlandite), poorly crystallized analcime, and x-ray amorphous alkali-rich calcium silicate phases which may also contain iron and aluminum as determined by EDX analyses. This material was referred to as fine-structure particles in the morphology and microstructure studies and includes matrix/aggregate reaction products. Minor amounts of hydrogarnet (tentatively identified) and possibly C-S-H gel (diffuse d-spacings at 3.04, 2.80, and 1.80Å) were also identified in x-ray patterns of some of the -1-μm matrix fractions extracted from these specimens. It was not possible to determine if the analcime is the result of alteration of pozzolana (volcanic ash) or rock fragments (pumice) which may have been included in the matrix separation, or if it is formed by partial crystallization of sodium-substituted CASH gel material. SEM morphologic analyses were not conclusive.

Additional information on the fine fraction subcrystalline matrix materials was obtained in trimethylsilylation experiments. These pozzolana/hydrated lime building materials contained silicate monomer, dimer, and differing amounts of pentasilicate and polymer condensates containing possibly up to eight silicons per unit. These species are similar to those in modern portland cement hydration products. Crystalline calcium silicates, such as tobermorite, xonotlite, and hillebrandite, were not detected in x-ray diffraction patterns or thin sections of any of the pozzolana/hydrated lime-containing composite specimens.

4. Summary and Conclusions

4.1 Summary

Mortars, plasters, and concretes resembling modern counterparts have been discovered in the remains of many ancient structures. Many have maintained mechanical integrity and could function in their intended capacity today. The present study has characterized recently collected concretes, mortars, and plasters up to 2200 years old from sites in Italy dating back to Early Republican age (about third century BC); some from Late Republican age (200-50 BC); many from Early Imperial (50 BC-50 AD); and from High Empire

(50-250 AD) ages. Despite centuries of use and exposure to adverse environmental conditions, which include atmospheric carbon dioxide, dissolved species in soil waters, and warm climatic conditions, such materials have endured, sometimes better than the stone or brick found in the same structures.

The results of the current studies of ancient materials, when integrated with information from prior work, provide insight into the long-term durability of cement-containing materials, complementary to that gained from other sources such as thermodynamic (Sarkar et al., 1982) and experimental (Scheetz and Roy, 1985) investigations. Such data provide the only direct long-term information on the response of various man-derived cementitious materials to the environments to which they were exposed.

A number of specific findings are summarized below:

1. The cementitious matrices of the materials investigated here and previously have been classified into four categories based upon chemical composition expressed in terms of (CaO + MgO) versus (Al_2O_3 + Fe_2O_3), supplemented by knowledge of the carbonate and sulfate contents. The categories are: (a) hydraulic (siliceous) hydrated lime cements and hydrated lime cements; (b) hydraulic aluminous and ferruginous/hydrated lime cements (±siliceous components); (c) volcanic ash (pozzolana)/hydrated lime cements; and (d) gypsum cements.

2. All of the ancient building materials collected from Italy contain pozzolana/hydrated lime cements except CS-1, CS-2A, and CS-3 from Cosa and OS-2 and OS-27 from Ostia. The latter specimens originally were composed of hydrated lime matrices which have subsequently carbonated. OS-27 contains coarse angular terra-cotta fragments but was not considered to be a true example of opus signinum, which is reported to be composed of finely crushed reactive terra cotta plus slaked lime.

3. Hydrated ("pure") lime cements had limited use in ancient mortars and plasters, where they originally contained randomly oriented portlandite crystals. Cementitious reactions in these materials may be represented as follows: $CaO + H_2O = Ca(OH)_2$; $Ca(OH)_2 + CO_2 = CaCO_3$. In contrast, hydraulic hydrated lime cements were extensively used in ancient multimodal mortars and plasters. The cementitious reactions in the latter materials probably took place as follows: (1) $CaO + {}'C_2S' \pm {}'C_3A \pm C_4AF' + H_2O \rightarrow Ca(OH)_2$

+ partially formed C-S-H* gel ± CAH ± CAFSH$^{\neq}$. (2) $Ca(OH)_2$ + partially hydrated phases + H_2O + CO_2 → $CaCO_3$ + C-S-H($\bar{C}$) ± CA(C)H ± CAF(C)H.*

4. Pozzolana/hydrated lime cements were extensively used in ancient Roman concrete construction. These cements contain intergrown crystals of calcite, 1 to 5 μm in size, and fine-structured particles >0.1 μm in size in addition to a very fine, partially reacted pozzolana aggregate component (10-500 μm). The fine-structure particles are amorphous, contain some polymerized silicate, display irregular morphologies, and generally have alkali-rich calcium silicate compositions. They also contain Al, Fe, and Mg. Additional crystalline phases such as analcime and, possibly, hydrogarnet were detected in the -1-μm disaggregated size fractions but may be the result of aggregate contamination. Well-developed, two-layer chemical and structural zoning was ubiquitous in the pozzolana/hydrated lime-containing specimens. Cementitious reactions in these composite materials are as follows:

CaO + volcanic ash + H_2O →

$Ca(OH)_2$ + KNCAFSH gel + additional hydrated crystalline phases

Hydrated phases + CO_2 →

$CaCO_3$ + KNCAFSH($\bar{C}$) ± hydrated crystalline phases

These reactions represent hydration and carbonation of the original mixes. If the lime used was hydraulic, then a 'C_2S' reaction as in 3. above may also take place.

5. For comparison, hydrated modern portland cements contain the following phases in the approximate proportions:

$Ca(OH)_2$ <15-20%

CAFH <10% (crystalline, calcium aluminoferrite hydrate)

---

* Cement abbreviations: Oxide formulas: C = CaO, S = SiO_2, A = Al_2O_3, F = Fe_2O_3, $\bar{C}$ = CO_2, H = H_2O, K = K_2O, M = MgO, N = Na_2O, $\bar{S}$ = SO_3. C-S-H refers to poorly crystalline nonstoichiometric hydrous calcium silicate. $^{\neq}$CAFSH, etc., similarly refer to nonstoichiometric C-A-F-S-H.

C-S-H <70% (nearly amorphous calcium silicate hydrates), differing somewhat from the mineralogy observed in ancient hydraulic hydrated lime cements and pozzolana/ hydrated lime cements.

6. As a result of increasing time and, depending on the degree of exposure to air, precipitation and ground water, modern portland cements undergo the following chemical and structural changes: $Ca(OH)_2$ and CAFH phases partially carbonate to form calcite and CAFH$\bar{C}$, and the nearly amorphous C-S-H polymerizes to form higher order condensates. The C-S-H incorporates some alumina in its structure, which may affect its polymerization. Extended aging of the ancient cementitious materials examined in this study has also resulted in carbonation of $Ca(OH)_2$ to form calcite [because of conventional practices, much of the $Ca(OH)_2$ in porous materials was probably carbonated relatively quickly; where exposed to carbonate-containing ground waters, denser materials would proceed to carbonate slowly in the direction defined by limits of phase stabilities (Sarkar et al., 1982)]. Limited evidence shows that there is increased polymerization of the C-S-H (actually KNCAFMSH) structure over that in modern concrete, though the total content of such C-S-H is small. The presence of less strong network formers such as Al and Fe balanced by the network modifiers K and Na (in the KNCAFMSH amorphous component) may be responsible for the limited size of polymeric structural units formed, or for the breakdown of initially formed polymers into smaller units. Current data, however, suggest that sorption properties resulting from the presence of Al in C-S-H or in the crystalline calcium silicate hydrate, tobermorite (Komarneni and Roy, 1983), produce certain advantages.

7. The extent of interaction of matrix with aggregate in the plasters, mortars, and concretes observed was variable depending upon the specific matrix and the mineralogy and microtexture of the specific aggregate. Hydraulic hydrated lime mortars often showed little matrix/aggregate interfacial reaction. However, in some cases a complex reaction was observed resulting in a two-layer interfacial region consisting of a film overlying the aggregate, which in turn was attached to the bulk paste by a layer of fine particles growing from the film. The pozzolana/hydrated lime cements showed extensive development of such

two-layer interfacial regions. In these respects they resemble microstructures in modern concretes (Langton and Roy, 1980).

8. Mechanical compaction, when a plaster is worked or compressed, appears to have been used in some instances in these materials to achieve low water/"cement" ratio materials. Although no direct evidence was found for the presence or use of organic materials as "admixtures" to increase workability in these particular materials as is commonly done in modern concrete technology, the proper sizing of materials and the extent of mechanical methods used appeared to achieve a similar effect. [Others have given evidence for use of organics in other ancient and more recent materials. Idorn (1959) has cited evidence for use of air entraining admixtures in concrete at Provence; Miao Ji-Sheng et al. (1981) for use of rice gluten, tung oil, and animal blood in ancient China; and Malinowski (1979) for use of quick lime-oil expanding mixtures in Jerusalem.]

4.2 Conclusions

These investigations have provided detailed knowledge of the chemical, mineralogical, microstructural, and macroscopic characteristics of some collections of durable ancient concretes, mortars, and plasters. Long-term durability of ancient cementitious materials, as compared to modern portland cement-containing counterparts, is a function of matrix mineralogy, particle size, and porosity and the aggregate type, grading, and proportioning.

Hydrated lime-binding materials generally were not very versatile or strong [exceptions are those in which low porosities (very low equivalent water/"cement" ratios) were achieved probably by compaction]. Eventually these types of cements were largely superseded in their use by the chemically different hydraulic hydrated lime-based materials and by lime-pozzolanic cements, the latter in Italy. The latter two categories are also generally more workable than gypsum or hydrated lime cements. Because of the multiphase content, they tend to have wider particle size distributions, allowing higher density of packing and permitting lower water/cement ratios. Mechanical means of densification, indeed almost "polishing," appear to have been used for placing layered plasters to line aqueducts, ore-washing basins, and other water-bearing structures (Vitruvius, 1960 translation). As

described by Malinowski (1979), the polished compacted surface helped to assure the impermeability of such structures. Similar plasters were investigated in the present study. In modern concrete materials, chemical admixtures are often used to achieve the same effects more efficiently.

Many of the ancient cementitious materials possess very fine, dense microstructures. This results from the intergrowth of the minute calcite crystals, formed by carbonating slaked lime, with somewhat lesser amounts of the finer particulate complex (partly carbonated) of amorphous and partially crystalline aluminoferrite and silicate hydrates that surrounds intermixed coarser fractions, unreacted volcanic ash, and mineral and rock fragments. In pozzolanic cements, which are capable of setting under water and frequently have higher strengths than the nonpozzolanic materials, the lime and alkalis continue to react with a silica-rich pozzolan to produce a complex hydrated material. Such fine microstructures generally give rise to greater strength, and the products are likely to have low permeability.

The sand and larger size fraction aggregates of these mortars, concretes, and plasters consist of many types of sedimentary and igneous rocks, as well as crushed terra cotta. Some coarser materials showed excellent grading of coarse to fine fractions, which appeared to be responsible in part for their mechanical stability.

These ancient cementitious materials have been shown to be remarkably durable, and the fact that not more remain is related to deliberate demolition, rebuilding by successive rulers, and willful destruction and vandalism (Lanciani, 1967; Frank, 1924). Those that survive attest to their long-term durability. The durability shown by these 2000-year-old cementitious materials is significant. In some cases, the cementitious mortar was more durable than the stone it "cemented."

The exposure of the cementitious materials to surface and near-surface conditions in a warm, relatively dry climate resembles the prospective exposure conditions for candidate borehole and shaft sealing materials for near-surface application in a nuclear waste repository as currently conceptualized for the NNWSI Project (Fernandez and Freshley, 1984). The durability of the cementitious materials is of further significance, since both their overall chemical composition and the fact that they incorporate volcanic ash and crushed tuff

as aggregate produce a strong resemblance to candidate NNWSI Project sealing materials and the host rock environment conditions for seals in a tuff repository. Evidence from the detailed investigation of these analog materials suggests that modern sealing materials compositionally and microstructurally similar to the ancient pozzolanic cementitious materials are likely to adjust slowly to a near-surface tuff repository environment. The results, furthermore, provide a base for comparison with data generated in future related sealing material property investigations, for such areas as thermodynamic properties and experimental durability studies.

Acknowledgements

We would like to express appreciation for the encouragement of the late T. A. Wertime, Smithsonian Associate, and Joan Mishara, Conservation Scientist, the Smithsonian Institution. Special thanks are also given for the aid of Professor F. E. Brown, of the American Academy in Rome, for obtaining specimens from Cosa. Appreciation is also expressed to Drs. Rosemary Vidale and Clarence Duffy, Los Alamos contract managers during the course of the study. R. Prave, L. D. Wakeley, and D. Wolfe-Confer assisted in some technical tasks.

References

Blake, Marion E. (Completing work begun by E.D. Van Beman), *Ancient Roman Construction in Italy from the Prehistoric Period to Augustus*. Carnegie Institution of Washington, Washington, DC, Publ. #570 (1947).

Brown, F.E., *Cosa I (History and Topography)*, Memoirs of the American Academy in Rome **20** (American Academy in Rome, Rome, Italy, 1951).

Calza, Guido, and Giovanni Becatti, *Ostia*, 9th Edition (updated by Maria Forieni Squarciapino; orig. 1927) (Istituto Poligrafico della Stato, Rome, Italy, 1974).

Courtault, B., "Couplage Microthermogravimetrie - Spectrometrie de Masse Analyses," Analysis **7** (11), 481-488 (1979).

Efstathiadis, Efstathios, *Greek Concrete of the Three Milleniums* (Research Center of the Hellenic Ministry of Public Works, Athens, Greece, 1978).

Fernandez, J.A.,and M.D. Freshley, "Repository Sealing Concepts for the Nevada Nuclear Waste Storage Investigations Project," Sandia National Laboratories report SAND83-1778 (June 1984).

Frank, Tenney, "Roman Buildings of the Republic. An Attempt to Date Them from Their Materials," Papers and Monographs of the American Academy in Rome, Vol. 3 (American Academy in Rome, Park Ave., New York, 1924).

Glasser, L.S. Dent, E.E. Lachowski, M.Y. Quereshi, H.P. Calhoun, D.J. Embue, W.D. Jameson, and C.R. Masson, "Identification of Some of the Polysilicate Components of Trimethylsilylated Cement Paste," Cem. Concr. Res. **11**, 775-780 (1981).

Idorn, G.M., "Mikroskopiske Glimt af Betonteknikkens Historie" [History of Concrete Technology-Through a Microscope]. Beton-Teknik 4, 119-141 (1959).

Komarneni, S., and D.M. Roy, "Tobermorites: A New Family of Cation Exchangers," Science **221**, 647-648 (1983).

Lanciani, Rodolfo, *Ancient Rome in the Light of Recent Discoveries* (Revised 1967, orig. 1888) (Benjamin Blom, New York, 1967).

Langton, C.A., and D.M. Roy, "Morphology and Microstructure of Cement Paste/Rock Interfacial Regions," in Proc., 7th International Congress on the Chemistry of Cement, Vol. III, Communications, Septima, Paris (1980), pp. VII-127 - VII-133.

Langton, C.A., and D.M. Roy, "Longevity of Borehole and Shaft Sealing Materials: Characterization of Ancient Cement-Based Building Materials," in Scientific Basis for Nuclear Waste Management, G. McVay, Ed. (International Atomic Energy Agency, Vienna, 1984), pp. 543-549.

Lea, F.M. *Chemistry of Cement and Concrete* (Arnold, London, 1970).

Lugli, Guiseppe, *The Roman Forum and the Palatine* (Bardis Editore, Rome, Italy, 1970.)

Mackenzie, R.C., *Differential Thermal Analyses*, Vol. 1 (Academic Press, New York, New York, 1970).

Malinowski, R., "Concrete and Mortars in Ancient Aqueducts," Concr. Internat., 66-76 (1979).

Meiggs, R., *Roman Ostia*, 2nd Ed. (Clarendon Press, Oxford, 1973).

Miao, Ji-Sheng, Xiu-Ying Li, Rong-Kiu Cheng, and Bao-Shan Lu, "A Preliminary Investigation of Cementing Materials Used in Ancient China," Res. Inst. Build. Mat. Wuhan **9** (2), 234-240 (June 1981.)

Ramachandran, V.S., *Applications of Differential Thermal Analysis in Cement Chemistry* (Chemical Publishing Co., New York, New York, 1969).

Roy, D.M., and C.A. Langton, "Longevity of Borehole and Shaft Sealing Materials: 2. Characterization of Cement-Based Ancient Building Materials," report ONWI-202, prepared by the Materials Research Laboratory, The Pennsylvania State University, for the Office of Nuclear Waste Isolation, Battelle Memorial Institute, Columbus, Ohio (1982).

Roy, D.M. and C.A. Langton, "Characterization of Cement-Based Ancient Building Materials in Support of Repository Seal Materials Studies," report BMI/ONWI-523, prepared by the Materials Research Laboratory, The Pennsylvania State University, for the Office of Nuclear Waste Isolation, Battelle Memorial Institute, Columbus, Ohio (1983).

Roy, D.M., M.W. Grutzeck, and P.H. Licastro, "Evaluation of Cement Borehole Plug Longevity," report ONWI-30, prepared by the Materials Research Laboratory, The Pennsylvania State University, for the Office of Nuclear Waste Isolation, Battelle Memorial Institute, Columbus, Ohio (1979).

Sarkar, A.K., M.W. Barnes, and D.M. Roy, "Longevity of Borehole and Shaft Sealing Materials: I. Thermodynamic Properties of Cement and Related Phases Applied to Repository Sealing," report ONWI-201, prepared by the Materials Research Laboratory, The Pennsylvania State University, for the Office of Nuclear Waste Isolation, Battelle Memorial Institute, Columbus, Ohio (1982).

Sarkar, A.K., and D.M. Roy, "A New Characterization Technique for Trimethylsilylated Products of Old Cement Pastes," Cem. Concr. Res. **9**, 343-352 (1979).

Scheetz, B.E., and D.M. Roy, "Performance Evaluation and Characterization of a Cementitious Seal Material for Application in the Topopah Spring Tuff at the Nevada Test Site," in Scientific Basis for Nuclear Waste Management, Vol. 8, C.M. Jantzen, J.A. Stone, and R.C. Ewing, Eds. (International Atomic Energy Agency, Vienna, 1985), pp. 935-942.

Tamas, F.D., A.K. Sarkar, and D.M. Roy, "Effect of Variables Upon the Silylation Products of Hydrated Cements," in Hydraulic Cement Pastes: Their Structure and Properties

(Cement and Concrete Association, Wexham Springs, Slough SL3 6PL, UK, 1976), pp. 55-72.

Uchikawa, H., and R. Furuta, "Hydration of C_3S-Pozzolana Paste Estimated by Trimethylsilylation," Cem. Concr. Res. **11**, 65-78 (1980).

Vitruvius, P., *Vitruvius - The Ten Books on Architecture*, translated from the Latin by M.H. Morgan (Dover Publications, Inc., New York, New York, 1960 trans.).

Znaczko-Janworski, I.L., "Experimental Research on Ancient Mortars and Binding Materials," Q. Hist. Sci. Technol. **3**, 377-407 (1958).

APPENDIX A
SITE LOCATIONS AND DESCRIPTIONS

A-1 Site Location at Cosa

Four specimens were collected by Professor F. E. Brown from ancient Cosa (Ansedonia); the total site consists of a Roman city built on a small hill with adjacent port. It is located north of Rome. The town was apparently little changed after mid-first century BC, keeping to earlier methods, and appears to contain little evidence of later Empire building methods using structural concrete.

Roman buildings of the third century and second century BC utilized squared stone masonry, random lime mortared rubble work or opus incertum (layered unshaped stone/mortar work), and occasionally brick work. The chief building material was the hill's grey limestone, occasionally a hard calcareous sandstone and rarely a soft yellow sandstone, a purplish tuff, plus roofing tile, sometimes crushed, and peppery-looking sea sand (Brown, 1951).

A-2. Site Locations in Rome

Two principal areas in Rome were investigated for source material: the Roman Forum and the Palatine; site descriptions follow. Additionally, limited samples were collected from nearby Trajan's Forum, from the Baths of Caracalla, from Hadrian's Tomb (now Castel St. Angelo), and from the Colosseum. Locations maps can be found in Lugli (1970).

Among the oldest concrete structures was the base of the Temple or Castor; the concrete samples (CF-2,4) were collected at its base, which was built in about 117 BC (Blake, 1947). Mortar/concrete specimens were also obtained from the Basilica Aemilia (FP-11,12), possibly from the first or second century AD, and from the Rostra (FP-18).

A mortar was also collected from the wall of Trajan's Forum (T-1) nearby. Outside the Roman Forum area, the Baths of Caracalla provided third century AD samples of pumice-bearing vault concrete (CR-1 and CR-2) and an outside concrete wall sample (CR-9). Hadrian's Tomb, remodeled later to contain the Castel St. Angelo, still included

concrete material in the base walls of probable 139 AD age, in the area on the far side from the entrance.

The Palatine hill towers above the Forum and was perhaps the earliest permanent dwelling place of Rome, being built and rebuilt with residences of emperors and other wealthy householders (Lanciani, 1967). The site dating from perhaps eighth century BC contains the remains of numerous palaces, buildings, and their substructures, which have actually extended the hill and remain to emphasize its importance. A plaster-lined third century BC cistern is perhaps the oldest well-dated structure. A plaster sample was taken from walls of the House of Livia (House of Augustus) (FP-15).

According to Tenney Frank (1924), Blake (1947), and others, Cato knew how to make concrete, but the fact that much of what survives in Rome is mid-second century BC or later is related to the fact that it was not generally recognized that Roman volcanic ash ("pit sand") was a good substitute for the superior pozzolanic ash described by Vitruvius, from the region of Vesuvius. The better quality concretes were usually of Imperial or later age, with Roman structures built during the reigns of Julius Caesar (54-44 BC) and Augustus (43 BC-14 AD), employing gray pozzolanic "pit sand" or a reddish brown or red local sand. The Temple of Concord (121 BC) is said to be the earliest well-dated concrete (Frank, 1924; Blake, 1947), and the concrete collected at the Temple of Castor is of similar age (117 BC).

The Pantheon (no sample procured) is perhaps the best known structure in Rome, built in 27 BC and still functioning today as a church.

A-3 Site Locations in Ostia

A great deal remains as a record of Imperial Ostia, Rome's port city with about 50,000 inhabitants in its heyday, although it was mostly abandoned by the fifth century AD. Excavated during this century, the general plan of Ostia Antica can be found in Calza (1974). Meiggs (1973) provides an enlarged plan . Although the city's origins were

earlier (~330 BC), much of the building took place after 43 AD under Claudius and his successors. Up to three- and four-story buildings were constructed, of which many of two stories remain. The development of Roman building techniques is illustrated through well-preserved structures.

Specimens OS-1A, OS-1B OS-12, OS-13, OS-18, OS-27, and OS-33 were collected from Ostia.

Apartment blocks and individual houses; civic buildings; temples, forums, and theaters; many baths; mercantile structures; granaries; and butcher shops are all present in Ostia as well as port structures and tombs.

APPENDIX B
TERMINOLOGY AND DEFINITIONS

The terminology proposed by Roy and Langton (1982), which was based on age of structures or on the age of the cementitious materials used in these structures, has proven useful for describing the wide range of samples analyzed in this study. Terminology based on function and composition of archaeological specimens (Roy and Langton, 1982) also has proved necessary for consistent characterization in both field and laboratory analyses.

As a result of the present study, two additional terms were found to be useful in describing the construction of masonry walls. The following nomenclature was found to be suitable for describing archaeological structures:

Ashlar Masonry - Masonry which incorporates hewn or squared stones with or without the use of mortar.

Rubble Masonry - Masonry which incorporates stones in their natural form, that is, uncut fieldstones with or without the use of mortar.

In addition, as a result of the present study, it becomes necessary to better define the term plaster. This need arose because of the common application of plasters on floors in the pre-Roman era. Since many of these plasters were multimodal with respect to their aggregate distributions, they initially appeared to be concretes. However, upon more detailed examinations, these plasters were similar or identical to those used for walls in the same structures. Therefore, in addition to the previous definition, plasters were defined as those layered materials which were emplaced onto surfaces with trowels or trowel-like tools as opposed to concretes which were poured between rigid forms.

Additional terms used occasionally:

Opus recticulatum - reticulate work: squared cross-section stone work usually used as facing on concrete walls

Opus incertum - layered, unshaped stone "rubble" mortar work

Random rubble work - completely irregular stone bound by mortar

Opus signinum - plaster or mortar prepared of lime and crushed terra cotta, usually crushed fine, and often

"worked" to line structures used to hold water

C-S-H or C-S-H gel - the semi-amporphous calcium silicate hydrate of room temperature hydrated portland cements

"Cement" nomenclature - $C = CaO$, $A = Al_2O_3$, $S = SiO_2$, $H = H_2$, $N = Na_2O$, $K = K_2O$, $F = Fe_2O_3$, $\bar{S} = SO_3$, $M = MgO$

Pozzolana - volcanic ash or deposit which is reactive with lime, named after type locality, Pozzuoli (L. Puteoli) near Vesuvius

Hydraulic cement - cements that set and harden by chemical interaction with water and that are capable of doing so under water.

APPENDIX C
FIELD DESCRIPTION OF SAMPLES AND SITES

TABLE C-1. Field Descriptions of Ancient Building Materials and Sites for Samples Collected in Italy

Sample No *	Sample Description**	Site Description
	COSA	
0980 CS-1	mortar from west corner ∿160 BC	Capitolium
0980 CS-2	wall plaster; exterior southwest; mid-3rd century BC	Capitolium
0980 CS-3	concrete floor; early 1st century BC	Edge House
0980 CS-4	mortar; ∿180-190 BC; N. corner	Bldg. APII
	OSTIA	
0980 VIII OS-1A	irregular reddish mortar, lower right of brick wall column	E. of city walls
0980 VIII OS-1B	grayish, mortar; locale same as OS-1A	E. of city walls
0980 VIII OS-2	wall plaster; building in cemetery (S. side 1st St. to left ent. small cemetery); from Columbaria bldg. (C2-22, VIII-3)	cemetery; E. of city walls
0980 VIII OS-12	plaster from wall of house; 2nd century AD (Hadrianic or Antonine) (IX-3)	House of the Charioteer, Calza, 1974, pp. 99, 123 (Insula degli Aurighi)
0980 VIII OS-13	mortar sample; floor (baths of the Cisiarii)	Terme di Cisiarii (Calza, p. 113)
0980 VIII OS-18	brownish hearth mortar around heating duct entrance; bricks above, near Neptune's baths	furnace; near Neptune's Bath (Calza, p. 116)
0980 VIII OS-27	plaster lining small tank (cistern), S.W. of Decumanus Maximus, near Neptune's Baths	Adjacent to Decumanus Maximus, near Neptune's Baths (Calza, p. 75)
0980 VIII OS-33	concrete sample (buff) from lower concrete buttress or supporting wall; 2nd-3rd century AD	W. end of Theater (Calza, p. 78, left)
0980 VIII OS-7-MHN	mortar from brick (tile) facing concrete wall, linteled door	Wall in cemetery east of Porta Romana
	ROME	
0980 VII CA-1	hard mortar, base, rear; ∿139 AD	Hadrian's tomb (Castel St. Angelo, Blake, 1947, Plate 9)
0980 VII CA-2	wall; ∿139 AD, base, far side from entrance	Hadrian's tomb; Castel St. Angelo
0980 VII CF-2	two samples from wall at base, low; one sample loose (117 BC)	Temple of Castor (Blake, 1947, Pl. 37)
0980 VII CF-4	four samples from wall near blocks, low; Blake (1947), Plate 37 (1), ∿6 AD or earlier (117 BC?)	Temple of Castor
0980 VII CO-19	mortar/concrete	Colosseum

TABLE C-1. Continued.

Sample No.*	Sample Description**	Site Description
0980 II CR-1	vault concrete, pumice-containing	Terme Caracalla (baths)
0980 II CR-2	vault concrete, pumice-containing	Terme Caracalla
0980 II CR-9	sample outside wall	Terme Caracalla
0980 IV FP-7	might be OPUS SIGNINUM; behind top marble (Ref. Blake, 1947, Pl. 51; early Augustan? ∿41BC)	Forum; Lacus Iuturnae
0980 III FP-11A	small sample pulled from wall	Basilica Aemilia (Blake, 1947, Plate 33.2) ∿14BC
0980 III FP-11B	larger fragment dropped from same wall interior	Basilica Aemilia
0980 III FP-12	mortar from wall interior at the other end of the Basilica	Basilica Aemilia
0980 V FP-15	plaster from Fresco (domus Augustus)	"House of Livia"; Palatine (Blake, 1947, Pl. 31)
0980 III FP-18	concrete sample; rather friable	Rostra (Blake, 1947, Pl. 31); Forum
0980 T-1	mortar, south wall	Traiano (Trajan's) Forum

*Archive reference numbers. Abbreviated sample numbers have been used for convenience in the remainder of this text.

**Ages of all structures in Cosa, Ostia, and Rome which were sampled were built between 100 BC and ∿200 AD unless otherwise stated. In Appendix A, on appropriate plan locations, samples are located, using last no. (i.e. CS-1 = 1, etc., on Cosa plan).

APPENDIX D
DESCRIPTION OF METHODOLOGY

D-1 Preparation of Materials for Study

Two methods were used for separating the matrix from the bulk sample. These techniques are summarized below:

Method A

1. Remove coarse aggregate fraction from bulk specimen.

2. Separate matrix fraction from fine aggregate fraction by light crushing and sieving (<325 sieve).

Method B

1. Remove coarse aggregate fraction from bulk specimen.

2. Crush remaining sample to ~0.5 cm.

3. Ultrasonify in distilled water (5-10 min at ~20,000 HZ).

4. Decant liquid and retain coarser fraction.

5. Settle suspended matrix fraction (~20 -1 μm).

6. Concentrate <1-μm matrix fraction retained in suspension by evaporation of liquid.

Identification of the crystalline phases making up the matrix fractions of the materials analyzed in this study was accomplished first by x-ray diffraction (XRD) analyses, and complemented with data from differential thermal (DTA) and thermogravimetric (TG) analyses, SEM/EDX and microprobe analyses, with some information gained from thin sections. XRD, DTA, and TG techniques are bulk analysis tools and are sensitive to phases present in amounts greater than about two to five weight percent depending on the specific characteristics of the sample. Precision of thermal analysis results is dependent upon crystal size, degree of crystallinity, heating rates, and the composition of the atmosphere in which the experiments are conducted (Courtault, 1979; Ramachandran, 1969; Mackenzie,

1970). Petrographic microscope techniques result in a maximum magnification of about 1000X, which was insufficient for the resolution or identification of extremely small particles. However, it is adequate for easy detection of gypsum and calcite crystals greater than about 0.001 mm.

Amorphous phases were often apparent in the XRD pattern. In order to isolate and identify amorphous phases and also phases constituting a small percentage of the total matrix, several additional types of analyses were used in addition to x-ray and thermal techniques. Scanning electron microscopy was a useful technique for determinng the presence of phases which occurred in minor quantities and also for isolating calcium silicate and/or aluminate gel particles. Detection was accomplished primarily on the basis of morphologic characteristics of these matrix particles and supplemented by energy-dispersive x-ray analysis. Ultrasonic separation of the -1-μm size fraction in hydraulic cement-containing building materials produces concentrated samples of amorphous phases which were relatively easy to analyze by the previously described techniques.

Other methods for detecting the presence and degree of polymerization of calcium silicate and/or calicum aluminosilicate gel particles utilize chemical dissolution methods combined with chromatographic (gas and GPC) analyses.

D-2 Macroscopic Analysis

Macroscopic analyses of all samples studied were carried out by hand-specimen examination with the aid of a 14X hand lens and also a 40X binocular microscope. Emphasis was placed on describing a variety of parameters for the matrix (binder) materials, aggregates, and miscellaneous properties in each sample. The principal parameters are listed below:

Macroscopic Descriptions of Ancient Building Materials

Binder	Aggregates	Miscellaneous
1. degree of coherency	1. type (rock/mineral/ceramic/other)	1. sample size
2. color	2. size	2. charcoal
3. mottling	3. mineralogy	3. secondary mineral
4. relative porosity	4. angularity	4. vug fillings
5. degree of carbonation	5. color	5. other
6. relative amount	6. relative amount	

D-3 Petrographic Analysis

Petrographic analyses were carried out using a Reichert polarizing microscope in order to determine the mineralogy and homogeneity of the matrix material, nature of the aggregates, nature of the matrix/aggregate interfacial regions, and microtexture of the composite sample. The matrix phases were studied using an oil-immersion 100X objective lens which resulted in a total magnification of about 1000X. However, most observations were made over the magnification range of 45 to 720X.

Thin sections were prepared for each of the 38 ancient samples studied. Modifications of standard thin section preparation techniques for ancient cement-based materials have been discussed by Roy and Langton (1982). Specific sample parameters of interest in the thin section analyses included those listed for macroscopic analysis in Section 2.1 and Appendix E.

D-4 Scanning Electron Microscope Analysis

Scanning electron microscope (SEM) imagery, combined with qualitative elemental analysis as determined by characteristic x-ray emissions (EDX), proved to be very useful techniques for studying the microstructure of the bulk samples and the morphology of individual particles. The advantages of using SEM techniques included large depth of focus, sample preparation simplicity, high resolution, and qualitative elemental analysis of

crystalline and noncrystalline phases exposed on fractured surfaces. The maximum working magnification using a secondary electron signal was between 10,000 and 20,000X or higher, depending on the individual sample. However, the practical maximum magnification in the lower stage, which was coupled with EDX capabilities, was about 3,000X.

An ISI-DS130 SEM unit was equipped to analyze signals generated by secondary electrons, back-scattered electrons, and x-rays characteristic of individual elements with atomic numbers greater than neon (although Na is not very sensitive). Morphologic and chemical data were correlated with x-ray diffraction powder pattern data for final phase identification. Several examples of data obtained from SEM imagery are discussed in Section 2.3.

D-5 X-Ray Diffraction Analysis

X-ray diffraction analyses were conducted on the matrix (binder) fractions of all samples discussed in this report and also on selected aggregates. Separation of the matrix and aggregate fractions was performed according to the procedure (method B) described by Roy and Langton (1982) or by ultrasonic disaggregation (method B) described in D-1. All samples analyzed by x-ray diffraction techniques consisted of particles less than 45 μm in size. Each sample was then mounted on a standard pre-cleaned microscope slide by dispersing the powder in a collodion solution or packed in an aluminum sample holder when it was important to insure random orientation. X-ray data were obtained with a Philips automated powder diffractometer (APD-3600/01) by using Cu radiation, standard settings at 45 KV and 30 mA, and a Θ-compensating slit which eliminated the necessity of slit changes. A Data General Nova/4S computer was used to collect, store, and process data. Software programs were run from a fixed firm disk, whereas JCPDF (Joint Committee on Powder X-Ray Diffraction, 1979 standard) patterns were stored on a removable firm disk. All ancient cement data were stored on a special reserved disk in a library directory called ANCCEMENT. Peak searches were conducted using a second derivative algorithm employing background fitting, peak smoothing, and α_2 stripping capabilities. Data manipulation was done on a Tektronix CRT 4012 using an interactive mode with the

PLOT program. Comparisons were made with the JCPDF patterns using the COMPARE routine.

D-6 Thermal Analyses—DTA and TGA

Differential thermal analyses were performed using a Harrop DTA 716 coupled with a Harrop TA700 programmer, controller, and recorder unit. This instrument was calibrated using the transition temperature of quartz and the melting temperature of indium. The standardization procedure was carried out using a standard sample size of 80 mg of material which was packed and tamped into a quartz sample holder. Corundum, α-Al_2O_3, was used as the reference material for measuring the temperature differential between the sample and a standard inert phase. A heating rate of 10°C/min. was used, and the temperature differential was recorded in millivolts over the temperature range 26-1000°C. Platinum thermocouples were used. All experiments in this study were conducted under atmospheric conditions in accordance with the standard operating procedure described above.

Thermogravimetric analyses were performed using a Harrop TGA 176 coupled with a Harrop TA700 programmer, controller, and recorder unit. Thermocouples were standardized using the dehydration temperatures of copper sulfate pentahydrate, and weight calibration for the balance portion of the instrument was performed using Cahn calibrating weights. All experiments were conducted under atmospheric conditions at a heating rate of 10°C/min. over the temperature interval of 26 to 1000°C. Between 20 and 35 mg of crushed (-200 mesh) material was used for each of these analyses.

D-7 Quantitative Chemical Analyses

Approximately 500 mg of separated matrix material was required for each total analysis. Chemical analyses of the oxide components were conducted primarily by plasma emission spectrometry. Silica was determined gravimetrically, and calcium oxide was determined according to a wet chemical procedure based on getting the calcium into solution and then precipitating it as calcium oxalate by means of a solution of ammonium oxalate,

according to the reaction $Ca^{++} + C_2O_4^{=} \rightarrow CaC_2O_4$. The calcium oxalate was then ignited to form calcium oxide and the latter compound was weighed.

Total sulfur analyses were conducted using a rapid analysis technique which employed a Leco Sulfur Analyzer. The samples were placed in the sample chamber of this instrument, where they were heated and reacted with oxygen. SO_2 was formed, then titrated to determine the amount of sulfur present. Sulfate and sulfide were not distinguished by this analysis. The analyses were reported as weight percent SO_3.

Determinations of adsorbed water ($H_2O_{110°C}$), water incorporated in the crystal structure (H_2O_{total} - $H_2O_{110°C}$), and carbonate (reported as CO_2) were made by weight losses observed in the thermal gravimetric analyses. This procedure was described in the section on thermal analyses.

D-8 Chemical Structure Determination—TMS Technique

The trimethylsilylation (TMS) technique is a chemical method of studying silicate structure, particularly those of poorly crystalline or noncrystalline silicates, including cement-related compounds and their hydration products. The structure, or rather the degree of condensation of the silicate groups in the original phase, can be estimated by gas-liquid chromatographic measurements of trimethylsilyl derivates (T-derivatives). These derivatives are formed by the reaction between trimethylsilyl and silanol groups, the latter produced by acid dissolution of the original silicate compounds. The procedure used in this study was adapted from that of Tamas et al. (1976) and Uchikawa and Furuta (1980), and has been described by Roy and Langton (1982). Gel permeation chromatography (GPC) was performed by E. Lachowski according to methodology described by Glasser et al. (1981).

D-9 Other Methods of Investigations

Microprobe Analysis

Microprobe analyses of selected samples were carried out in order to obtain quantitative chemical data for unidentified matrix and aggregate phases and matrix/aggregate interfacial regions. Analyses were conducted using an ETEC-Autoprobe equipped with three variable spectrometers and a KEVEX energy analyzer. Samples were analyzed for aluminum, carbon, iron, potassium, magnesium, manganese, sodium, and silicon, and the Bence Albee Correction Routine was used to compute oxide percentages.

Compositional data resulting in oxide components totaling between 35 and 65 weight percent were typical for the samples analyzed. Even after the approximate weight percentages of H_2O and CO_2 (determined by TGA) have been taken into account, the resulting totals were well below acceptable values. Applications of these data are therefore limited, and caution must be used in interpreting the results.

Determination of Organic Constituents

Chemical analyses were conducted on selected samples to determine if organic compounds, such as oils, resins, or waxes, were incorporated in these materials to act as waterproofing agents. Two methods of analysis were used. The first involved crushing the sample and then leaching it in hexane for 48 hours in a soxhlet. This solution was filtered, concentrated, and then analyzed by liquid chromatography.

The second method used for detecting the presence of organic compounds incorporated into ancient building materials involved dissolution of 50 to 100 grams of sample in a 50 percent HCl solution at 60°C for 24 hours. This was followed by dissolution of the remaining solid material in a 1:1 mixture with 50 percent HCl and 50 percent HF at 60°C for 24 hours. This solution was diluted and filtered. Residue remaining on the filter paper was again treated with a 50 percent HCl solution for 12 hours. Since the organic polymers

anticipated to be present (naturally occurring compounds available to the ancient engineers) are not soluble in the acid solutions described above, they can be separated as a solid residue by filtration.

D-10 Effect of Techniques

Chemical compositions or the matrix fractions of the materials investigated in this study were determined by means of emission spectrometry, wet chemical analyses, and thermogravimetric analyses (volatile constituents). The matrix fractions were separated from the bulk by a mechanical method which involved light crushing, separation, and sieving (Roy and Langton, 1982) and/or by ultrasonic techniques. These methods may result in minor, undetermined amounts of contamination of the matrix by aggregates present in the bulk material.

Alternative methods for determining the bulk compositions (see Section 1.6.8) for selected areas in the matrix and also for determining the compositions of individual particles in the matrix fractions were investigated and include energy dispersive x-ray analysis (EDX) in conjunction with SEM analysis and microprobe analyses. The primary advantages in using any of these techniques are that they do not require separation of the matrix from the bulk sample, and individual particles in addition to selected areas can be analyzed. Qualitative chemical analyses of matrix particles and areas exposed on fractured surfaces were obtained by EDX/SEM analyses. A relatively thick (300-400Å) gold coating was required in order to obtain resolution at magnifications above 3000X. As a result of this thick coating, the intensities of lower energy signals were preferentially decreased with respect to higher energy signals. Therefore, definitive compositional data for the matrix or for particles within the matrix fractions were not obtained by using this technique; however, they provided useful complementary information. Microprobe analyses were conducted on several samples in order to obtain quantitative compositional data for the matrix fraction. The results obtained should be interpreted with caution because of the low values computed for the total oxides present. High porosity observed on even the polished surface (which was required for microprobe analysis) is believed to be responsible

for the loss of impinging electrons which excite the sample to produce a detectable signal, and for the adsorption of the resulting energy signals by epoxy filling these pores.

APPENDIX E
MACROSCOPIC DESCRIPTIONS OF ANCIENT CONCRETES, MORTARS, AND PLASTERS FROM ITALY

TABLE E-1 Macroscopic Descriptions of Ancient Concretes, Mortars and Plasters from Italy.*†

Sample No.	Matrix‡	Aggregates	Miscellaneous
		COSA	
CS-1	coherent, v. carbonated, white (N9)	1. large rock frag. comprises >50% of hand specimen; lt. grayish yellow (5Y8/4) carbonate fragments (probably a carbonate conglomerate) 2. f. agg.fract. includes leucite and augite crystals 0.1-0.4 cm	6x5x3.5 cm Agg/matrix interfacial regions are characterized by fractures; matrix shows map cracking (probably result of shrinkage) which extends into fractures around agg.; no v.fn. agg. fract.
CS-2 (A and B)	coherent, v. carbonated, v. pale orange (10 YR 8/2) <20% sample vol. (may contain pozzolana)	1. quartz sand, ~0.1 cm, rounded to subangular ~50% vol. of samp. 2. basic volcanic rock frag. and crystals (augite, leucite) up to 0.3 cm 3. carbonated lime chunks up to 0.3 cm.	8x8x1 cm (plus smaller frag.), probably a plaster; agg. fraction becomes finer towards the outer surface; outer surface is smooth; displays parting surface; outer layer ~0.3 cm thick, inner layer 0.6 to >1 cm thick.
CS-3	coherent, v. carbonated, white (N9) 40-50% sample vol.	1. terra-cotta frag. angular, ~1±0.5 cm, mod. reddish brown (10 R 4/6), ~50% sample vol. 2. ≤5% leucite and other crystals 3. ≤5% terra-cotta frag. of a grayish orange color (10 YR 7/4)	15x10x6 cm. Extensive map cracking in matrix which extends into agg./matrix interfacial regions (probably from shrinkage).
CS-4	somewhat crumbly inconerent, sandy, carbonated, white (N9) (may contain dk. gray pozzolana)	1. v.fn.gr. dark volcanic sand, ~70% 2. basic volcanic rock frag. <0.25 cm 3. chunks of carbonated lime, ≤10% (specimen is entirely rock)	9x9x6.5 cm. Volcanic sand can be rubbed off hand specimen; some plant fibers are present but these are recent; shrinkage cracks are present in white chunks (probably due to a volume decrease upon carbonation), charcoal frag. are present, abundant black fn. agg (augite) results in a v.fn. speckled appearance of the matrix.
		OSTIA	
OS-1A	mod. conerent to sl. crumbly, carbonated, lt. olive gray (5 Y 6/1) (may contain lt. gray pozzolana)	1. augite crystals 0.05 cm, black 2. leucite crystals 0.05 cm, clear-whitish 3. volcanic rock frag., rounded subangular, 0.2 cm	2x2x1.5 cm. Stringers and patches of a white phase throughout matrix; one side of the sample displays agg. pluck outs which suggests this side was the under surface of a plaster.

TABLE E-1 (continued)

Sample No.	Matrix*	Aggregates	Miscellaneous
		OSTIA (Continued)	
OS-1B	coherent, carbonated, v. pale orange (10 YR 8/2), 20% sample vol. (may contain lt.tan pozzolana)	1. tuffaceous volcanic rock frag., vesicular, somewhat crystalline, various colors (red, tan, dk.gray), rounded, up to 1 cm, ≥60% 2. crystals (leucite, augite, sodalite, others), ≤0.2 cm 3. v.fn. agg. fract.	4x4x3 cm. 5% HCl etches matrix material into a cellular texture; Agg./matrix interfacial regions are intact and show no signs of reaction rims.
OS-2	coherent, carbonated, white (N9), outer surface is v.pale orange (10 YR 81)	1. 10% small transparent crystals (leucite), <0.2 cm 2. <5% volcanic rock frag., <0.3 cm, rounded	6x3x0.5 cm. Plaster with smooth outer surface; under surface is irregular
OS-12	coherent, carbonated, v.pale orange (10 YR 8/2) 30% sample vol. (contains lt.gray or tan pozzolana)	1. carbonate rock frag., angular, up to 1 cm 2. basic volcanic rock frag. up to 0.2 cm, rounded 3. v.fn.agg.fract.	2x1x0.5 cm (2 pieces). Probably part of a fresco or painted wall plaster; one surface is smooth and is covered with red pigment which was subsequently coated with grayish orange sec. min. products (probably carbonate).
OS-13	crumbly, carbonated v.lt.gray (N8) (contains gray pozzolana)	1. volcanic rock frag., rounded, 0.1 to 0.5 cm, vesicular 2. small crystals and basic rock frag. <0.1 cm 3. v.fn. agg. fract.	1x1x0.5 cm (2 pieces plus smaller fragments). Agg. >70% vol. of sample; Agg./matrix interfacial regions are intact and show no reaction rims.
OS-18	coherent, carbonated, pale brown (5 YR 5/2) (contains pozzolana)	1. white garnet crystals ~0.2 cm 2. augite crystals <0.1 cm 3. leucite crystals <0.1 cm 4. other unidentified crystals 5. carbonate and basic volcanic rock frag.	3x2.5x1.5 cm (plus smaller fragments). Most of the hand specimen is a large piece of yellowish brown chalcedony with sec. min. in vugs.
OS-27	coherent, carbonated outer layer is pinkish gray (5 YR 8/1) inner layer is grayish orangish pink (5 YR 7/2) (contains reddish pozzolana--may be v.fn. terra-cotta)	1. terra-cotta frag. up to 2 cm, angular to rounded, relatively porous 2. volcanic rock frag., vesicular, subangular to rounded, up to 0.5 cm 3. leucite, augite, and other crystals <0.5 cm and mostly <0.1 cm 4. v.fn. agg. fract.	3x2x1 cm. Plaster (possibly 2 layers); outer surface layer is 0.15-0.1 cm thick; interface between the 2 layers is regular and parallel to the outer surface of the upper layer; under surface of inner layer is irregular; terra-cotta fragments characteristically are rimmed by a white zone; Agg. 30% of sample.

TABLE E-1 (continued)

Sample No.	Matrix ∓	Aggregates	Miscellaneous
		OSTIA (Continued)	
OS-33	coherent, carbonated, grayish yellow (5 Y 8/4) (contains lt. brown or tan pozzolana)	1. volcanic rock frag. angular to rounded, up to 1.5 cm, vesicular 2. leucite and augite crystals up to 0.1 cm 3. white, chalky crystals could be analcime or garnet up to 0.2 cm 4. v.fn.agg.fract.	6x5x3 cm. Abundant patches of white v.fn.gr. material; Agg./matrix interfacial regions are intact and show no reaction rims; Agg. ≳70%.sample vol.
OS-7-MHN	coherent, carbonated, v.lt.gray (N8) ≲25% of sample vol. (contains grayish pozzolana)	1. volcanic rock frag. (trachytic tuff), rounded, dk. gray, <0.5 cm 2. v.fn.agg., <0.05 cm 3. carbonated lime chunks, <0.1 cm 4. small crystals (augite), 0.1 cm	4x3x2 cm (2 pieces). acid treatment results in residual cellular texture in cement matrix; Agg./matrix interfacial regions are intact and show no reaction rims.
		ROME	
CA-1	coherent, carbonated, v.lt.gray (N8) on weathered surface to buff pinkish gray (5 YR 8/1) on fresh surface; ≲20% vol. of sample (contains grayish and/or reddisn pozzolana)	1. weathered volcanic frag. (trachytic tuff) rounded to sub-angular, vesicular to dense, crystals of augite, hornblende, >70% 2. tuffaceous frag., ≲5%, yellow br. (10 YR 5/4) 3. occasional chunks of carbonated lime <0.3 cm 4. v.fn. red agg.fract.	4x3.5x2.5 cm (irregular shape) plus smaller pieces. Good sorting and grading of the agg. fract; Agg./matrix interfacial regions are intact and show no reaction rims.
CA-2	coherent, sl.-mod. carbonated, v.lt.gray (N8) grading into buff pinkish gray (5 YR 8/1) due to concentration and color of v.fn. agg. fract. (contains gray pozzolana)	1. coral frag., ~4x3x2 cm 2. volcanic frag. (trachytic tuff) crystal-rich (augite-rich), sub-angular to rounded, <0.05-2 cm, black to reddish (5 R 3/4), >70% 3. tuffaceous volcanic frag., m. vel. brown (10 YR 5/4), <0.05-2 cm, subangular 4. carbonated lime chunks <0.5 cm 5. v.fn.agg.fract.	12x6x3 cm (irregular shape). Agg. sorting and grading is good; weathered surface contains vugs filled with white sec. min.; Agg./matrix interfacial regions are intact and show no reaction rims; coral/matrix interface is intact except where broken due to handling.
CF-2	coherent, carbonated, pinkish gray (5 YR 8/1), ≲20% vol. of sample (contains pinkisn gray pozzolana)	1. volcanic rock frag. (trachytic tuff) rounded to subangular; weathered dk. reddish brown (10 R 3/4) to grayish brown (5 YR 3/2) to lt. brown (5 YR 5/6) 2. v.fn.agg. fraction	6x5x3 cm (2 pieces), 7x5x2.5 cm (one piece). Agg./matrix interfacial regions are intact and show no reaction rims; tendency for agg. to pluck out; vugs up to 0.5 cm in diameter are filled with v.fn.gr. white needle-shaped and massive crystals; outer weathered surface is slightly darker than bulk specimen.

TABLE E-1 (continued)

Sample No.	Matrix‡	Aggregates	Miscellaneous
		ROME (Continued)	
CF-4	coherent, carbonated, pinkish gray (5 YR 8/1) ≲20% vol. of sample (contains yellowish grayish brown pozzolana)	1. volcanic rock frag. (tracnytic tuff) dk. gray to orangish brown, rounded to sub-angular, <0.05-1.5 cm, contains alkali feld., augite, garnet crystals 2. v.fn.agg.fract.	sample consists of 4 small fragments labeled A, B, C, D, each ≈2x2x1 cm; B and C appear to be crystal-rich (feldspar, augite, biotite, garnet analcime) tuffaceous rocks; A and D may be concretes with vug fillings; Agg./matrix interfacial regions are intact and show no reaction rims.
CO-19	m.coherent-sl. crumbly, carbonated v.lt.gray (N8) ≳35-40% vol. of sample (contains reddish gray pozzolana)	1. volcanic rock frag. (trachytic tuff), vesicular, rounded, reddish-brown, up to 1.5 cm, agg. contain white vug fillings 2. v.fn.agg.fract.	3x2x1 cm (2 pieces) plus smaller frag. V. thin white stringers throughout entire sample of sec. min.; larger aggregates are concentrated on one surface of the sample.
CR-1	coherent, carbonated, buff pinkish gray (5 YR 8/1) (contains reddish gray pozzolana)	1. one large volcanic frag. (crystal-rich trachytic tuff) contains biotite, augite, and other phenocrysts 2. v.fn.agg.fract.	7x5x2 cm. Most of the hand specimen is a large pumice fragment; cement matrix is present as a thin (<0.5 cm thick) coating over a small portion of this rock which was fractured from larger concrete specimen. Agg./matrix interface is intact and shows no macroscopic reaction rim; due to vesicular agg., interface is very intricate.
CR-2	coherent, carbonated, buff pinkish gray (5 YR 8/1) (contains reddish pozzolana)	1. one large volcanic frag. (crystal-rich trachytic tuff) contains augite, leucite, and analcime; vesicular reddish brown 2. smaller volcanic rock frag. rounded to subangular, <0.3 cm 3. v.fn.agg. fraction <0.05 cm	10x8x6 cm. >85% of sample consists of one large pumice frag.; Agg./matrix interface is very intricate due to the vesicular nature of the agg. but shows no reaction rims; cement is present as a coating <1 cm thick on this rock.
CR-9	coherent, carbonated, pinkish gray (5 YR 8/1) <30% vol. of sample (contains v. grayish red pozzolana)	1. volcanic rock frag. (trachytic tuff) contains leucite up to 0.5 cm, feld., analcime, augite, and garnet rounded to subangular 2. one terra-cotta fragment, 5x3.5x2 cm 3. v.fn.agg.fract.	6x7x2.5 cm = largest of 4 pieces. Volcanic agg./matrix interfacial zone is intact and shows no reaction rim; terra-cotta/matrix interfacial zone is characterized by visible white line around terra-cotta edge.

TABLE E-1 (continued)

Sample No.	Matrix†	Aggregates	Miscellaneous
		ROME (Continued)	
FP-7	conerent, carbonated, lt. gray (N7) <30% sample vol. (contains gray pozzolana)	1. volcanic rock frag., dense to vesicular, rounded, <0.5 cm, reddish-brown 2. crystals of primarily leucite, feld., analcime, sodalite 3. cnalcedony frag. grayish orange (10 YR 7/4) 4. v.fn.agg.fract.	2x2x3 cm. Agg./matrix interfacial region is intact and snows no reaction rim; Agg. including small crystals ≥70% sample vol.
FP-11A	thin coating on agg., carbonated, pinkish gray (5 YR 8/1) (contains pozzolana)	1. coating may contain v. fn. agg., 0.05 cm but no larger agg.	2.5x2x1 cm. >95% of this hand specimen is one trachytic pumice frag., dk.reddish brown (10 R 3/4); which was an agg. in a concrete; cement is a coating on the agg.
FP-11B	coherent, carbonated, pinkish gray (5 YR 8/1) (contains reddish pozzolana)	1. volcanic rock frag. (crystal-rich trachytic tuff) up to 1 cm, reddish to brownish, contains augite, alkali feldspar, few quartz grains 2. v.fn.agg.fract.	4x3.5x2.5 (2 pieces). Agg./matrix interfacial zone is intact and snows no reaction rims; tendency for some crystals to be plucked out; Agg. >80% of sample vol.
FP-12	m.coherent to crumbly, carbonated, lt. gray (N9) to v.lt. brownish gray (5 YR 6/1) (contains grayish pozzolana)	1. v.fn. volcanic rock frag., <0.1 cm 2. leucite, feldspar, and garnet crystals <0.1 cm 3. patches of carbonated lime ≤0.1 cm	3x3x2.5 cm (2 pieces) plus several smaller pieces. May be a plaster or mortar since coarser volcanic rock frag. are concentrated towards one surface.
FP-15	m.coherent, carbonated, white (N9) to yellow gray (4 Y 8/1) to v.pale orange yellow (10 YR 8/2) (may contain pozzolana)	1. crystals of leucite and augite plus other unidentified crystals all <0.1 cm, ≥75% agg.	2.5x1.5x0.75 cm. Plaster as evidenced by smooth outer surface; the outer-most surface layer (0.025-0.05 cm) may have been applied separately since it has a distinct texture and lacks agg.; crystal/matrix interfacial zones occasionally display a white rim around the crystal.
FP-18	m.coherent to crumbly, carbonated, lt. gray (N7) (contains gray pozzolana)	1. volcanic rock frag. (trachytic tuff) dense to vesicular, ≤0.5 cm, rounded 2. crystals of leucite, feldspar, and augite, ≤0.1 cm 3. v.fn.agg. fraction <0.05 cm.	3x3x0.5 cm (plus numerous small frag.); >80% agg. and v.fn.agg.fract.

TABLE E-1 (continued)

Sample No.	Matrix‡	Aggregates	Miscellaneous
		ROME (Continued)	
T-1	coherent, carbonated pinkish gray (5 YR 8/1) <30% sample vol. (contains brownish tan pozzolana)	1. basic volcanic rock frag., >1 cm, med. brown (5 YR 4/4), vesicular to dense, rounded to sub-angular, some frag. are crystal-rich (leucite, feldspar, analcite, sodalite with white reaction rim, augite) 2. med. size volcanic agg., ~0.1-0.5 cm, same as above 3. v.fn.agg. fraction <0.05 cm	4 5x4x2 cm. Agg /matrix interfacial regions are intact although there is some pitting of agg., reaction zones are not characteristic.

*The Geological Society of America Rock Color Chart was used to designate colors as indicated by the symbol enclosed within parentheses following each color description. T = presence of carbonate phases was determined by effervescence upon contact with 5% HCl solution.

+Macroscopic descriptions were compiled from the samples as received. They do not take into account alteration of the samples as the result of further analyses.

‡The basis for describing some matrices as possibly containing pozzolana was that these matrices have textures and colors which suggest that they contain ultrafine material similar to but finer grained than the very fine volcanic aggregate fraction (<0.05 cm in size).

APPENDIX F
X-RAY DIFFRACTION PATTERNS FOR SEPARATED CEMENTITIOUS MATERIALS

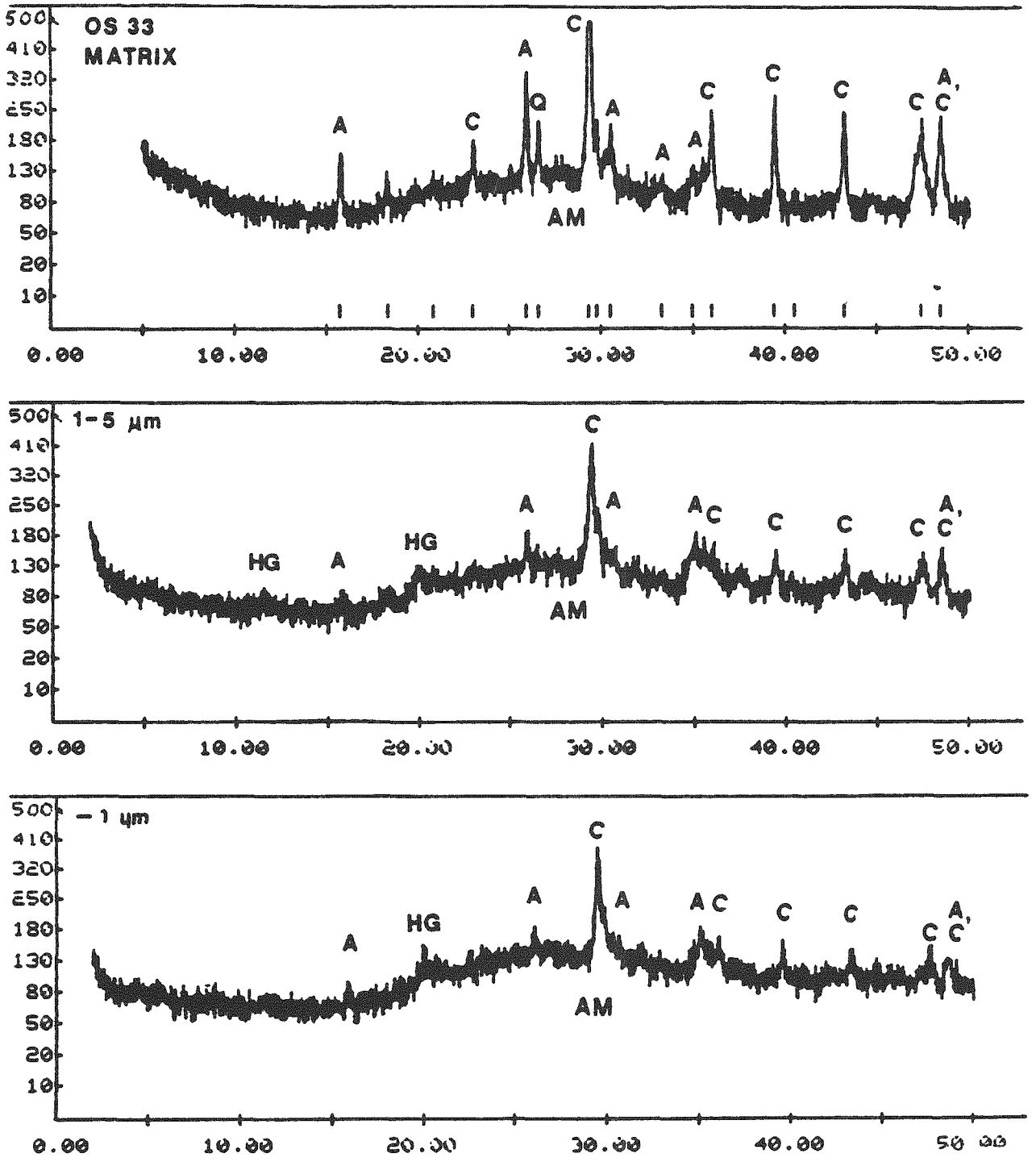

Fig. F-1. X-ray diffraction powder patterns of the matrix fraction of OS-33. Top pattern was obtained by light crushing and sieving (Method A). Middle pattern was obtained by settling 1- to 5-μm particles from suspension (Method B). Bottom pattern was obtained from -1-μm particles retained in suspension (Method B). A = analcime, AM = x-ray amorphous material, C = calicte, HG = possible hydrogarnet, and Q = quartz.

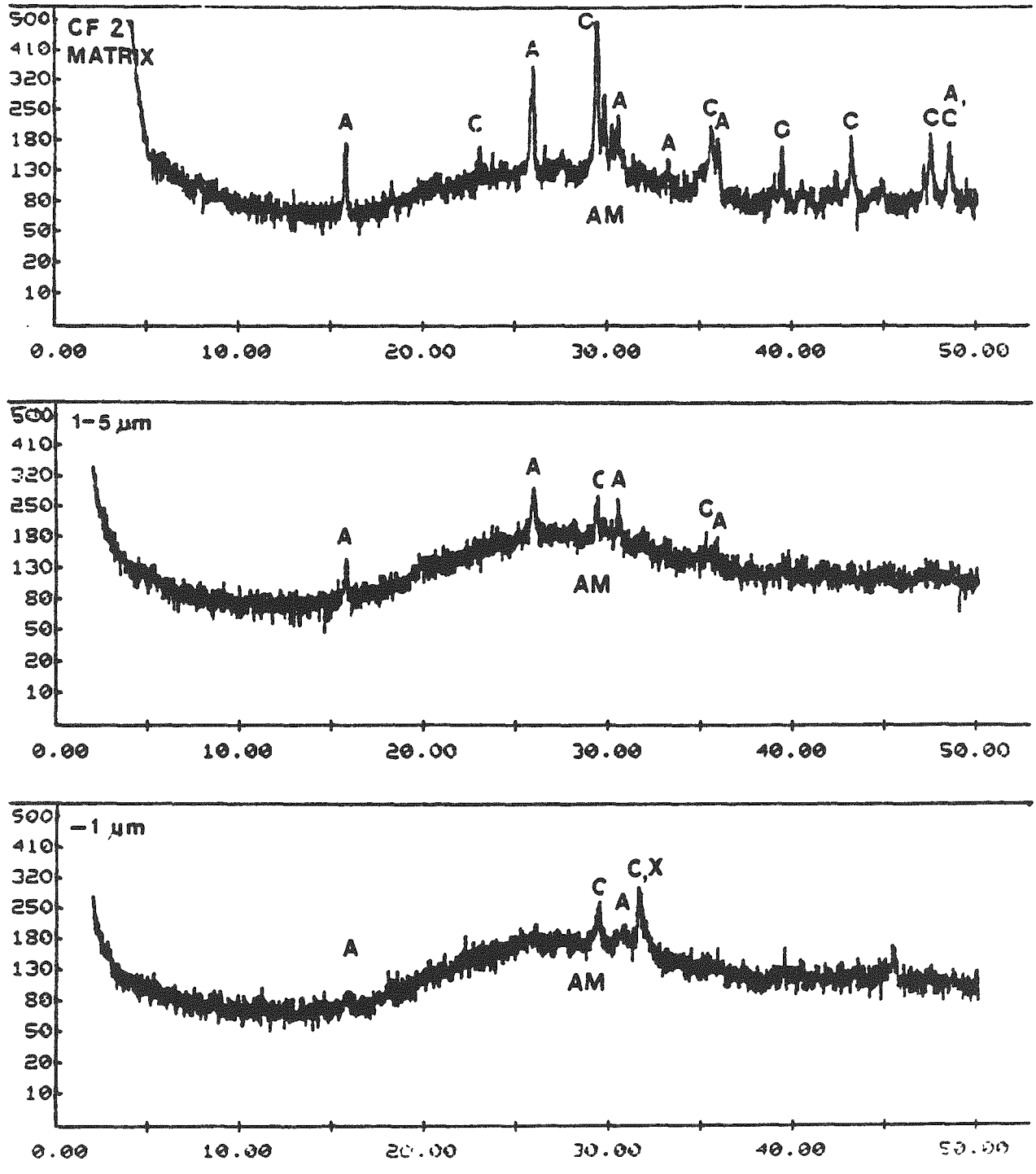

Fig. F-2. X-ray diffraction powder pattern of the matrix fraction of CF-2. Top pattern same as in Fig. F-1; X = poorly crystalline hydrated calcium silicate phase resembling C-S-H gel (which may or may not be carbonated). Abbreviations as in Fig. F-1.

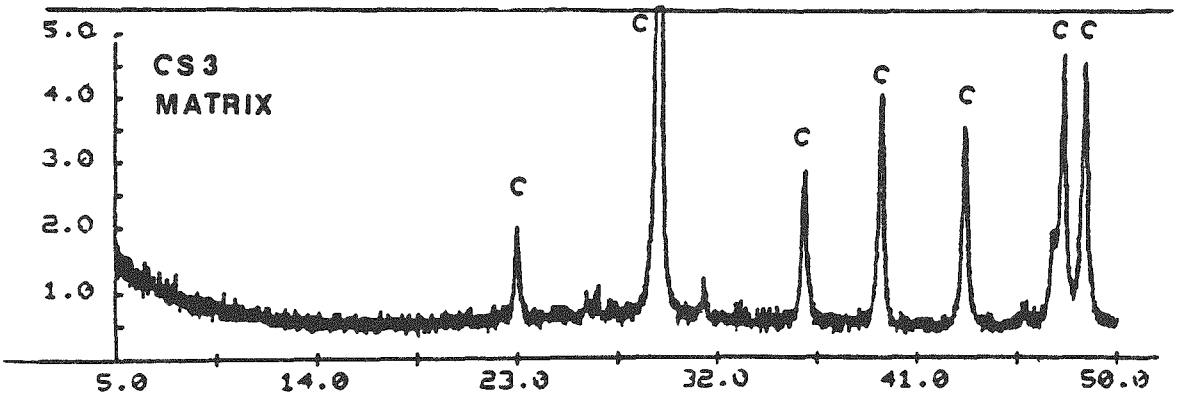

Fig. F-3. XRD pattern of CS-3. C = calcite.

APPENDIX G
THERMAL ANALYSIS RESULTS

[Thermogravimetric Analyses (TGA) and Differential Thermal Analyses (DTA) for CS-1, OS-33, FP-12, and FP-18 Samples]

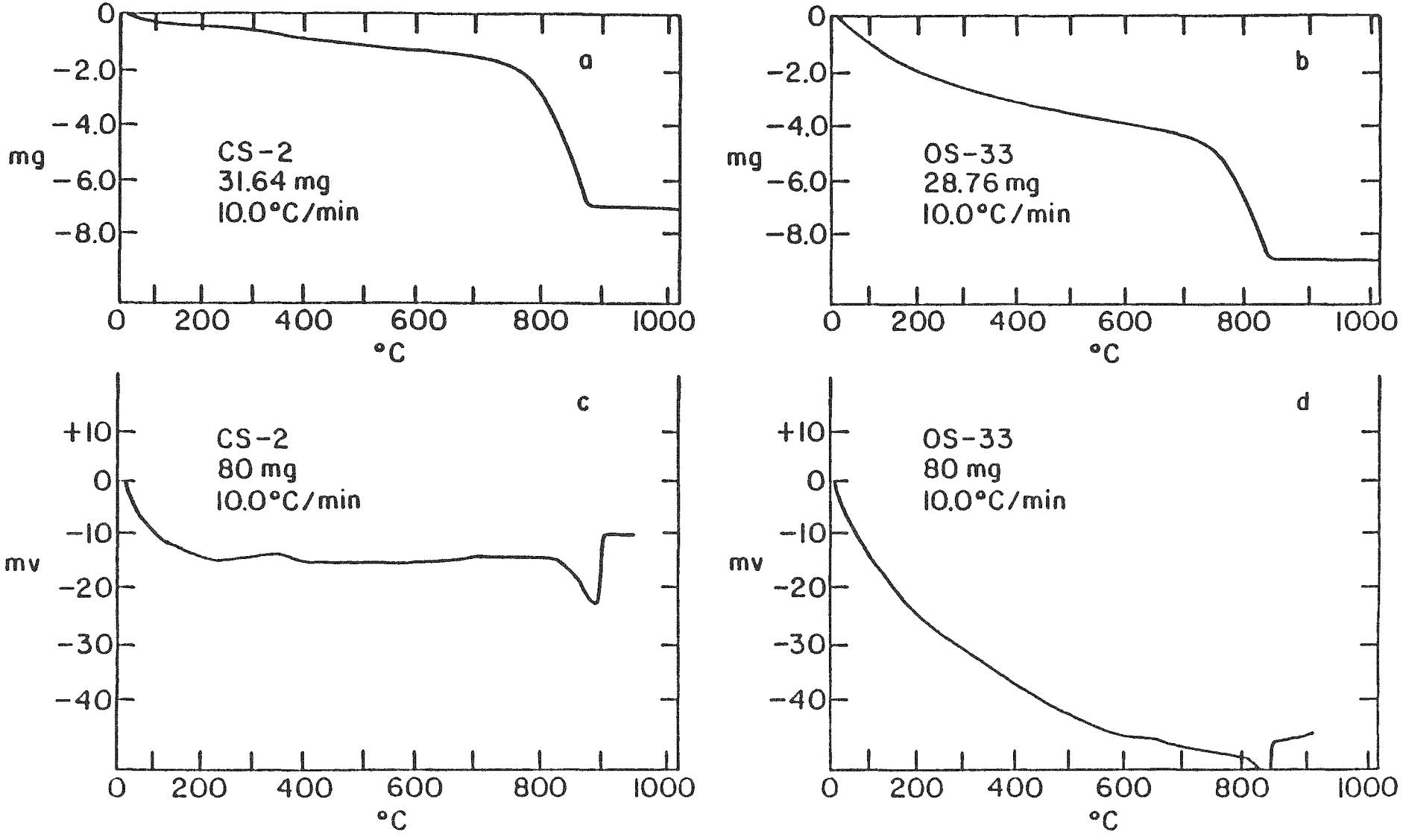

Fig. G-1. TGA (a and b) and DTA (c and d) data for CS-2 and OS-33, respectively.

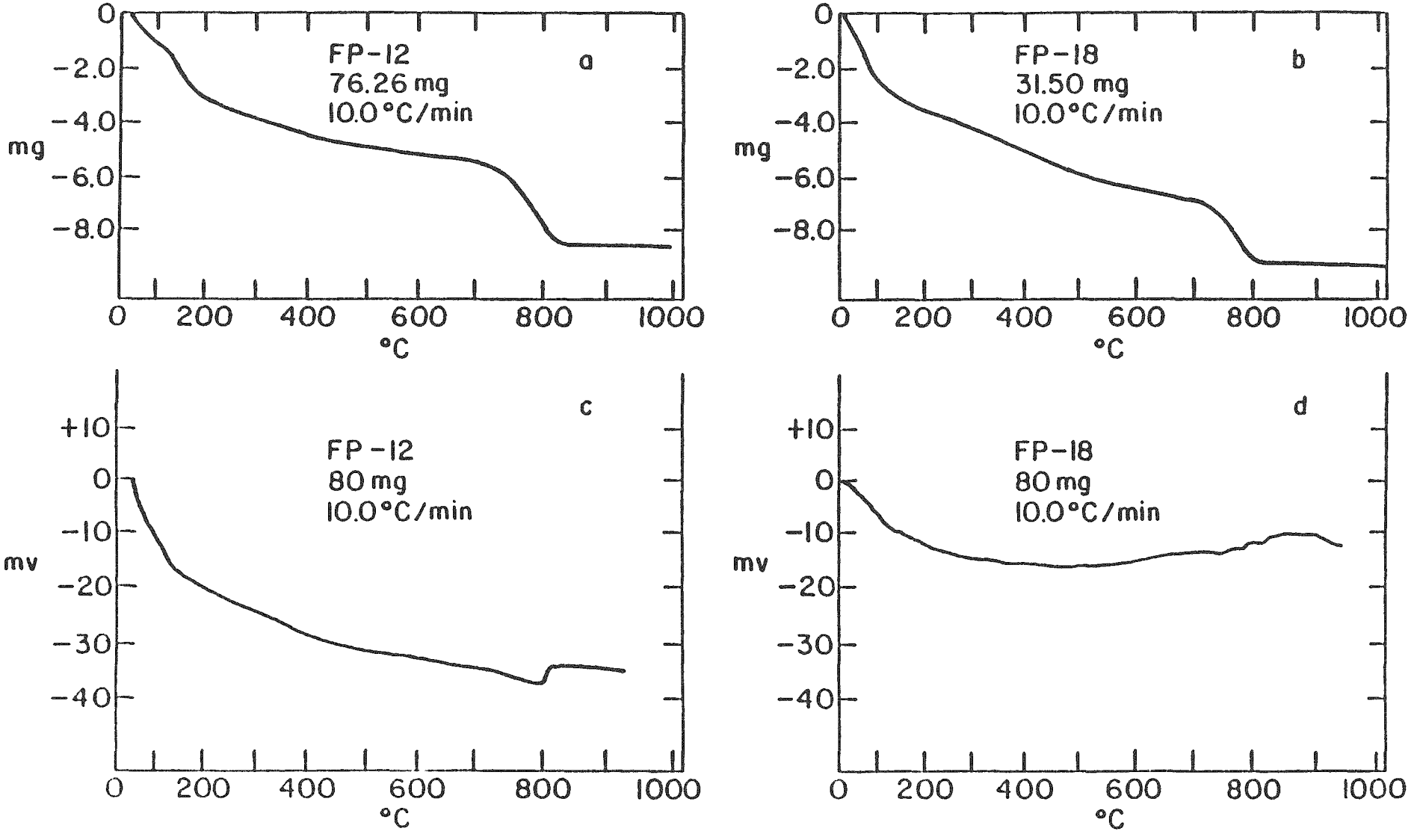

Fig. G-2. TGA (a and b) and DTA (c and d) data for FP-12 and FP-18, respectively.

Table G-1. Summary of Thermal Effects in TGA Analysis

CS-2	50-210°C = dh.EW and SW, 900°C = dc.C
FP-12	50-150°C = dh.EW and SW, 150-170°C = dh.SW, 770°C = d.c.C
FP-18	50-220°C = dh.EW and SW, 700-950°C = dc.C
OS-33	50-110°C = dh.EW, 110-600°C = dh.SW, 845°C = dc.C

---

dh = dehydration, EW = evaporable water, SW = structural water, dc = decomposition, C = calcite

APPENDIX H

CHROMATOGRAPHIC ANALYSES OF TRIMETHYLSILYLATED DERIVATIVES OF CEMENTITIOUS MATRIX FROM ANCIENT CEMENTITIOUS MATERIALS AND AN ALKALI-SILICA GEL FROM DENMARK

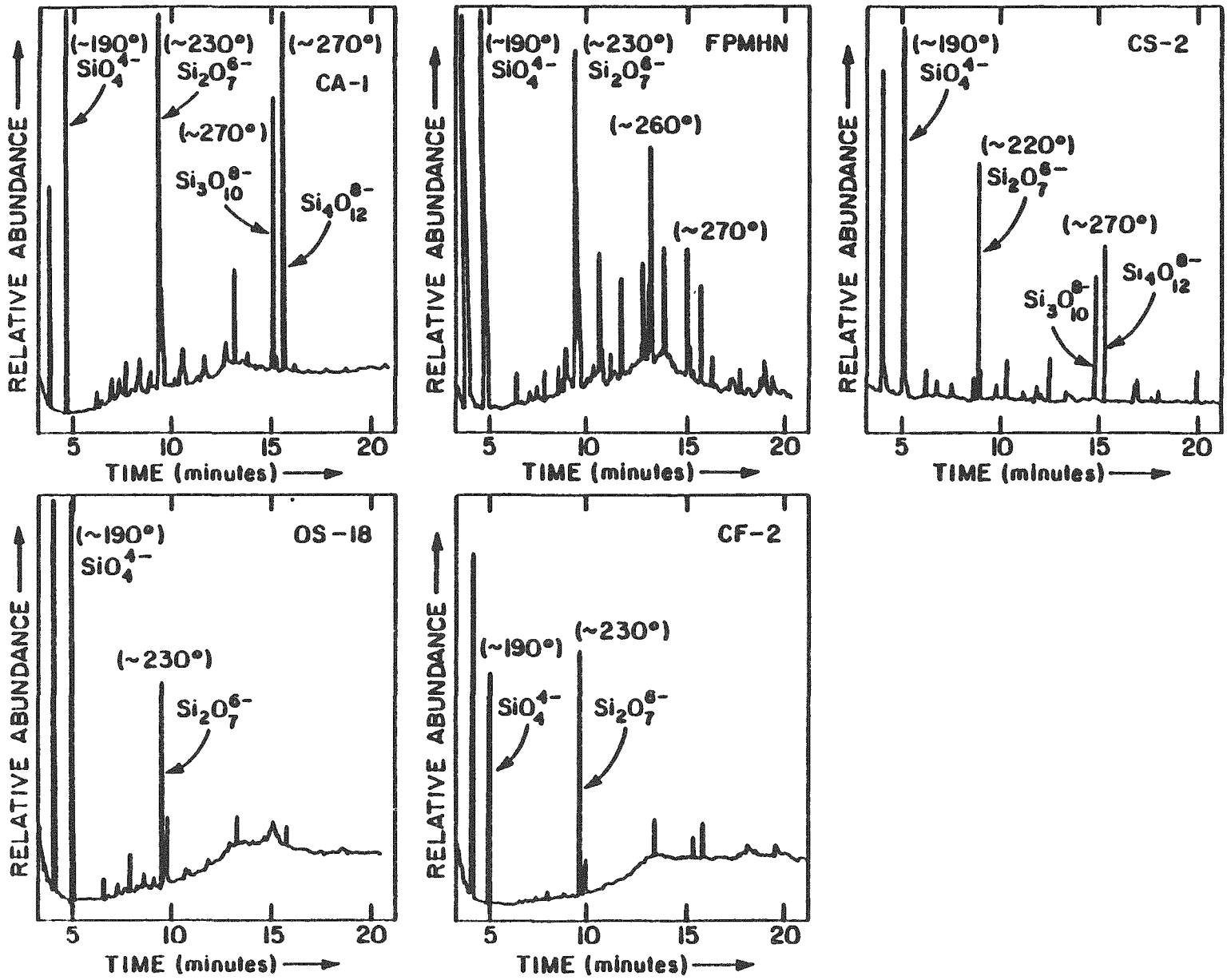

Fig. H-1. Gas-liquid chromatograms of the silylated reaction products from the matrix fractions of selected ancient building materials from Italy.

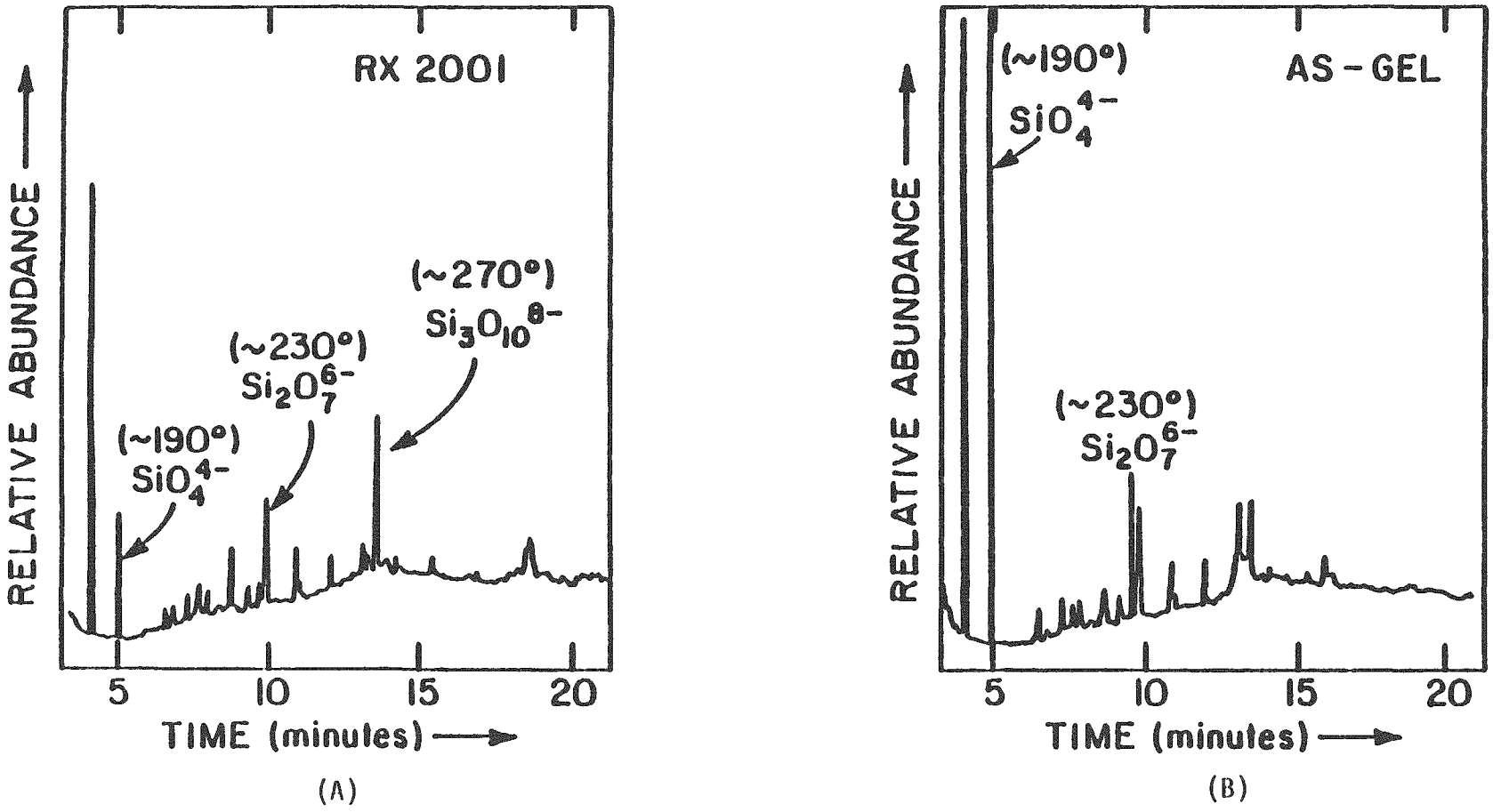

Fig. H-2. Gas-liquid chromatograms of the silylated reaction products from a trachytic tuff, Rome, and alkali-silica gel from concrete in Denmark (alkali-silica gel, courtesy of Dr. G. M. Idorn).

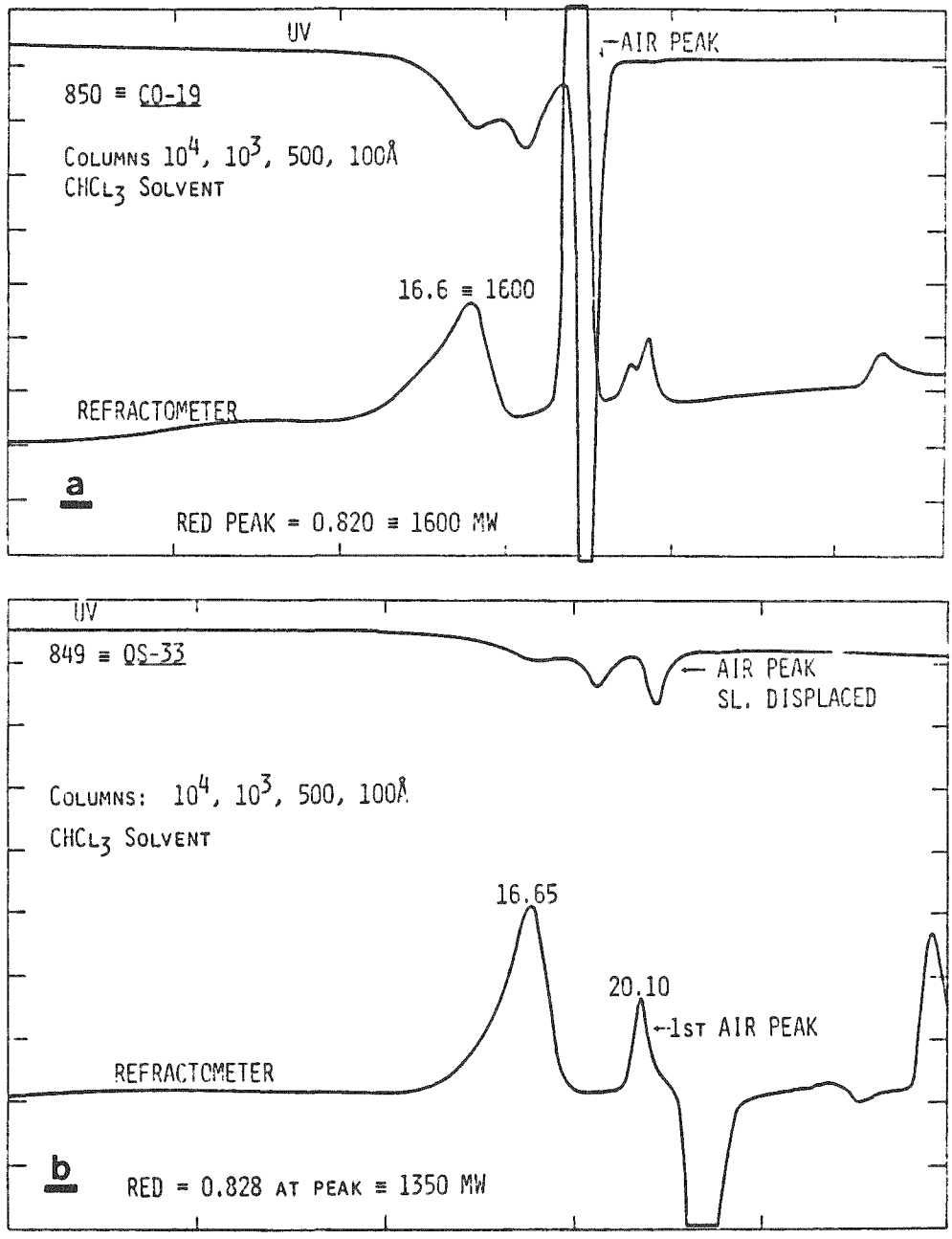

Fig. H-3. GPC results on (a) CO-19 and (b) OS-33 cementitious materials. GPC chromatograms courtesy of Dr. E. Lachowski.

☆ U.S. GOVERNMENT PRINTING OFFICE: 1989-673-034/00111